



# Annual Report 2023

MLZ is a cooperation between:

Bavarian State Ministry of  
Science and the Arts



SPONSORED BY THE



Federal Ministry  
of Education  
and Research

**The Heinz Maier-Leibnitz Zentrum (MLZ):**

The Heinz Maier-Leibnitz Zentrum is a leading centre for cutting-edge research with neutrons and positrons. Operating as a user facility, the MLZ offers a unique suite of high-performance neutron scattering instruments. This cooperation involves the Technische Universität München, the Forschungszentrum Jülich GmbH and the Helmholtz-Zentrum hereon GmbH. The MLZ is funded by the German Federal Ministry of Education and Research, together with the Bavarian State Ministry of Science and the Arts and the partners of the cooperation.

**The Forschungs-Neutronenquelle Heinz-Maier-Leibnitz (FRM II):**

The Forschungs-Neutronenquelle Heinz-Maier-Leibnitz provides neutron beams for the scientific experiments at the MLZ. The FRM II is operated by the Technische Universität München and is funded by the Bavarian State Ministry of Science and the Arts.

# **Joint Annual Report 2023**

## **of the MLZ and FRM II**



**234**  
articles

**55**

Third-Party Funding  
Projects at MLZ with a total  
volume of €13.2 million

**626**  
media  
articles



**2,013**  
followers on  
social media

**40**  
news  
articles  
on the  
web pages



**€ 8.61**  
million



**€ 1.68**  
million



**€ 1.27**  
million



**€ 1.65**  
million

from other  
institutions

PUBLICATIONS AND COMMUNICATION

THIRD-PARTY FUNDING

# 2023 IN NUMBERS

SCIENTIFIC EVENTS

EVENTS FOR THE PUBLIC

**539** participants at  
the European Conference  
on Neutron Scattering  
(ECNS) hosted by MLZ



**250** participants  
registered  
for the MLZ  
User Meeting

More  
than **50**  
participants  
at the MLZ  
Conference  
“Neutrons for  
Biomaterials”

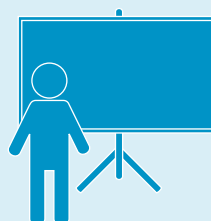


**90** children and  
**270** adults  
participating in FRM II tours  
at the “Open-Door-Day  
with the Mouse”

**3,296**  
visitors



Around  
**80** participants at the  
SR2A Conference on Synchrotron  
Radiation and Neutrons in Art  
and Archaeology



More than  
**100** participants  
at the “Science for  
Everyone” lecture  
(by Deutsches Museum)

## **Perseverance will prevail..... 7**

### **Scientific Highlights**

Closer to the dream of nuclear fusion with positrons.....	10
Blockage in batteries .....	11
AI optimizes beamtime .....	12
Analyzing rocks to store CO <sub>2</sub> .....	13
Bone fragments discovered inside an 800-year-old piece of jewelry .....	14
Non-toxic cleaner for paintings .....	15
Clarifying the structure of the skin barrier.....	16
Milk from green leaves .....	17
Safe alternative – solid-state batteries .....	18
Discoveries in the realm of microorganisms.....	19

### **Scientific Reports**

Materials Science .....	22
Soft Matter .....	31
Structure Research.....	36
Quantum Phenomena .....	43
Neutron Methods.....	48

### **News from the instruments**

Update from the instruments .....	58
-----------------------------------	----

### **Reactor & Development**

An undesirable saga continues: more than 1300 days without neutrons, but a busy year for the FRM II .....	66
Experiments to support conversion of FRM II to Low Enriched Uranium (LEU).....	68

### **Facts & Figures**

The year in pictures .....	72
Workshops, Conferences and Schools .....	83
Changing media presence.....	90
MLZ hosted the European community.....	94
Organization, Staff and Budget .....	96
Publications & Theses .....	100
Cover pages .....	102
Committees .....	103
Partner institutions.....	108
Imprint.....	112



# Perseverance will prevail

The famous German poet and illustrator, Wilhelm Busch, once said: “Perseverance is rewarded sooner or later – but usually later.” After four years without neutrons at the FRM II and MLZ, Busch’s “later” has often felt very true. And yet, as Busch also stated, perseverance will eventually pay off. Looking back at these past four years, we are proud to note that many technical challenges have been overcome, making us hopeful that regular operation is within our grasp!

The great progress made would not have been possible without the uncompromising dedication of the staff at FRM II. The operating team has been making exceptional efforts to restart FRM II as soon as possible. At the same time, our scientists, as supported by our scientific advisors and the community, have been advancing our suite of instruments and experimental methods. In addition, they have been supporting our users in every conceivable manner to advance their research activities. For the long-term future, the MORIS upgrade program has been submitted to our funding agencies.

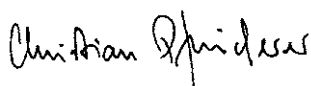
The wide range of activities and disciplines at MLZ is reflected, for instance, by the European Conference for Neutron Scattering (ECNS), which was held in Garching in March 2023, attracting over 500 participants. Similarly, we were delighted to welcome over 200 participants to our annual User Meeting in December. Further highlights in 2023 included the MLZ Conference on “Neutrons for Biomaterials” in Fürstenried as well as the SR2A 2023 conference at Munich’s Pinakothek der Moderne, which highlighted synchrotron and neutron applications in art and archaeology. All of these events demonstrated an enduring passion and interest for neutron-based research at the MLZ.

We are especially grateful for the strong political support and financial commitment of the Federal Ministry of Education and Research and the Bavarian State Ministry of Science and the Arts. Both have demonstrated their encouragement wholeheartedly, recognizing the importance of our scientific contributions as well as our efforts to convert FRM II from highly enriched to low enriched fuel.

As the end of 2023 approached, a change of the board of directors took place. Following a term of almost six years, Prof. Dr. Peter Müller-Buschbaum decided to dedicate more time to research, in particular the Bavarian Keylab TUM.Solar, the Federal Cluster of Excellence e-Conversion, and the TUM Sustainability Board.

Starting on January 1<sup>st</sup>, 2024, Prof. Dr. Christian Pfeleiderer took office as the Scientific Director of FRM II and MLZ. Holding the professorship for the Topology of Correlated Systems at TUM, Prof. Pfeleiderer has been intimately involved with many scientific and technological developments at MLZ for many years.

With the annual report 2023, we wish to highlight the key scientific achievements of studies carried out at MLZ, as well as the technological progress made towards future user operation. We trust that you will enjoy reading this report and hope you may share the extraordinary spirit at FRM II and MLZ, helping us to prevail despite these challenging times without neutrons.



Christian Pfeleiderer



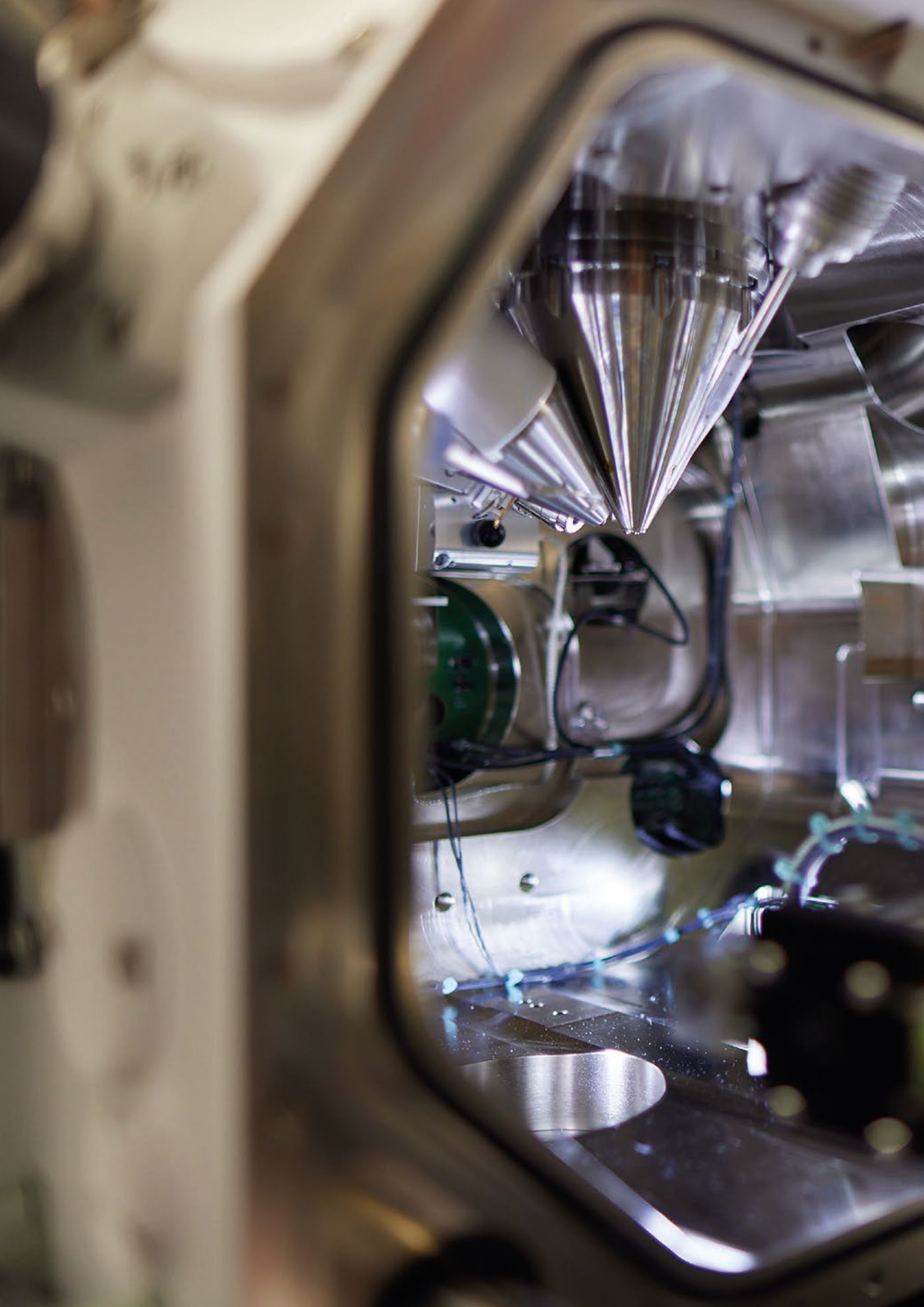
Martin Müller



Axel Pichlmaier

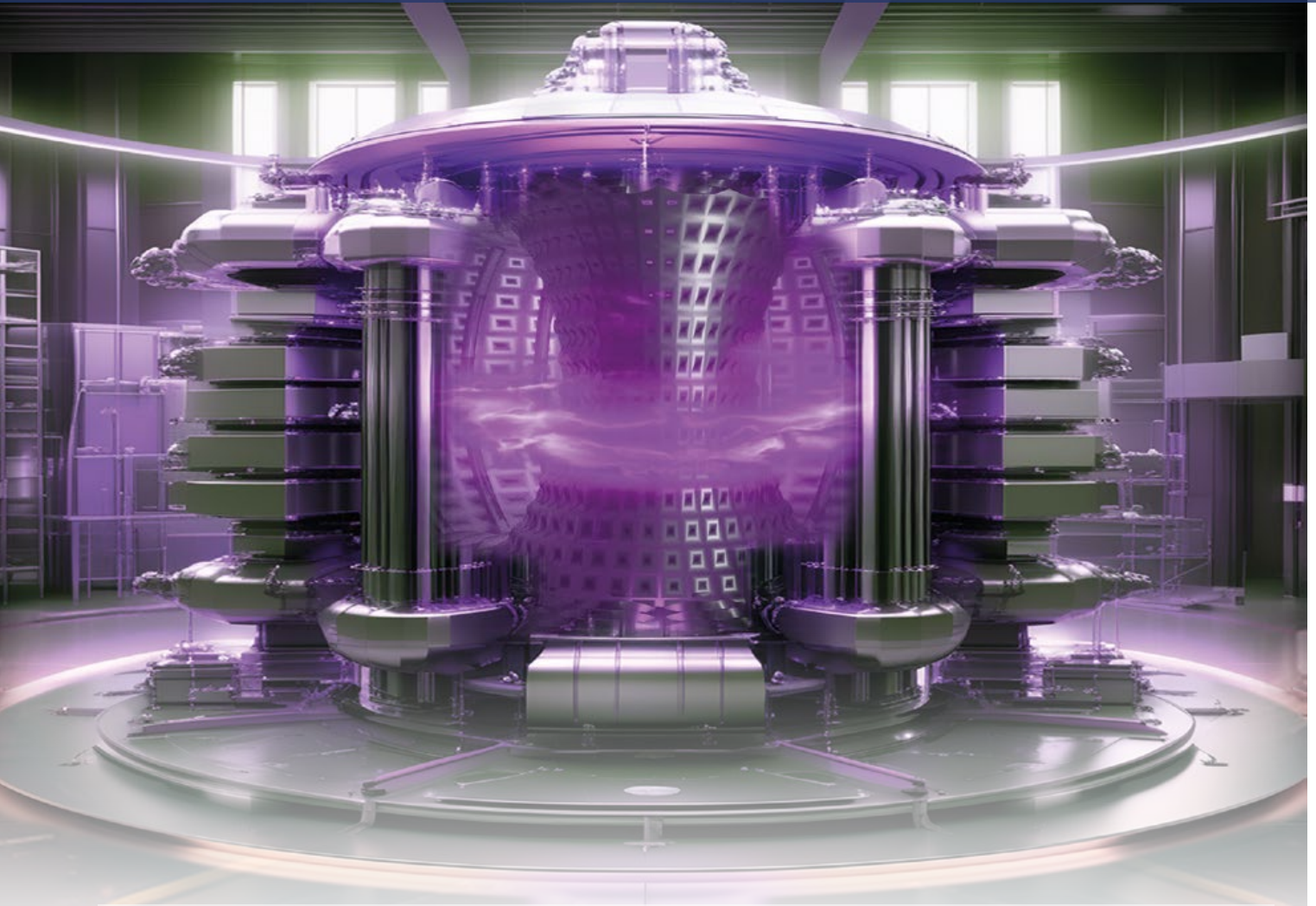


Robert Rieck



# Scientific Highlights





## CLOSER TO THE DREAM OF NUCLEAR FUSION WITH POSITRONS

**Nuclear fusion could help solve the energy problem in the future. However, there are still numerous challenges to overcome before then. Among other things, the inner walls of the fusion reactor must be able to withstand extreme conditions.**

### **How can an artificial sun be shielded?**

Candidates as material for the reactor wall include tungsten and Eurofer 97, a steel alloy made of iron, molybdenum and other elements. The steel is exposed to particle and gamma radiation in the fusion reactor, which detaches individual atoms from their lattice position in the metal. Individual helium nuclei can initially be deposited in these tiny voids, gradually forming larger and larger pores. The mechanical stability deteriorates as a result of this pore formation.

### **Getting to the heart of steel with positrons**

The positron source NEPOMUC generates a beam that is 100 times stronger than conventional sources. As a result, the identification and spectroscopy of defects can

be performed in significantly shorter measurement times and allows sample analysis up to a depth of one micrometer. Researchers can use this data to draw conclusions about the size and type of defects on an atomic level.

### **Limiting the helium loading in tungsten**

Further tungsten investigations revealed that the targeted introduction of vacancies act as effective barriers, limiting helium penetration. These findings are important for developing optimal wall materials for fusion reactors and ensuring their safe operation.

*A. Kärcher, T. Schwarz-Selinger, V. V. Burwitz, L. Mathes, C. Hugenschmidt, W. Jacob, The influence of displacement damage on helium uptake and retention in tungsten, Nucl. Mater. Energy 34, 101370 (2023)*

*DOI: 10.1016/j.nme.2023.101370*

*Experiments were carried out at NEPOMUC.*

## BLOCKAGE IN BATTERIES

**When developing new batteries, researchers are challenged by effects that reduce the storage capacity. Using neutrons, an international team has investigated one of these effects: the blocked transport of lithium ions in the cathodes of commercial batteries.**

In the past, cathodes were made of lithium cobalt oxide. However, the cobalt oxide can promote ignition of the cell and is very rare worldwide.

### From blocking atoms

“Nickel was considered a promising alternative for cobalt”, explains Tobias Hölderle, a doctoral student at the MLZ. However, one defect reduces capacity and energy density: cation mixing. The positively charged nickel and lithium ions swap their positions due to their similar atomic radius. “During charging and discharging, nickel ions can sit firmly in the lithium positions, blocking the diffusion paths of the lithium,” says Hölderle.

### Batteries installed in Tesla S

To improve structural stability, manufacturers do not entirely replace the cobalt atoms in the cathodes with nickel. Instead, most use a proportion of cobalt and nickel. Empirically, manufacturers have found mixes for long lasting, safe

and low priced batteries. Batteries of this type are also installed in the first generation of the Tesla Model S. While cation mixing for cells with nickel-manganese-cobalt (NMC) has already been proven, the occurrence in nickel-cobalt-aluminum cathodes (NCA) has remained controversial.

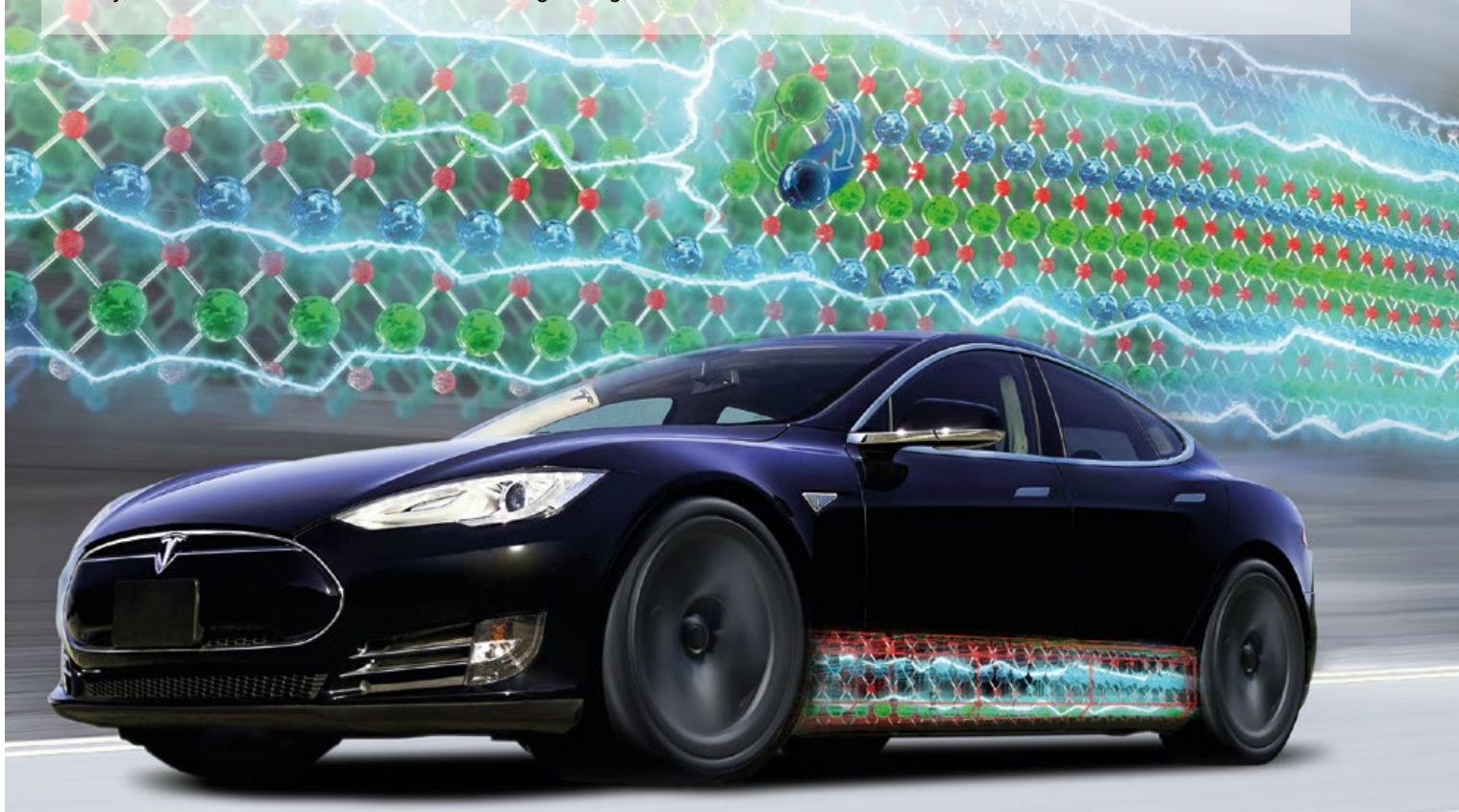
### Neutrons observe the atoms

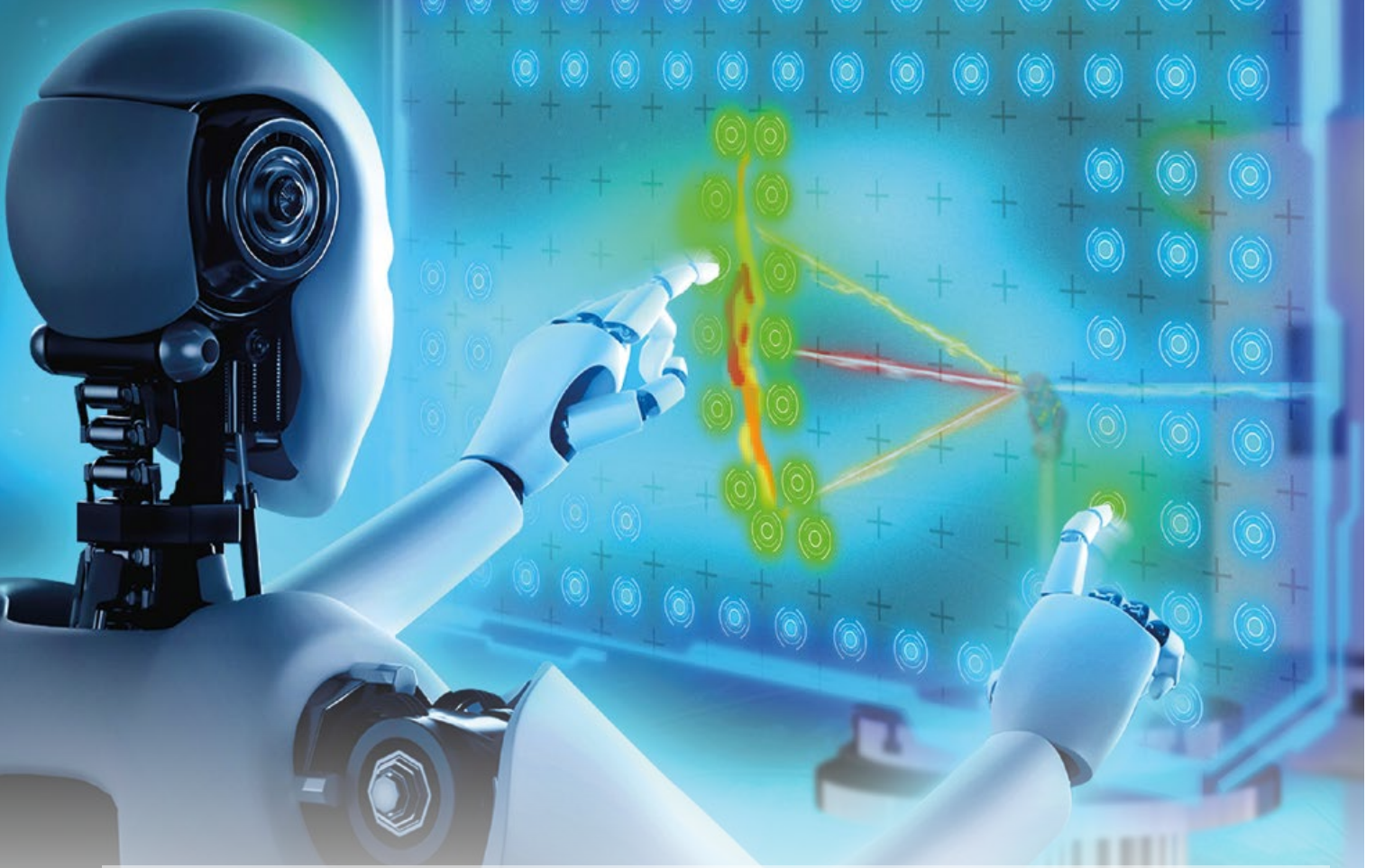
Hölderle and his co-authors examined commercial NCA cathodes in different states of charge using neutrons at the MLZ and ANSTO in Australia. Neutrons make the position of the lithium particularly visible. Hölderle summarizes the results: “In contrast to the NMC cathode material, there is no cation mixing in the NCA cathodes.”

*T. Hölderle, M. Monchak, V. Baran, O. Dolotko, S. Bette, D. Mikhailova, A. Voss, M. Avdeev, H. Ehrenberg, P. Müller-Buschbaum, A. Senyshyn, The structural behavior of electrochemically delithiated  $\text{Li}_x\text{Ni}_{0.8}\text{Co}_{0.15}\text{Al}_{0.05}\text{O}_2$  ( $x < 1$ ) battery cathodes, J. Power Sources 564, 232799 (2023)*

*DOI: 10.1016/j.jpowsour.2023.232799*

*Experiments were carried out at SPODI.*





## AI OPTIMIZES BEAMTIME

**A scientific team from Forschungszentrum Jülich has improved the efficiency of neutron spectroscopy experiments and successfully tested for this. They optimized data acquisition using an active learning artificial intelligence approach. This reduces the time per experiment and makes better use of the scarce resource of measurement time, especially in the first hours of an experiment.**

### Noise signals avoided as far as possible

In neutron spectroscopy, some of the neutrons are scattered by the atoms of the sample, while some pass through without interacting. Only the scattered neutrons contain information; for example, how much energy the neutrons have gained or lost. The other neutrons produce what is known as “noise”.

In order to waste as little time as possible measuring noise signals, the algorithm developed by Dr. Mario Teixeira Parente and his colleagues first takes measurements using a coarse grid. The algorithm then uses this initial data to identify areas in which further measurements would be useful. With each additional measurement point, the algo-

rithm continuously supplements its own database and then autonomously decides on the next measurement position. Because of the feedback loop, this approach is also referred to as active learning. Mario Teixeira Parente explains: “Over time it figures out for itself where it is relevant to measure.”

### Test passed in real experiment

The researchers demonstrated the advantages of their approach in real neutron experiments. Using practical examples and realistic scenarios, they showed that the available measurement time is used more efficiently. Thus, there is nothing stopping an application on further three-axes spectrometers.

*M. T. Parente, G. Brandl, C. Franz, U. Stuhr, M. Ganeva, A. Schneidewind, Active learning-assisted neutron spectroscopy with log-Gaussian processes, Nat Commun 14, 2246 (2023)*

*DOI: 10.1038/s41467-023-37418-8*

*Experiments were carried out at EIGER (SINQ).*

## ANALYZING ROCKS TO STORE CO<sub>2</sub>

**Whether sedimentary rocks store fossil hydrocarbons or act as impermeable layers to prevent the rise of stored carbon dioxide – all depends on their porosity. The size, shape, organization, and connectivity of the pore spaces are decisive. At the MLZ, the networks of micropores were characterized using small and very small angle neutron scattering.**

Ranging from a few micrometers to sub-nanometers in size, the pores are formed during sedimentation and compacted over time, determining the permeability of rocks. However, how do you measure pores that are no bigger than bacteria? “Only small and very small angle neutron scattering is suitable for fully quantifying pores between a few nanometers and micrometers”, emphasizes Dr. Amir saman Rezaeyan, a researcher formerly at the Heriot-Watt University, Scotland, who, together with an international team, has analyzed the porosity of a dozen sedimentary rocks from Europe and America.

### Neutrons show atom-free pores

As neutrons only interact with the nuclei of atoms, they show the arrangement of the atoms and thus – indirectly – that of the atom-free pores. Rezaeyan, currently at the

University of Calgary, Canada, correlated the measurements with the microscopic properties of the rocks. The result: The more clay, the greater the probability of smaller pores. Rocks with a high clay content are therefore potentially well suited for sealing a disposal or storage place underground as an impermeable layer.

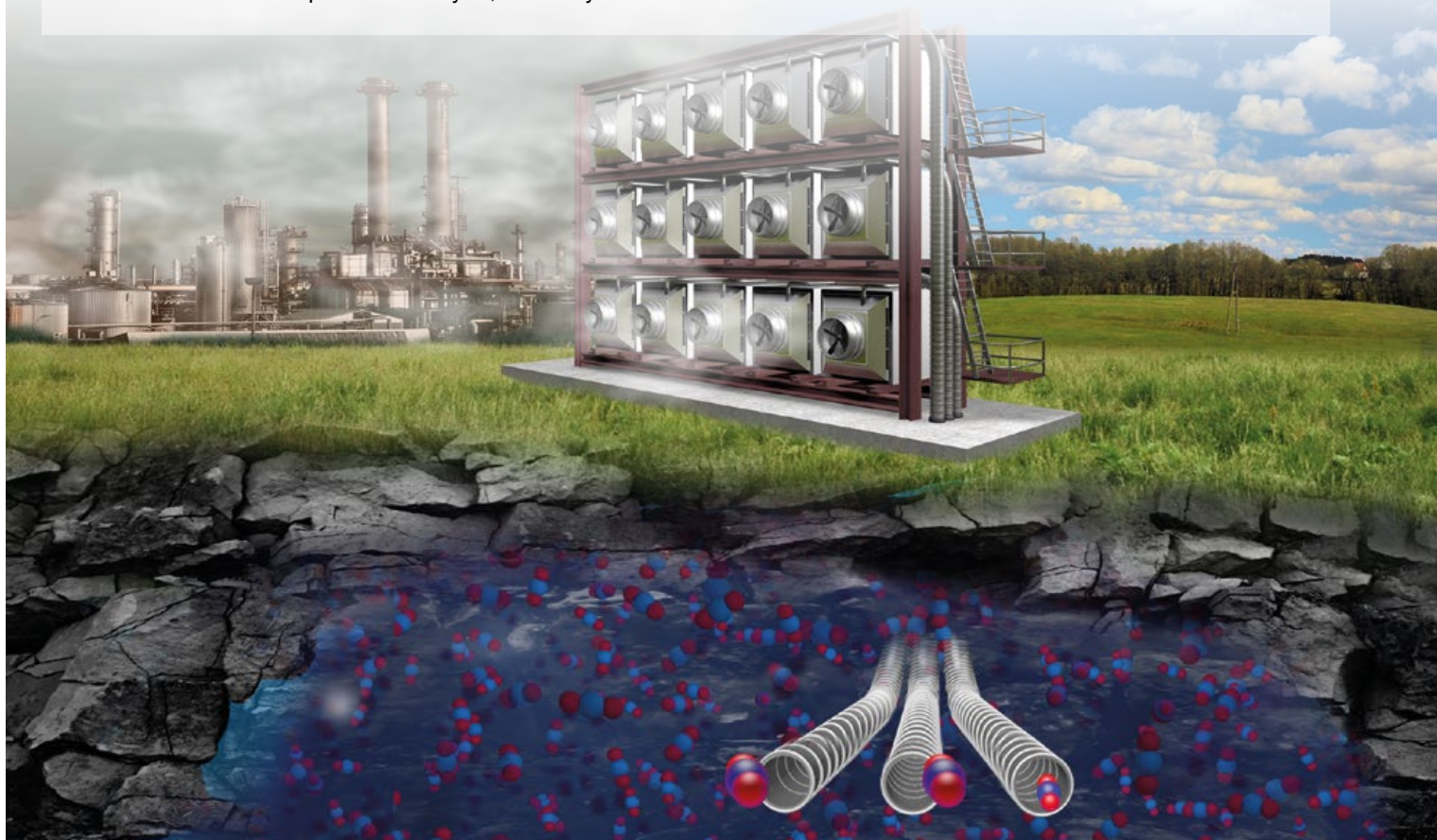
### Nuclear waste repositories

Given these results, it should be possible in future to estimate the physical properties of fine-grained sedimentary rocks based on the sedimentation conditions and to find out whether they are suitable as impermeable layers for nuclear waste repositories and CO<sub>2</sub> storage sites.

*A. Rezaeyan, N. Kampman, V. Pipich, L. C. Barnsley, G. Rother, C. Magill, J. Ma, A. Busch, Evolution of Pore Structure in Organic-Lean and Organic-Rich Mudrocks, Energy Fuels 37, 16446 (2023)*

*DOI: 10.1021/acs.energyfuels.3c02180*

*Experiments were carried out at KWS-1 and KWS-3.*



**EARTH, ENVIRONMENT AND CULTURAL HERITAGE**



## BONE FRAGMENTS DISCOVERED INSIDE AN 800-YEAR-OLD PIECE OF JEWELRY

**The mystery of a gilded pendant found in a medieval garbage pit in the old town of Mainz in 2008 has been unravelled. Non-destructive neutron examination of the object reveals tiny fragments of bone inside, presumed to be relics.**

Five individual pouches made of silk and linen emerged, each containing bone fragments. Due to centuries of corrosion, the object, especially the locking mechanism, is badly damaged, and opening it would mean irreversibly destroying it.

### **Bones of a saint?**

During restoration, a fragment of cord was discovered in the suspension loop, which, upon closer examination, was identified as silk. This is the first evidence that such pendants might have been worn around the neck on a silk cord. Whether the bones belong to saints and which saint the bone fragments can be attributed to cannot be determined. Unlike most receptacles containing relics, the usual parchment strip bearing the name of the saint is missing here.

### **Storage containers for relics**

Only three other reliquaries of this kind, called Phylacterium (translated from the Greek as a preservative or protective substance), have been discovered to date. The exterior of the gilded copper pendant is enameled with images of Jesus, the four Evangelists, Mary, and four female saints. Archaeologists date it to the late 12<sup>th</sup> century and attribute it to a workshop in Hildesheim, Lower Saxony.

*M. Heinzel, E. Kluge, D. Kemper, B. Schillinger, C. Stieghorst, Discovery of a 12<sup>th</sup>-Century Enamelled Reliquary Pendant: Elemental Analysis and Content Visualisation Using Prompt Gamma Neutron Activation Analysis and Neutron Tomography, METAL2022 Proceedings of the interim meeting of the ICOM-CC METALS working group, September 5-9, 2022, 184-191 (2022)*  
ISBN: 978-2-491997-61-8

*Experiments were carried out at ANTARES and PGAA.*

## NON-TOXIC CLEANER FOR PAINTINGS

The restoration of artworks often involves toxic solvents. Now, researchers have succeeded for the first time in creating a non-toxic and sustainable cleaning agent for paintings. They investigated the structure of the agent, referred to as an organogel, using neutrons at the MLZ.

Paintings are irreplaceable works of art, which should be preserved for future generations. However, with the passing of the years, a patina of dust, aggressive air pollutants and microorganisms makes their surfaces look dark and muted. “In order to remove the patina from water-sensitive surfaces, restorers usually use liquid organic solvents which are however hazardous to humans and are also a burden on the environment,” says Prof. Piero Baglioni, chemist at the University of Florence. Together with an international research team, the scientist has now developed a cleaning agent for paintings. Its main component is castor oil, a natural and inexpensive product. Stiff gels can be made from castor oil.

### Gels can carry solvents

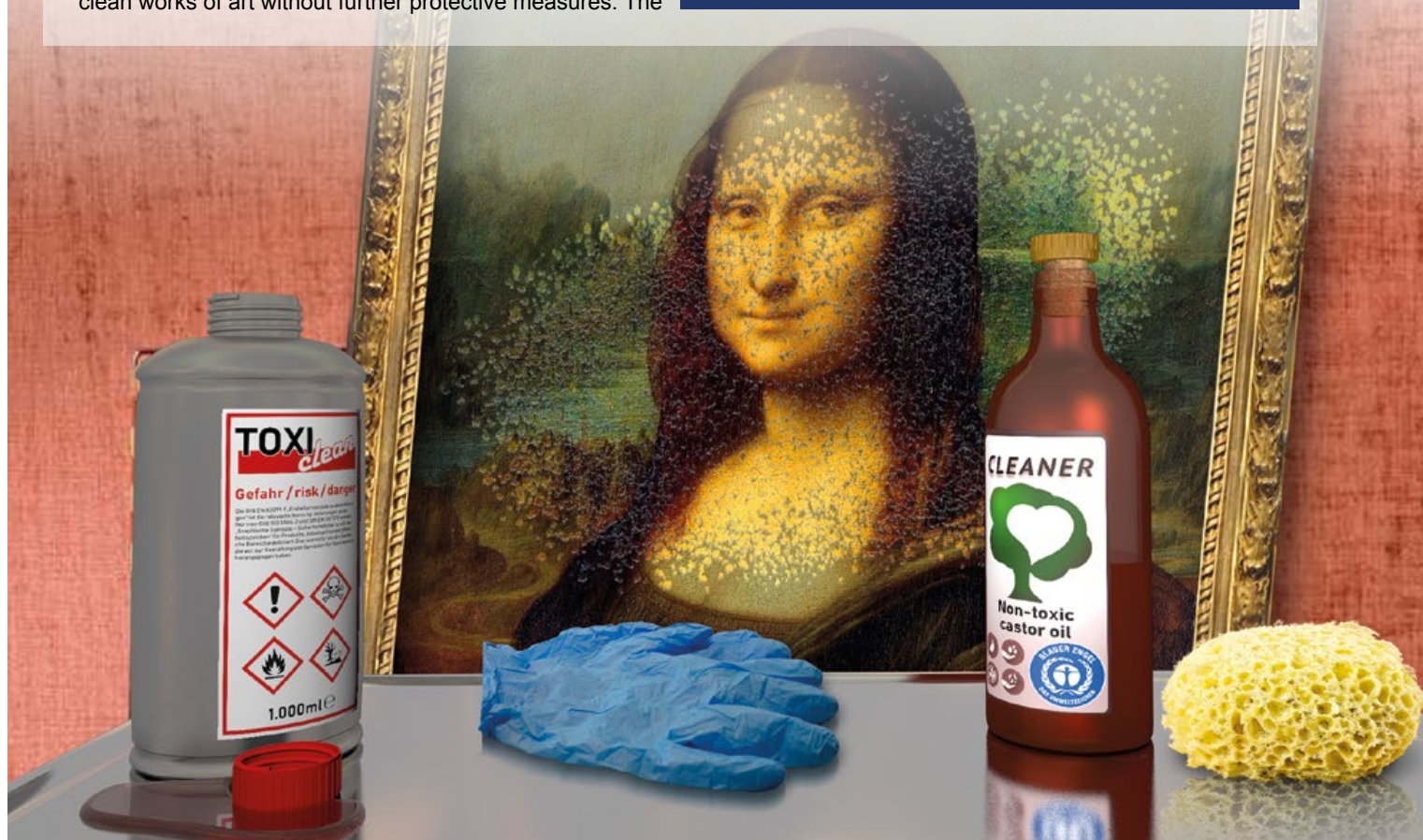
These organogels are able to integrate organic solvents into their molecular networks: “The gels carrying the solvent clean works of art without further protective measures: The

restorer can remove them together with the dust and dirt,” Baglioni explains.

**Neutrons render the structure of the organogels visible** “Neutrons are absolutely necessary in order to understand the structure and dynamics of the organogels,” Baglioni points out. “The investigations at MLZ reveal for the first time their nanostructure and provide information on how the structure changes when the polymers are charged with organic solvents,” says Baglioni. The team used the results of the investigation to optimize the new cleaning agent. In a practical test, restorers at the Peggy Guggenheim Museum in Venice successfully cleaned a painting by Giorgio de Chirico.

*G. Poggi, H. D. Santan, J. Smets, D. Chelazzi, D. Noferini, M. L. Petruzzellis, L. Pensabene Buemi, E. Fratini, P. Baglioni, Nanostructured bio-based castor oil organogels for the cleaning of artworks, J. Colloid Interface Sci. 638, 363 (2023) DOI: 10.1016/j.jcis.2023.01.119*

*Experiments were carried out at SANS-1.*



**EARTH, ENVIRONMENT AND CULTURAL HERITAGE**



## CLARIFYING THE STRUCTURE OF THE SKIN BARRIER

**The promises of skin creams range from relief for dry skin to rejuvenating effects. On the skin, ceramides together with other lipids form a very thin film between the horny cells of the outermost skin layer. As a result, they prevent the body's moisture from evaporating and at the same time prevent the penetration of substances from the environment.**

Moisturizing creams provide ceramides when the skin itself cannot supply enough. Ceramides are a group of molecules consisting of a long chain of carbon and hydrogen atoms. In order to understand exactly how they work, the structure in which the lipids arrange themselves in the skin and thus how water-permeable they are needs to be better investigated – a question that is important for the optimization of moisturizers.

### **Structures dependent on temperature**

Using X-ray measurements, it was possible to show that the ceramides can arrange themselves into two different structures, the so-called “short lamellar phase” (SLP) and

the “medium lamellar phase” (MLP). Which of the two is adopted depends on the environmental conditions and, in particular, on the temperature and humidity.

### **Neutrons decode the functioning of ceramides**

Thanks to the neutrons, we were able to obtain additional information about the water distribution within the MLP repeat unit for the first time and gain a better understanding of how ceramides function.

*P. Pullmannová, B.A. Čuříková-Kindlová, V. Ondřejčková, A. Kováčik, K. Dvořáková, L. Dulanská, R. Georgii, A. Majcher, J. Maixner, N. Kučerka, J. Zbytovská, K. Vávrová, Polymorphism, Nanostructures, and Barrier Properties of Ceramide-Based Lipid Films, ACS Omega 8, 422 (2023)  
DOI: 10.1021/acsomega.2c04924*

*Experiments were carried out at MIRA.*

## MILK FROM GREEN LEAVES

**Milk alternatives made from sugar beet leaves – this is the vision of a research team. They have examined milk proteins in cow's milk products and oat drinks using X-rays to find out what the structure must be like in order for them to be stable, appealing and nutritious.**

### Alternatives to cow's milk

"We are looking for sustainable alternatives to milk," says Dr. Theresia Heiden-Hecht from Forschungszentrum Jülich. In terms of the circular economy, it would be sustainable to produce food with sugar beet leaves, instead of using them as fertilizer during harvesting. It is well known that proteins help the oil droplets to form a stable milk liquid. Plant milk must also be nutritious and appealing to all the senses. "We know what it looks like, but the underlying macro- and micro-structure of the milk can only be identified using X-rays or neutrons," says Heiden-Hecht.

### Milk in X-ray and neutron light

For this reason, the food technologist first examined classic cow's milk, yoghurt, Gouda cheese and oat drinks more closely using different techniques at MLZ. Subsequently,

Heiden-Hecht's team used X-ray scattering to unravel details of a milk emulsion. "We were able to identify interfacial details of the oil droplet in water with the help of X-rays," says Heiden-Hecht.

### Sugar beet leaves as milk suppliers

A methodology has now been developed. Next, the team will focus on plant proteins such as those from sugar beet leaves and has planned neutron measurements. The aim is to highlight the differences to milk and dairy products and to find out what potential the proteins from green leaves have.

*T. Heiden-Hecht, B. Wu, M.-S. Appavou, S. Förster, H. Frielinghaus, O. Holderer, Multiscale Structural Insight into Dairy Products and Plant-Based Alternatives by Scattering and Imaging Techniques, Foods 12, 2021 (2023) <https://doi.org/10.3390/foods12102021>*

*Experiments were carried out at KWS-X.*



# HEALTH AND LIFE



## SAFE ALTERNATIVE – SOLID-STATE BATTERIES

**One of the most important differences between solid-state batteries and conventional batteries is the form of the electrolyte. Electrolytes ensure that electricity is stored and released again by securing the exchange of ions between the anode and cathode.**

### Conventional batteries

This is not a problem with a liquid electrolyte; the ions are present in a solution and can flow to where they are needed. However, safety precautions are necessary due to the highly flammable and difficult to extinguish components, especially lithium. This is associated with very high costs, especially for larger energy storage systems.

### Decoding the ion transport mechanism

Solid-state electrolytes have been the subject of intensive research for some time now, as they could be a more stable and safer alternative to liquid electrolytes. One class of solid-state electrolytes are compounds similar to the mineral argyrodite. Researchers are using X-ray diffraction and neutron spectroscopy to investigate the mechanism of

ion transport in this material. By heating the electrolyte to temperatures of 80°C, individual atoms vibrate so strongly that the ions diffuse through a solid material.

### Optimization of new solid-state electrolytes

The findings help to develop stable and safe solid-state batteries. In the future, this could reduce the cost of large energy storage systems with a high energy density, e.g. batteries for long-distance vehicles such as trains, vessels and trucks, as well as mobile devices.

*Q. Ren, M. K. Gupta, M. Jin et al., Extreme phonon anharmonicity underpins superionic diffusion and ultralow thermal conductivity in argyrodite  $\text{Ag}_8\text{SnSe}_6$ , Nat. Mater. 22, 999 (2023)*

*DOI: 10.1038/s41563-023-01560-x*

*Experiments were carried out at TOFTOF and AMATERAS at J-PARC.*

## DISCOVERIES IN THE REALM OF MICROORGANISMS

**Cyanobacteria, which are commonly found in freshwater and in the sea, engage in photosynthesis much like plants. While light absorption is desirable for harvesting solar energy, excessive sunlight may also be harmful to the bacteria. So, how do bacteria protect themselves from excessive sunlight?**

### **Built-in sun protection within the cells**

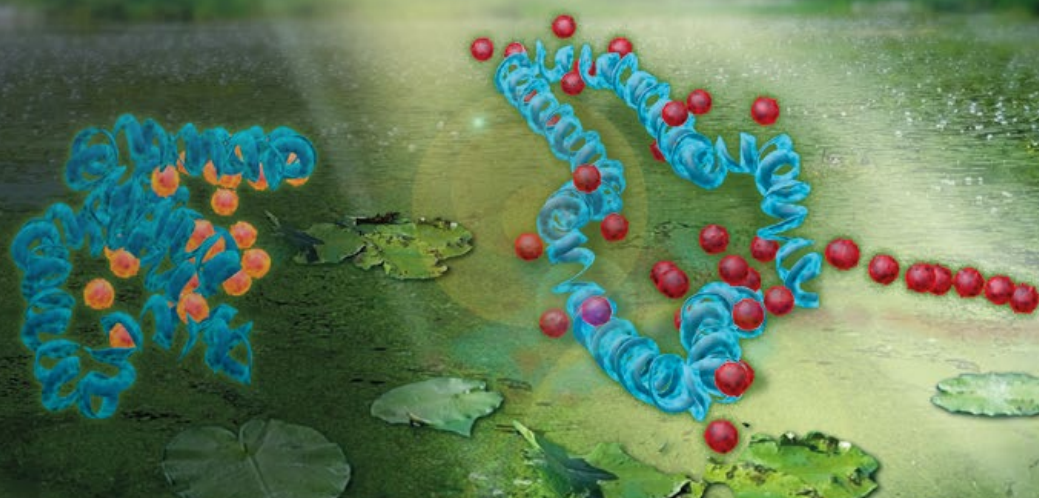
Proteins constitute one of the essential building blocks in living organisms. They are composed of long-chained assemblies of amino acids that fold into complex three-dimensional arrangements. In cyanobacteria, the orange-carotenoid protein (OCP) is employed to absorb and dissipate excessive light energy for the protection of the organism. Following light illumination, the complex three dimensional structure changes to a more open extended conformation, which is the essential prerequisite for the energy dissipation of the excessive light. After the light is switched off, OCP returns to its 'dark' ground state and the cycle can start again.

### **In-operando studies – proteins at work**

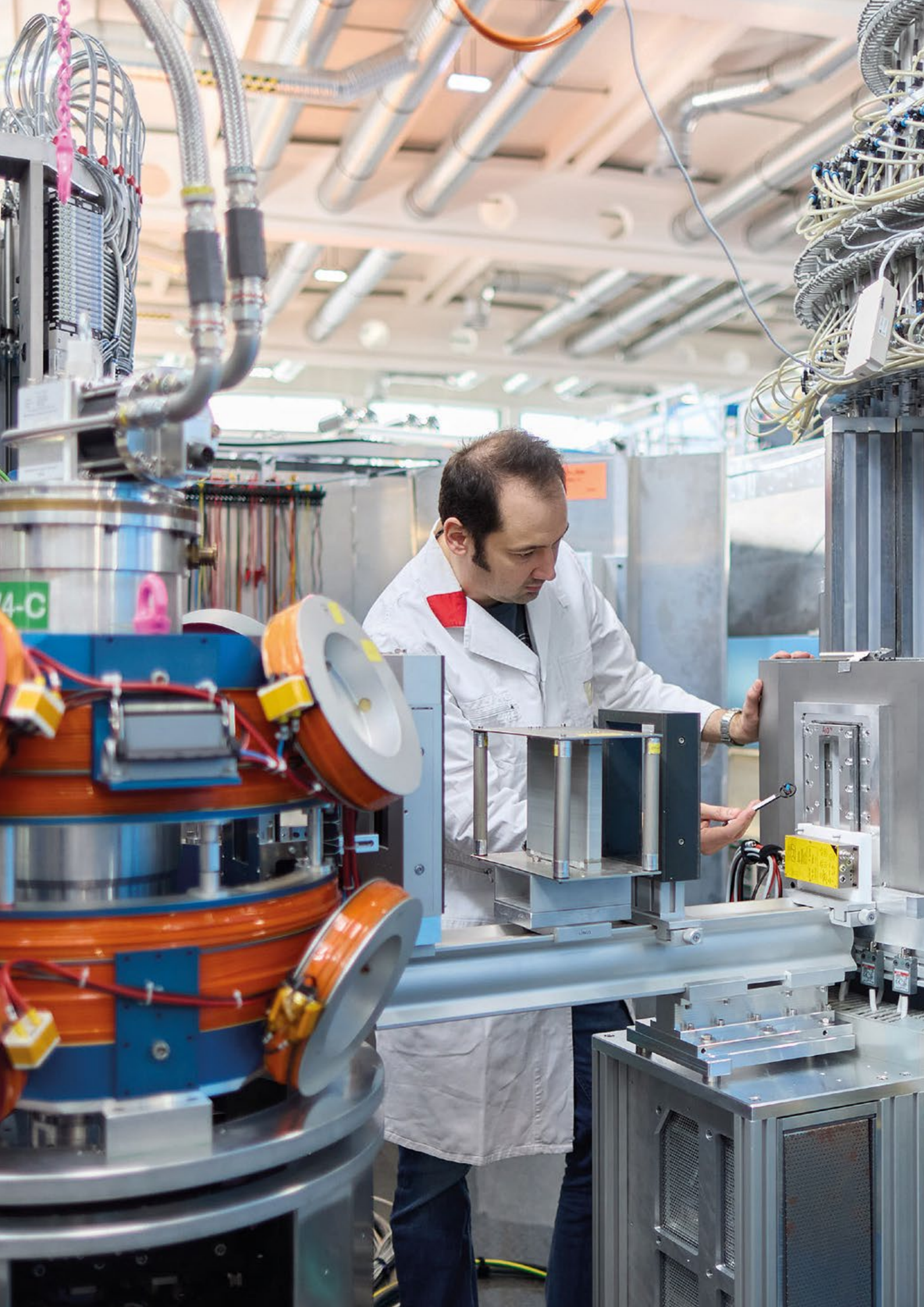
The photoprotective mechanism of OCP was studied for the first time under operational conditions by neutron spectroscopy, addressing the alteration of the internal protein dynamics as the OCP switches from the 'dark' to the extended 'light' conformation. The experiments reveal the biological trick: the higher flexibility in the active state of OCP enables the necessary structural change and provides additional means of non-radiative decay for the conversion of excess energy into heat.

*M. Golub, M. Moldenhauer, F.-J. Schmitt, W. Lohstroh, T. Friedrich, J. Pieper, Light-Induced Conformational Flexibility of the Orange Carotenoid Protein Studied by Quasi-elastic Neutron Scattering with In Situ Illumination, J. Phys. Chem. Lett. 14, 295 (2023)*  
DOI: 10.1021/acs.jpcclett.2c03198

*Experiments were carried out at TOFTOF.*



**BASIC RESEARCH**



# Scientific Reports



Collision-accumulation processes of  
planetesimals as evidenced by pallasitesN. P. Walte<sup>1</sup>, C. Howard<sup>1,2</sup>, G. Golabek<sup>3</sup><sup>1</sup>Heinz Maier-Leibnitz Zentrum (MLZ), Technical University of Munich, Garching, Germany, <sup>2</sup>ISIS facility, STFC Rutherford Appleton Laboratory, Chilton, Didcot, UK, <sup>3</sup>Bayerisches Geoinstitut (BGI), University of Bayreuth, Bayreuth, Germany

**P**allasite meteorites were formed by two colliding planetesimals in the early solar system. We measured the particle size distributions of eight pallasites and compared them to samples created by deformation experiments with SAPHiR. Our results help to constrain the collision stages and the mixing of core and mantle material, which represent the early steps of the accumulation process that finally led to the formation of terrestrial planets.

**Pallasites, witnesses of a violent past**

The early history of the solar system involved the aggregation of material from the primordial disk into small bodies. These planetesimals grew by collision into planetary embryos and, finally, into terrestrial planets. Pallasites, meteorites composed of large olivines embedded in iron-nickel, were formed by the collision of planetesimals, thereby witnessing this important stage of solar system evolution. During the impact, the olivine-rich mantle of the host body was fragmented and intruded by liquid core-metal of the impactor. In order to constrain the collision, we investigated the particle size distribution (PSD) of olivines in different pallasites that stem from a single parent body. PSD plots have been widely used for characterizing brittle and impact-related rocks from Earth. It is suggested that the PSD of such rocks follows a power law equation:

$$N(d) \sim d^{-D}$$

with the grain diameter  $d$ ,  $N(d)$  the number of particles larger than  $d$ , and  $D$  the slope of a linear size distribution in a double-logarithmic plot.

**Understanding cosmic collisions**

PSD plots of fragmental pallasites, meteorites that are composed of shard-like particles (Fig. 1a), display two linear sections, while PSD plots of angular pallasites, meteorites that were formed by fracturing along former grain boundaries, only display linear sections above their respective grain size (Fig. 1b). Metal-melt bearing deformation experiments with SAPHiR created similar structures and PSDs (Fig. 1c). We explain the PSDs with the impact-stages that

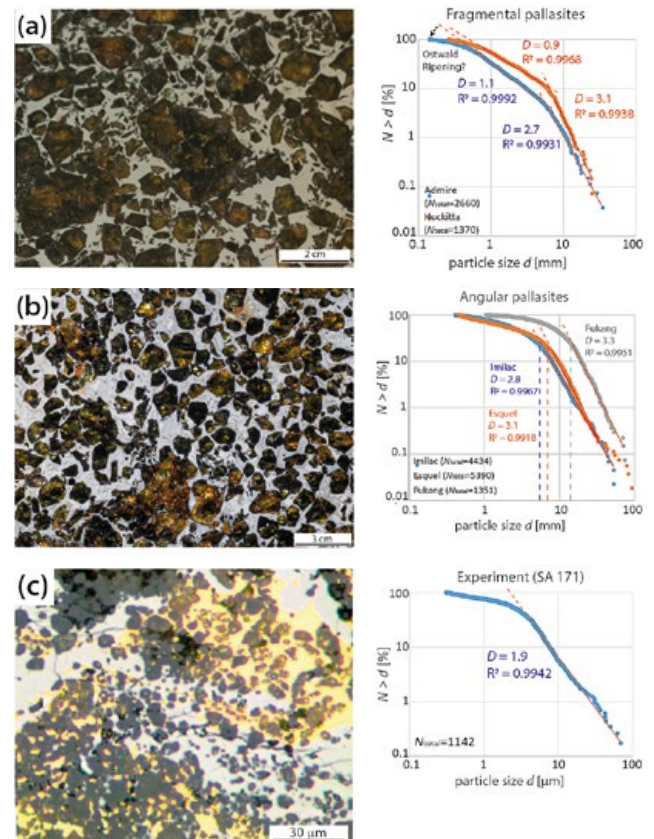


Figure 1: Images and PSD plots of pallasites (a)–(b) and of the SAPHiR samples (c). Dark particles are olivine, bright matrix is metal. (a) Fragmental pallasites were likely situated close to the impact site. (b) Angular pallasites display PSDs with power law distributions above their respective grain size (stippled lines), indicating deeper-lying mantle areas. (c) SAPHiR deformation experiment that created a microstructure similar to angular pallasites.

occur during a collision: Fragmental pallasites were situated closest to the impact where the compressional shock-wave formed the dominantly small particle size population, which is similar to impact ejecta from craters. On the other hand, angular pallasites sample deeper, more protected parts of the mantle. They were mainly effected by the secondary rarefaction wave coupled with the gravitationally downwelling liquid core-metal of the impactor that led to extensional deformation.

[1] N. P. Walte et al., *Mantle fragmentation and incomplete core merging of colliding planetesimals as evidenced by pallasites*, *Earth Planet. Sci. Lett.* 617, 118247 (2023)

DOI: 10.1016/j.epsl.2023.118247

## Designing high-performance metallic laminates assisted by in situ diffraction

H. Wu<sup>1</sup>, M. Huang<sup>2</sup>, Y. Xia<sup>3</sup>, X. Li<sup>1</sup>, R. Li<sup>1</sup>, C. Liu<sup>1</sup>, W. Gan<sup>4</sup>, T. Xiao<sup>5</sup>, L. Geng<sup>3</sup>, Q. Liu<sup>1</sup>, G. Fan<sup>1</sup>

<sup>1</sup>Key Laboratory for Light-weight Materials, Nanjing Tech University, Nanjing, China; <sup>2</sup>Structural Technology Department, Hardware Technology Center, OPPO Guangdong Mobile Communications Co., Ltd., Dong Guan, China; <sup>3</sup>School of Materials Science and Engineering, Harbin Institute of Technology, Harbin, China; <sup>4</sup>German Engineering Materials Science Centre (GEMS) at MLZ, Helmholtz-Zentrum hereon GmbH, Garching, Germany; <sup>5</sup>Shanghai Synchrotron Radiation Facility, Shanghai Institute of High Energy Applied Physics, Shanghai, China

The interfacial stress-affected zone (ISAZ) is a key factor in determining the mechanical properties of layered composites. Here, we provide the direct experimental evidence to confirm the presence of the ISAZ using high-energy X-ray diffraction and neutron diffraction. The ISAZ dimension is then directly correlated with the mechanical property, which addresses the long-standing but unsolved ISAZ effect of heterogeneous layered composites.

### Interesting findings

For our study, we designed a series of Ti/Al laminated composites with different thickness ratios. The thickness of the Al layers varied progressively from 70 to 10  $\mu\text{m}$ , while that of the Ti layers remained constant at 70  $\mu\text{m}$ . Tensile testing revealed the peak of the strain hardening capacity of the Al layer to be 35  $\mu\text{m}$  in thickness. Deviations from this thickness threshold resulted in rapid strain softening promptly after yielding. Moreover, the 35  $\mu\text{m}$  Al thickness layer sample exhibited the greatest uniform flow capacity and the most dispersed crack distribution among all the Ti/Al laminated composites.

### Inspiration from in situ diffraction

First, we confirmed the presence of the interfacial stress-affected zone (ISAZ) and quantified its size as about 15  $\mu\text{m}$  by in situ high-energy X-ray diffraction. Remarkably, the optimal Al layer thickness of 35  $\mu\text{m}$  is nearly double the ISAZ size, indicating that the soft Al layer was almost fully filled by two adjacent ISAZs. Such a perfectly-coated stress field strengthened the constituent layers, enhancing the interfacial constraint effect to achieve superior strength-ductility synergy.

Subsequently, the influence of the ISAZ on the deformation mechanism was then fully investigated via in situ tension measurements at STRESS-SPEC. A notable observation was the elimination of “nominal” elasticity when the Al layer thickness was only 20  $\mu\text{m}$  (Fig. 1a). This phenomenon is attributed to the complete coverage and locally partial overlap of two adjacent ISAZs, and further suggests that a “nominal” elasticity of the composite was mainly contributed by Al layers that were not encompassed by the ISAZ (Fig. 1b). This insight is crucial for the development of high-performance metallic laminates.

[1] H. Wu et al., *The importance of interfacial stress-affected zone in evading the strength-ductility trade-off of heterogeneous multi-layered composites*, *Int. J. Plast.* 160, 103485 (2023)  
DOI: 10.1016/j.ijplas.2022.103485

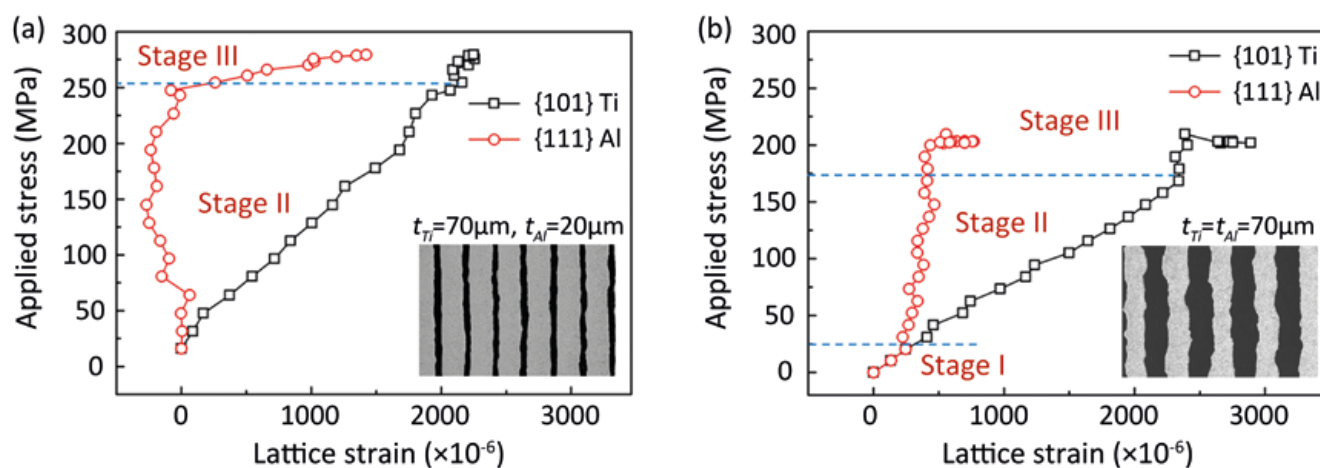


Figure 1: Lattice strain evolution of Ti and Al via in situ neutron diffraction of laminates with Ti 70  $\mu\text{m}$  composed with Al 20  $\mu\text{m}$  (a) and 70  $\mu\text{m}$  (b), respectively.

## Residual stresses in Cu matrix composite surface deposits after laser melt injection

X.X. Zhang<sup>1</sup>, J. Rebelo Kornmeier<sup>1</sup>, J. Bunn<sup>2</sup>, S. Cabeza<sup>3</sup>, F. Fritzen<sup>4</sup>, A. Langebeck<sup>5</sup>, M. Hofmann<sup>1</sup>

<sup>1</sup>Heinz Maier-Leibnitz Zentrum (MLZ), Technical University of Munich, Garching, Germany; <sup>2</sup>Neutron Scattering Science Division, Oak Ridge National Laboratory, Oak Ridge, USA; <sup>3</sup>Institut Laue-Langevin, Grenoble, France; <sup>4</sup>Stuttgart Center for Simulation Science, Institute of Applied Mechanics (CE), University of Stuttgart, Stuttgart, Germany; <sup>5</sup>BIAS – Bremer Institut fuer angewandte Strahltechnik GmbH, Bremen, Germany

**W**ear protection coatings made from metal matrix composites (MMC) can significantly increase the lifetime of heavy-duty tools.

However, during laser melt injection of MMC surfaces, thermally induced residual stresses (RS) are generated, having a detrimental effect on service life and wear resistance. Neutron diffraction measurements were used to determine the effects of processing parameters on the RS state of WC/W<sub>2</sub>C particles coated with Cu materials.

## Laser melt injection

To improve wear resistance, novel metal matrix composite (MMC) coatings have been developed over the last few years that consist of a metal matrix containing up to ~54 vol% spherical fused tungsten carbide (WSC, containing WC and W<sub>2</sub>C). The composite deposits were manufactured via laser melt injection (LMI, Fig. 1a). Due to high-temperature gradients during manufacturing and property mismatches between phases, macro- and micro residual stresses arise in the WSC/metal composite coating. These stresses affect the performance of the composite and might even diminish the integrity of the composite layer on the substrate.

Two types of WSC/metal composites were studied. The first was a WSC particle reinforced pure Cu serving as a reference material (labelled WSC/Cu). The other used as substrate material a CuAl10Ni5Fe4 bronze material (labelled CuAl) on which 5 tracks of WSC particles were injected (Fig. 1b). This material was selected as a typical material used in real-time engineering applications. The measurements were performed in the depth direction from the composite surface layer into the bulk of the substrates

using neutron diffraction measurements at the instruments HB-2b (Oak Ridge National Laboratory) and SALSA (ILL Grenoble).

## Measured residual stresses

Residual stresses (RS) in the WSC/Cu composite deposit showed very low stresses with a maximum tensile residual stress of 98 MPa in the Cu matrix on the top surface. This can be explained by the high preheating temperature of 400°C necessary (due to the high laser reflectivity of the pure Cu substrate) to produce these samples, causing a lower elastic modulus and decreased yield stress in Cu compared to ambient conditions.

In contrast, the RS in the WSC/CuAl composite deposit are higher. This is mainly because no preheating was necessary for the LMI process of the WSC particles in CuAl bronze. In addition, a pronounced compressive stress was found around a depth of 0.6 mm, where the highest density of WSC particles is found (Fig. 1c). This is primarily due to an effective thermal expansion mismatch between the composite layer and the CuAl substrate, resulting in a macroscopic compressive stress in the longitudinal (LD) and transversal (TD) direction in the fusion zone.

These results are used to develop and validate a thermo-mechanical coupled finite element model to predict residual stresses in MMC composites after LMI.

[1] X.X. Zhang et al., *Residual stresses in Cu matrix composite surface deposits after laser melt injection*, *Strain* 59(6), e12457 (2023)

DOI: 10.1111/str.12457

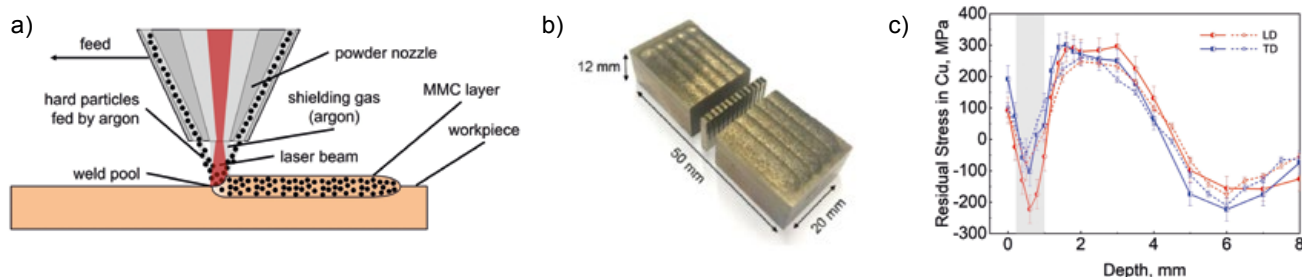


Figure 1: a) Schematic diagram of the manufacturing process using LMI; b) A CuAl composite brick sample was used for the measurements, including a cut-out d<sub>0</sub> reference comb; c) Residual stress depth profiles in LD and TD direction of the CuAl sample from 2 neutron measurements. The grey area indicates the composite layer with the WSC particles.

## Recrystallization texture evolution of cold-rolled Cu foils revealed by neutron diffraction

H. Shi<sup>1,2,3,5</sup>, W. Gan<sup>3</sup>, Y. Zhang<sup>2,5</sup>, E. Maawad<sup>4</sup>, C. Esling<sup>2,5</sup>

<sup>1</sup>Harbin Institute of Technology, Harbin, China; <sup>2</sup>Université de Lorraine, Metz, France; <sup>3</sup>German Engineering Materials Science Centre (GEMS) at MLZ, Helmholtz-Zentrum hereon GmbH, Garching, Germany; <sup>4</sup>Institute of Materials Research, Geesthacht, Germany; <sup>5</sup>Laboratory of Excellence on Design of Alloy Metals for low-mAss Structures (DAMAS), Metz, France

Neutron diffraction technique was employed to investigate the recrystallization texture evolution of thin copper foils with a thickness of around 10  $\mu\text{m}$ . The results showed that the crystallographic orientation of the recrystallized grains was influenced by both the intrinsic properties of the cold-rolled Cu foils such as deformation stored energy and grain boundary mobility, and external factors like thermal strain and surface energy.

Researchers are currently investigating the application of ultra-thin metal foils in instrument design, with the goal of creating more compact devices. A key focus of our study was to understand the behavior of such foils when subjected to heating after undergoing a cold-rolling process. This treatment induces changes in the size and orientation of the crystals in the metal, termed recrystallization, which strongly affects the mechanical properties of the foils. Our study aims to delve into the range of factors that control recrystallization to optimize the use of metal foils in compact instrument design.

### Texture evolution of thin Cu foils during heating

Neutron diffraction with the instrument STRESS-SPEC was used to measure the bulk texture of thin Cu foils in different states, such as the as-cold-rolled, and the samples heated to distinct terminal temperatures. The data obtained was presented in orientation density function (ODF) sections (see Fig. 1). Our measurements demonstrated that the texture of

thin Cu foils evolved from a cold-rolled type represented with typical cold-rolling texture components to a recrystallized type, which is dominated by several orientations.

### Screening factors for grain growth

At the nucleation state, the orientations of the nuclei were mainly inherited from the deformation texture components. In this state, the screening factor was the deformation stored energy. When the recrystallized nuclei grew to certain sizes (through the foil thickness) during heating, the geometrical 2D features of the foils induced an orientation dependent biaxial thermal constraint and imposed an orientation dependent surface constraint on the growing grains. The nuclei with both moderate biaxial moduli in the foil plane and moderate surface energy densities were favored for further growth. During the post-recrystallization grain growth, grain boundary mobility played an important role, i.e., certain grains with immobile grain boundaries were stabilized.

Our findings provide valuable insights into the recrystallization behavior of cold-worked metals, helping to improve our understanding of these processes.

[1] H. Shi et al., *Recrystallization texture evolution of cold-rolled Cu foils governed by microstructural and sample geometrical factors during heating*, *Mater. Charact.* 196, 112605 (2023)

DOI: 10.1016/j.matchar.2022.112605

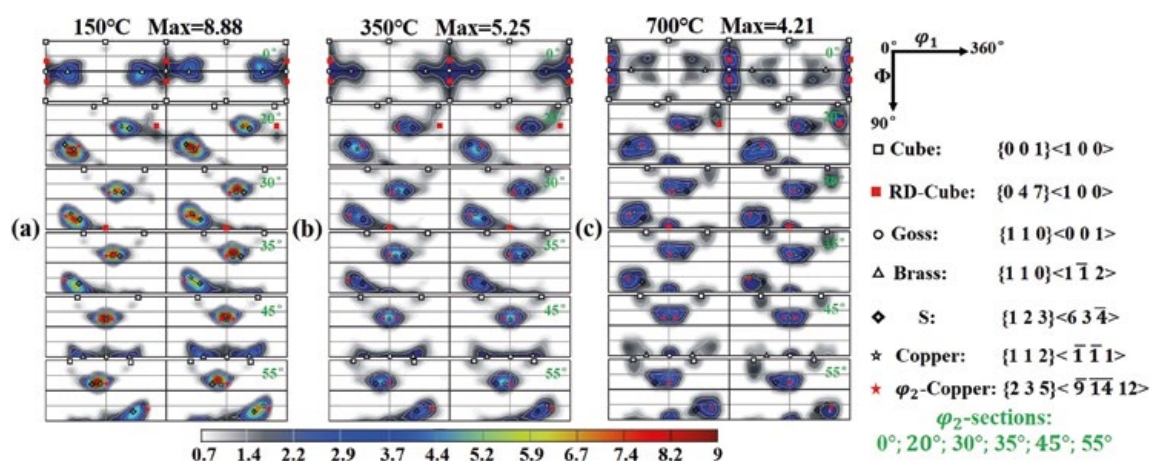


Figure 1: ODF sections ( $\phi_2 = 0^\circ, 20^\circ, 30^\circ, 35^\circ, 45^\circ$  and  $55^\circ$ ) of Cu foils heated to (a) 150°C, (b) 350°C and (c) 700°C measured by neutron diffraction technique on STRESS-SPEC.

# Spacing of quasifreestanding monolayer graphene on 6H-SiC(0001) determined by positron diffraction

M. Dodenhöft<sup>1</sup>, I. Mochizuki<sup>2</sup>, K. Wada<sup>2</sup>, T. Hyodo<sup>2</sup>, P. Richter<sup>3,4</sup>, P. Schädlich<sup>3,4</sup>, T. Seyller<sup>3,4</sup>, C. Hugenschmidt<sup>1</sup>

<sup>1</sup>Heinz Maier-Leibnitz Zentrum (MLZ) and Physics Department, Technical University of Munich, Garching, Germany; <sup>2</sup>Institute of Materials Structure Science, High Energy Accelerator Research Organization (KEK), Ibaraki, Japan; <sup>3</sup>Institute for Physics, University of Technology Chemnitz, Chemnitz, Germany; <sup>4</sup>Center for Materials, Architectures and Integration of Nanomembranes (MAIN), Chemnitz, Germany

**W**e have investigated the structure of hydrogen-intercalated quasifreestanding monolayer graphene (QFMLG) grown on 6H-SiC(0001) by employing total-reflection high-energy positron diffraction (TRHEPD). By performing a rocking curve analysis based on the full dynamical diffraction theory, we determined precisely the spacing between QFMLG and the SiC substrate to  $d_{\text{QFMLG}} = 4.18(6)$  Å in excellent agreement with density-functional theory calculations

## Graphene and Positron Diffraction

Graphene has been extensively studied due to its exceptional properties, such as extremely high thermal conductivity and mechanical strength, as well as massless charge carriers. Of the different approaches to producing large-area graphene, its synthesis on the surface of the wide band gap semiconductor SiC is particularly appealing for high-power or high-frequency electronics.

In this study, we investigated the surface structure of hydrogen-intercalated QFMLG on 6H-SiC(0001) using total-reflection high-energy positron diffraction (TRHEPD), i.e., positron diffraction in grazing incidence. In contrast to electrons, positrons experience a repulsive crystal potential that leads to an outstanding surface sensitivity. TRHEPD is particularly well suited to analysis of the potential buckling of two-dimensional (2D) materials and precise determination of the spacing between graphene and different substrates. Due to the requirement of a bright and coherent positron beam of adequate intensity, there are only two TRHEPD setups in the world, one at the Slow Positron Facility (SPF) of the KEK, Japan and our new positron diffractometer at NEPOMUC.

## Spacing between Graphene and the Substrate

The QFMLG sample was prepared by polymer-assisted sublimation growth of a buffer layer on 6H-SiC(0001) and subsequent hydrogen intercalation. Prior to TRHEPD, the sample was comprehensively precharacterized using XPS, AFM, LEED, and RHEED. The experimental rocking curves, i.e., the intensity of the specular spot as a function

of the glancing angle  $\theta$ , were recorded along the azimuthal direction  $7.5^\circ$  off the high-symmetry directions (one-beam condition) using the 10 keV positron beam at the SPF.

Since in the one-beam condition the contribution of in-plane diffraction is strongly suppressed, the analysis of the experimental data in Fig. 1(a) allows the out-of-plane atomic coordinates to be determined and yields the separation of atomic layers when their mean composition and occupation are included; see all values in Fig. 1(b).

[1] M. Dodenhöft et al., *Determination of the spacing between hydrogen-intercalated quasifreestanding monolayer graphene and 6H-SiC(0001) using total-reflection high-energy positron diffraction*, *Phys. Rev. B* 108, 155438 (2023) DOI: 10.1103/PhysRevB.108.155438

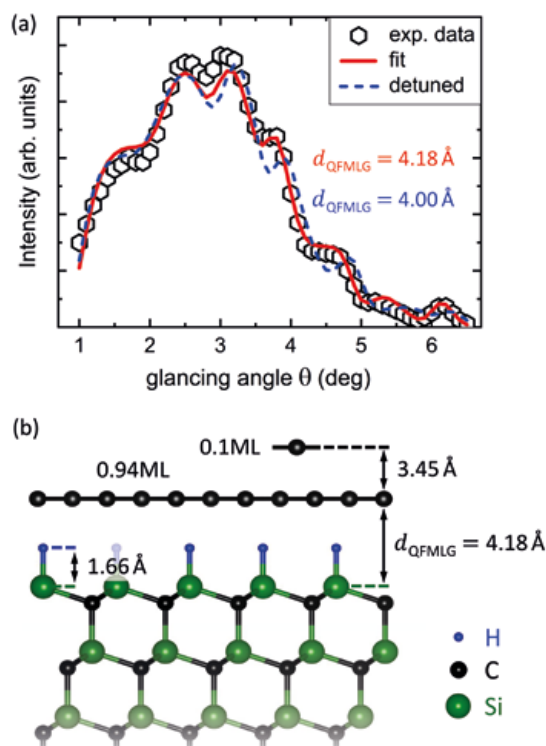


Figure 1: (a) TRHEPD one-beam rocking curve analysis of QFMLG. The model employed to perform the fit (red line) is based on the structure depicted in (b), including six fit parameters: occupations and spacings of QFMLG and graphene bilayer, the spacing of the H atoms, and the lattice relaxation of the top Si layer. The rocking curve is particularly sensitive to the spacing  $d_{\text{QFMLG}}$ : When detuned by  $0.18$  Å (dashed blue line), some features change completely and worsen the fit.

## Novel data analysis tool for coincident doppler broadening spectroscopy

L. Chryssos<sup>1</sup>, C. Hugenschmidt<sup>1</sup>

<sup>1</sup>Heinz Maier-Leibnitz Zentrum (MLZ) and Physics Department, Technical University of Munich, Garching, Germany

**C**oincident Doppler Broadening Spectroscopy (CDBS) of the 511 keV positron electron annihilation line is one of the commonly used positron annihilation spectroscopy techniques utilized at the NEutron induced POsitrone source MUniCh (NEPOMUC). CDBS can be used to investigate defects and extract elemental signatures at the positron annihilation site. Due to the requirement of significant data processing and lack of open-source software solutions, a new program was created.

### CDBS Data Acquisition

Contrary to Doppler Broadening Spectroscopy (DBS), CDBS records the energy of both of the electron positron annihilation gamma quanta. Instead of a 1D energy spectrum, the data is represented as a 2D histogram, where each axis corresponds to one of the two gamma energies. Since the electron positron annihilation always results in a total annihilation energy of 1022 keV, the Doppler broadened peak can be separated from background events within the 2D histogram.

### New ROI Based Software

In order to separate the annihilation line from background data, the new software (Software Tools for Analyzing CDB Spectra – STACS) cuts the 2D histogram into segments using a Region Of Interest (ROI) that is fitted to the histogram. As the ROI boundaries do not correspond to the pixel boundaries of the histogram, a simple linear interpolation algorithm is used to avoid artifacts. The ROI is subsequently segmented into energy bins to project the annihilation line onto one dimension, at which point information on the elemental composition can be extracted.

An additional background subtraction step further improves the signal to noise ratio of the projected annihilation line, as shown in the figure. This further improves the already excellent sensitivity of CDBS to detect element specific signatures, for example in Al alloys. STACS offers an open-source easy-to-use python-based software solution for CDB spectroscopy, greatly improving data analysis workflows.

[1] L. Chryssos et al., *Novel data analysis tool for coincident doppler broadening spectroscopy*, *Nucl. Instrum. Methods Phys. Res., Sect. A*, Vol. 1050, 168171 (2023)  
DOI: 10.1016/j.nima.2023.168171

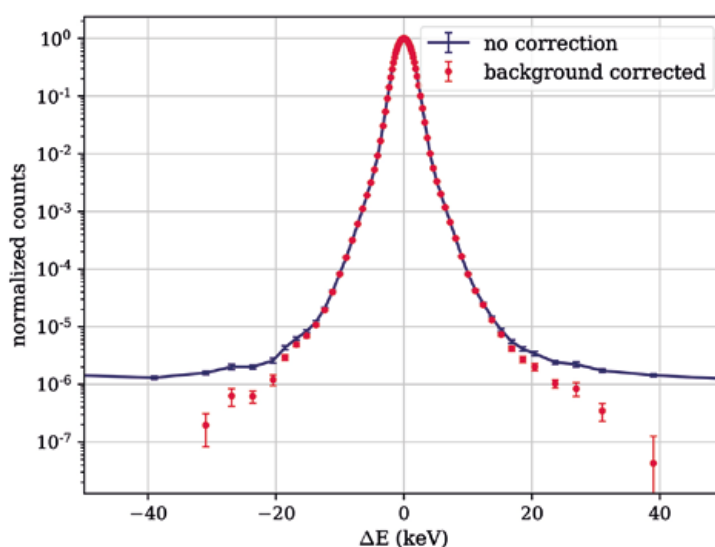


Figure 1: Projection of the Doppler broadened electron positron annihilation line of a tungsten sample with and without background correction. The background correction achieves an additional order of magnitude of signal to background ratio.

## Assessment of delayed hydrogen cracking behavior and the impact of hydrogen diffusion coefficient on various microstructures of the Zr-2.5%Nb alloy

A. Gómez<sup>1</sup>, J. Páez Ponce<sup>2</sup>, M. Grosse<sup>3</sup>, S. Soria<sup>4</sup>, A. Condó<sup>5</sup>, A. Flores<sup>2</sup>, M. Schulz<sup>6</sup>, P. Vizcaino<sup>7</sup>, J.R. Santisteban<sup>8</sup>

<sup>1</sup>Instituto Sabato, Universidad Nacional de San Martín and Comisión Nacional de Energía Atómica. Departamento de Tecnología de Aleaciones de Circonio, Centro Atómico Ezeiza, Buenos Aires, Argentina; <sup>2</sup>Comisión Nacional de Energía Atómica, Departamento de Tecnología de Aleaciones de Circonio, Centro Atómico Ezeiza, Buenos Aires, Argentina; <sup>3</sup>Karlsruhe Institute of Technology, Karlsruhe, Germany; <sup>4</sup>Comisión Nacional de Energía Atómica and CONICET, División Física de Metales, Centro Atómico Bariloche, Argentina; <sup>5</sup>Comisión Nacional de Energía Atómica and CONICET, Instituto Balseiro (UNCUYO), Centro Atómico Bariloche, Argentina; <sup>6</sup>Heinz Maier-Leibnitz Zentrum (MLZ) and Physics Department, Technical University of Munich, Garching, Germany; <sup>7</sup>Comisión Nacional de Energía Atómica and CONICET, Departamento de Tecnología de Aleaciones de Circonio, Centro Atómico Ezeiza, Buenos Aires, Argentina; <sup>8</sup>Comisión Nacional de Energía Atómica and CONICET, Laboratorio Argentino de Haces de Neutrones, Argentina

This study explores the degradation mechanism of delayed hydride cracking (DHC) within different microstructures of the Zr-2.5Nb alloy, aiming to identify potential causes. The DHC phenomenon involves accelerated crack propagation through hydrides precipitated perpendicular to the applied stress field, typically in front of stress concentrators like cracks or flaw tips in the material. Hydrogen diffusion is notably influenced by the morphological aspects of the microstructure.

### Samples with different microstructures

Various microstructures resulting from different processes were deliberately chosen for examination, including those from cold deformation, stress relief, and recrystallization heat treatments below the monotectoid temperature. Additionally, microstructures resulting from high-temperature heat treatments above the monotectoid temperature, followed by cooling under quasi-equilibrium conditions, were included. Using a cantilever beam configuration, samples underwent testing to observe the behavior of the DHC phenomenon and determine the stress intensity factor KIH, a crucial parameter characterizing crack arrest in DHC.

### Dependence of DHC on metallurgical processing

The findings reveal that the increase in ultimate tensile strength (UTS) and hardness, attributed to metallurgical processing, heightened susceptibility to DHC. This was evidenced by a reduction in the stress intensity KIH from 11.8 to 8.5 MPa√m, accompanied by an increase in crack propagation velocity from  $1.6 \times 10^{-8}$  to  $4.5 \times 10^{-8}$  m/s.

### Results of the hydrogen diffusion studies at ANTARES

Conducting in situ hydrogen diffusion experiments at the cold neutron imaging facility ANTARES on two of these materials illuminated the impactful role of recrystallization

treatment-induced  $\beta$ -phase lamellae discontinuity in the parent material on hydrogen diffusion (see Fig. 1). This discontinuity resulted in a 35% reduction in the diffusion coefficient compared to the parent material and a decrease in the terminal solid solubility (TSS). Consequently, there was a slight increase in KIH (7%), an extended hydride incubation time, and a decrease of approximately 20% in crack propagation velocity [1, 2].

[1] A. Gómez et al., *Evaluation of the delayed hydrogen cracking behavior and the hydrogen diffusion coefficient for different microstructures of the Zr-2.5%Nb alloy*, *J. Nucl. Mater.* 587, 154725 (2023)

DOI: 10.1016/j.jnucmat.2023.154725

[2] S.R. Soria et al., *Development of in-situ Delayed Hydride Cracking tests using neutron imaging to study the H redistribution in Zr-2.5%Nb*, *J. Phys. Conf. Ser.* 2605, 012036 (2023)  
DOI: 10.1088/1742-6596/2605/1/012036.

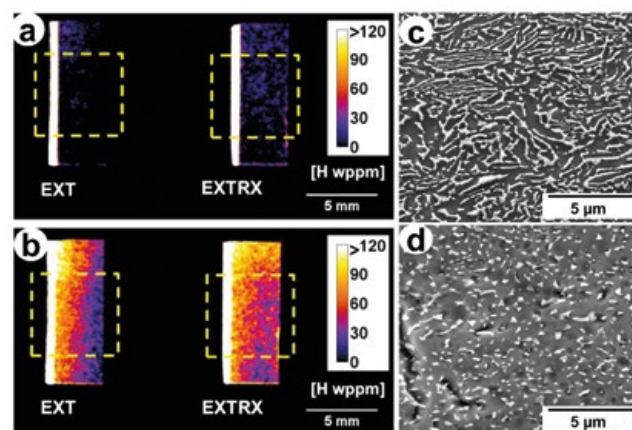


Figure 1: H concentration maps (a) before (0 min) and (b) after the experiment (210 min) at 300°C. The brighter zone on the left side of the samples shown in (a) are the initial hydride layers formed by cathodic charge. The region limited by the dashed yellow line was used to obtain the hydrogen concentration profiles. (c) SEM image obtained using secondary electrons (SEs) of the tube extruded Zr-2.5%Nb microstructure (EXT), (d) EXT material after a recrystallization treatment at 600°C/4hs.

# High-resolution Bragg-edge neutron radiography for visualization of grain morphology

I. Serrano-Munoz<sup>1</sup>, B. Pfretzschner<sup>1</sup>, A. Kromm<sup>1</sup>, N. Nadammal<sup>1</sup>, N. Kardjilov<sup>2</sup>,  
H. Markötter<sup>1,2</sup>, T. Neuwirth<sup>3</sup>, M. Schulz<sup>3</sup>, A. Griesche<sup>1</sup>

<sup>1</sup>Bundesanstalt für Materialforschung und -prüfung (BAM), Berlin, Germany; <sup>2</sup>Helmholtz-Zentrum Berlin für Materialien und Energie (HZB), Berlin, Germany; <sup>3</sup>Heinz Maier-Leibnitz Zentrum (MLZ) and Physics Department, Technical University of Munich, Garching, Germany

One of the main advantages of metal additive manufacturing (MAM) is its ability to produce parts with site-specific microstructural features. However, microstructural defects and lack of reproducibility remain major problems in MAM. Here, we use high-resolution Bragg-edge neutron 2D imaging (HR-BENI) to perform a robust and concise analysis of the quality of crystallographic textures in a MAM material at cm-length scales.

## Advantages of MAM

With the continuous improvement of MAM, efforts are now turning to the development of desirable microstructure-property relationships. Specifically, the possibility of creating components with site-specific properties has been identified as a new design direction leading to enhanced performances. However, it remains difficult to evaluate the quality of the tailored microstructures on the component level. The characterization of MAM components is commonly performed destructively via electron backscatter diffraction (EBSD). In this context, neutron 2D imaging can result an attractive complementary tool for the characterization and optimization of MAM materials.

## Neutron 2D imaging

Specifically, we investigated a laser powder bed fusion (PBF-LB/M) IN718 material using both conventional

(ANTARES beamline at FRM II of MLZ) and high-resolution BENI (CONRAD-2 beamline at BER II of HZB) neutron radiography. A first overview using the  $\{111\}$  cut-off indicates that there are regions where the solidified material remelts locally when the next stripe is being printed. This leads to an increase in the number of  $\langle 111 \rangle \parallel Z(\text{BD})$  grains growing in these regions (shown as black lines in Fig. 1a and outlined in white in Fig. 1b). A higher number of these grains increases neutron scattering and, therefore, a lower intensity is recorded by the detector. In addition, the grey level within the stripes is observed to change with a periodicity of four, due to the influence of the processing parameters.

When using HR-BENI, the localized texture is clearly distinguishable in the vicinity of stripe overlaps, and it is particularly noticeable within stripes 1 and 2 (e.g., Fig. 1d). Remarkably, the lamellar  $\langle 100 \rangle \parallel Z(\text{BD})$  grains formed at the center of the melt pools (which are not visible in Fig. 1) are also resolved (Fig. 1b–d). Thus, the contrast information provided by HR-BENI can be exploited to gain further insights into the development of two-dimensional crystallographic textures within MAM materials.

[1] I. Serrano-Munoz et al., High-resolution Bragg-edge neutron radiography detects grain morphology in PBF-LB/M IN718, *Materialia* 30, 101827 (2023)  
DOI: 10.1016/j.mtla.2023.101827

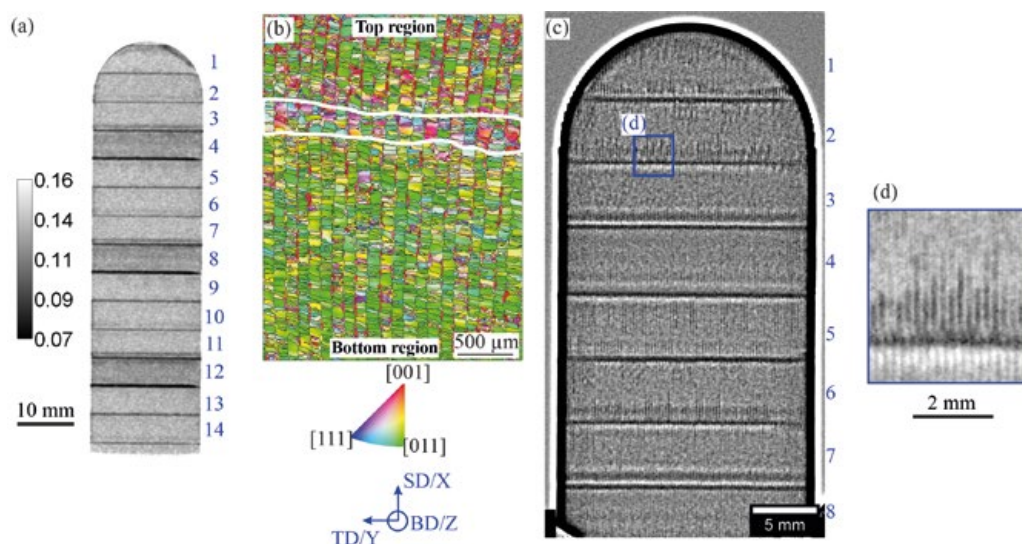


Figure 1: (a) Transmission image at 3.9 Å. (b) EBSD representative orientation map with respect to the BD of one of the overlaps between stripes. (c) Stitched high-resolution BENI image, from which a zoom-in detail is shown in (d).

## Deeper understanding of how a “saltwater battery” works

J. Schubert<sup>1</sup>, L. Grossmann<sup>2</sup>, S. Seidlmayer<sup>2</sup>, K. Pettinger<sup>1</sup>, M. Danzer<sup>3</sup>, R. Gilles<sup>2</sup>

<sup>1</sup>Technology Center for Energy – University of Applied Science Landshut, Ruhstorf a. d. Rott, Germany; <sup>2</sup>Heinz Maier-Leibnitz Zentrum (MLZ), Technical University of Munich, Garching, Germany; <sup>3</sup>Chair of Electrical Energy Systems, University of Bayreuth, Bayreuth, Germany

**S**afety and environmental aspects are increasingly important for the growing battery market. A candidate which meets these criteria is the dual-ion “Saltwater Battery”. This technology utilizes an aqueous electrolyte containing lithium and sodium ions, a lithium manganese oxide (LMO) cathode and a sodium titanium phosphate anode. The results show that lithium is the dominant active species in both electrodes.

### Working principle

This study analyzes the “Saltwater Battery” working principle and compares it with previous results from the literature. The working principle of the active materials in the electrodes is believed to be an intercalation process. There are different studies in which a manganese oxide structure works as host for both sodium and/or lithium. Manganese oxide structures can intercalate both ions, depending on the selected electrolyte and thus the available ion. It is assumed that the cathode interacts with both ions during operation. The lithium containing manganese oxide as produced changes to a  $\lambda$ -manganese phase with empty space for sodium ions. Nevertheless, lithium may be preferred due to its smaller ion radius. In all three possible reaction cases – only sodium, only lithium or both ions – the working principle is intercalation into the LMO host.

### The role of Li and Na

We focused on the single electrodes to investigate the active species by cyclic voltammetry (CV) as well as X-ray diffraction (XRD). Additionally, we performed full cell measurements with electrolytes containing only one ion type to analyze the performance by exclusion. X-ray diffraction studies were carried out in the Physics Lab of the MLZ with support from Dr. Alexander Book.

The findings of this work support the assumption that the anode material can interact with lithium and sodium in a reversible reaction. In contrast to that, contrast voltage measurements indicate that the activity of the manganese oxide structure is limited to lithium only and does not intercalate sodium to any significant degree. Phase analysis of XRD patterns (Fig. 1) support this conclusion and substantiate the described intercalation process on the cathode side.

The active species on the cathode side is clearly identified as lithium (Fig. 1c). Interestingly, sodium deteriorates the cell performance, as is apparent from electrochemical full cell measurements. In this respect, lithium also seems to be the only active species on the anode side.

This research was funded by BMWK, grant number 03EI3046F and BMBF “ExZellTUM III”, project number 03XP0255.

[1] J. Schubert et al., Identifying the active species in dual ion “Saltwater battery” based on lithium manganese oxide, sodium titanium phosphate and aqueous electrolyte, *Energies*, 16(11), 4485. (2023)

DOI: 10.3390/en16114485

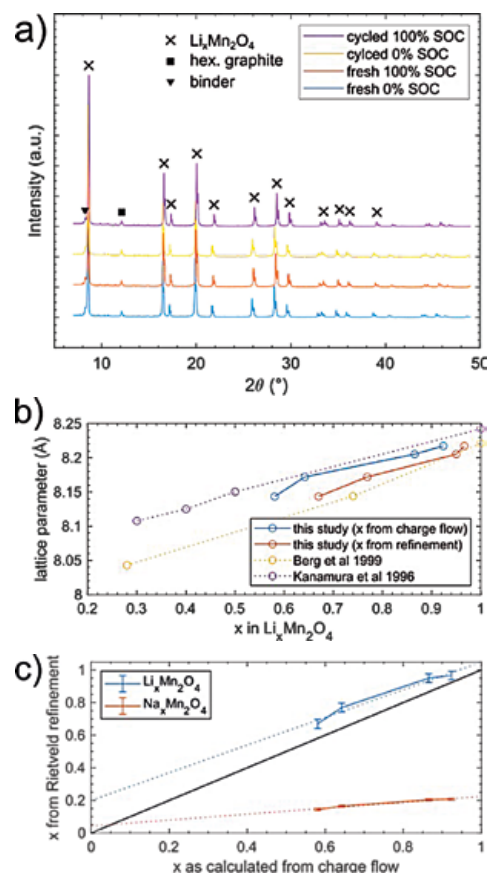


Figure 1: XRD patterns of  $\text{Li}_x\text{Mn}_2\text{O}_4$ -cathode a) as well as  $\text{NaTi}_2(\text{PO}_4)_3$ -anode b) shows the experimental lattice parameter as a function of  $x$  in  $\text{Li}_x\text{Mn}_2\text{O}_4$ . Thereby,  $x$  can be extracted from the charge flow measured by the potentiostat, assuming the (de)intercalation of 1  $\text{Li}^+/\text{e}^-$  or Rietveld refinement. Here, our data are compared with the literature where only  $\text{Li}^+$  was intercalated. c) Comparison of molar fraction  $x$  of the active ion, assuming either intercalation only in  $\text{Li}_x\text{Mn}_2\text{O}_4$  (blue) or  $\text{Na}_x\text{Mn}_2\text{O}_4$  (orange). Fraction values  $x$  obtained from charge flow recorded by the potentiostat and Rietveld refinement.

## Determination of the cooperativity length in glass forming liquids and polymers

R. Zorn<sup>1</sup>, Y.Z. Chua<sup>2,3</sup>, J.W.P. Schmelzer<sup>2,3</sup>, O. Holderer<sup>4</sup>, M. Zamponi<sup>4</sup>, C. Schick<sup>2,3</sup>

<sup>1</sup>Forschungszentrum Jülich GmbH, Jülich Centre for Neutron Science (JCNS-1) and Institute for Biological Information Processing (IBI-8), Jülich, Germany; <sup>2</sup>Institute of Physics, University of Rostock, Rostock, Germany; <sup>3</sup>Competence Centre CALOR, Faculty of Interdisciplinary Research, University of Rostock, Rostock, Germany; <sup>4</sup>Jülich Centre for Neutron Science (JCNS) at MLZ, Forschungszentrum Jülich GmbH, Garching, Germany

In glass forming liquids, the size of cooperatively rearranging regions defining a cooperativity length plays an important role, but is very difficult to access experimentally. Recent experimental improvements, in both AC calorimetry and high-resolution neutron spin echo spectroscopy, allow access to this quantity. In this way, the fundamental question of whether temperature is a fluctuating quantity can be addressed.

### The thermodynamic mystery

Although the idea of a ‘characteristic’ or ‘cooperativity’ length scale  $\xi$  related to the glass transition is now widespread, there is much less consensus on whether this length scale can be related to thermodynamic fluctuations and, if so, whether one has to consider temperature fluctuations  $\delta T$ . The crucial experiment to this end must compare values of  $\xi$  from ‘thermodynamic’ formulae to independent values from structural-dynamics experiments.

### A new path towards a solution

Such an experiment was proposed some time ago by Ernst Donth. The basic idea is to assign a length scale to the AC-calorimetric relaxation time using the spatial resolution of quasielastic neutron scattering, as shown schematically in Fig. 1. The main challenge is to find a range of relaxation times that is accessible by both methods, especially

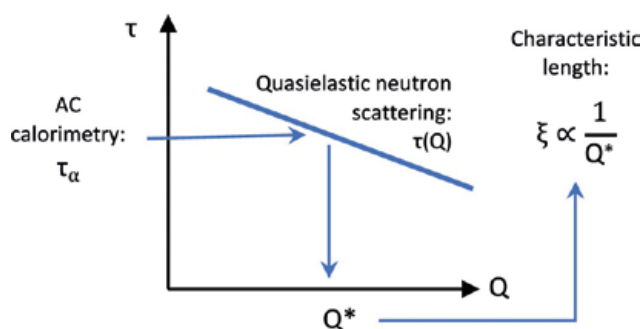


Figure 1: Combining AC calorimetry with quasielastic neutron scattering (with J-NSE and SPHERES) allows the cooperativity length in glass forming polymers to be determined [1].

because the QENS part requires neutron spin-echo with *incoherent* scattering (at J-NSE). A first experiment of this kind was realized on a glass-forming liquid, propylene glycol (PG) [Y.Z. Chua et al., J. Chem. Phys. 146, 104501 (2017)]. The result was that agreement with the thermodynamic calculations was better if temperature fluctuations were accounted for. Nevertheless, in PG the difference between the two thermodynamic estimates is small and the dynamics of the methyl groups overlaps with the  $\alpha$  relaxation. Therefore, a material with a higher ‘contrast’ between the alternatives was of interest and used in a second experiment, poly(ethylmethacrylate) (PEMA). The new results show agreement with the thermodynamic calculation involving temperature fluctuations while the calculation without is off by a factor of six (Fig. 2) [1]. The results strongly indicate that for the thermodynamical treatment of glass forming liquids temperature fluctuations must be taken into account.

[1] Y.Z. Chua et al., *Determination of the cooperativity length in glass forming liquids and polymers*, ACS Phys. Chem. Au 3, 172 (2023)

DOI: 10.1021/acspchemau.2c00057

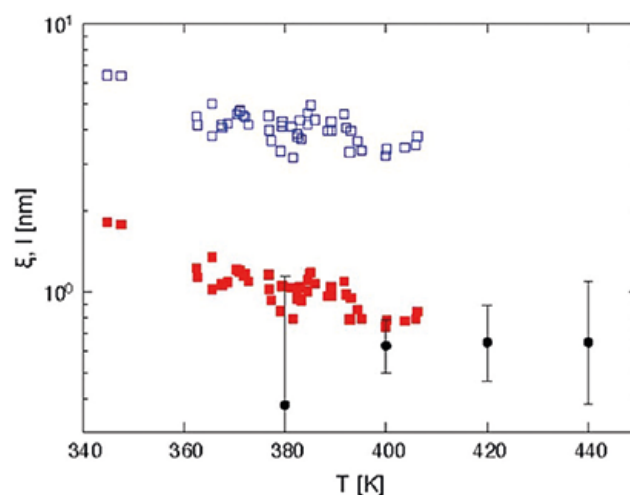


Figure 2: Comparison of the characteristic length  $\xi_\sigma$  from thermodynamic arguments with that from the combination of AC calorimetry and NSE:  $\xi_\sigma$  without considering temperature fluctuations (blue open squares),  $\xi_\sigma$  accounting for temperature fluctuations (red filled squares), from AC calorimetry and NSE (black circles) [1].

Block-copolymer adsorption on the  
surface of multi-walled carbon nanotubesI. Levin<sup>1</sup>, A. Radulescu<sup>2</sup>, Y. Cohen<sup>1</sup><sup>1</sup>Department of Chemical Engineering, Technion, Haifa, Israel;<sup>2</sup>Jülich Centre for Neutron Science (JCNS) at MLZ, Forschungszentrum Jülich GmbH, Garching, Germany

The adsorption morphology of block copolymer (BCP) dispersants of the styrene-*b*-4vinylpyridine family (S4VP) on the surface of multi-walled carbon nanotubes (MWCNT) in a polar organic solvent, *N,N*-dimethyl formamide (DMF) was evaluated by small-angle neutron scattering (SANS) measurements, using the contrast variation (CV) method. This is relevant for CNT-polymer interface in composites, with CNT-CNT contacts for electrical or thermal conductivity.

## The role of block copolymers

Amphiphilic BCPs have been successfully implemented to modify the solution behavior of CNTs. Their use is advantageous when the CNT dispersions are used for the fabrication of composite materials, providing integrity of the CNT/matrix interface yet allowing space for CNT-CNT contact when a conductive pathway is needed. Polymer blocks adsorbed on the CNT surface serve as an anchor, while solvophilic blocks extend into solution, providing stable dispersion by steric repulsion. MWCNT dispersions in organic solvents are used to fabricate composite polymer films and coatings in electric, optical, thermal-dissipation and anti-corrosion applications. Our research aims to characterize the density and layer thicknesses of S4VP copolymers (Fig. 1a) adsorbed on MWCNTs by CV-SANS, using mixtures of protiated and deuterated DMF (dDMF) solvents, as well as using BCPs with protiated and deuterated styrene (dS).

## SANS experiment

Clear dispersions were prepared with 0.5 wt% MWCNT and 2 wt% S4VP by sonication and centrifugation to remove aggregates and possible contaminants. Cryogenic transmission electron microscopy (TEM) imaging shows good dispersion (Fig. 1b). SANS measurements were carried out on the KWS-2 beamline at MLZ, at 2, 8 and 20 m sample to detector distances and 5 Å wavelength. Analysis was done using a cylindrical core-shells model considering the CNT hole partially solvent-filled, carbon shell, and solvent-containing adsorbed block layer and solvent-extended block shell. A simple core-shell model could be used at different contrast conditions achieved using different DMF/dDMF solvent mixtures and S4VP BCPs with either S or dS blocks (Fig. 1c, d).

## Adsorption of block copolymers

The results show that the BCP adsorbs onto the MWCNT surface as a continuous coverage of low polymer concentration. S-blocks form an adsorbed 20 Å layer of ~6 wt% S), which allows for sufficient free space of CNT-CNT contact, if needed. The 4VP blocks emanate extended into the solvent, forming a shell ~90 Å at dilute (<1 wt%) concentration, relevant for sufficient entanglement with dissolved matrix polymers for a strong interface in cast composites.

[1] I. Levin, et al., *Block-copolymer Adsorption on the Surface of Multi-walled Carbon Nanotubes for Dispersion in *N,N* dimethyl formamide*, *Nanomaterials* 13, 838 (2023)  
DOI: 10.3390/nano13050838

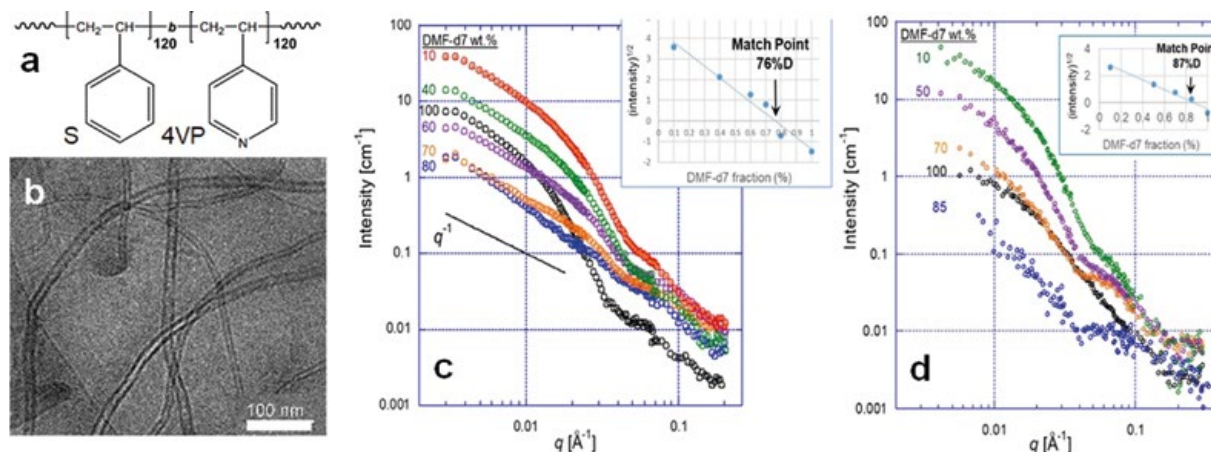


Figure 1: a) the S4VP copolymer; b) cryogenic-TEM image of 0.5% MWCNT dispersion in dDMF with 1% S4VP; c) and d) CV-SANS data of MSCNT dispersion in dDMF/hDMF mixtures, with: c) 1% S4VP and d) 1% dS4VP. Insets:  $(\text{Intensity})^{0.5}$  vs. dDMF content.

## Interchain hydrodynamic interaction and internal friction of polyelectrolytes

E. Buvalaia<sup>1</sup>, M. Kruteva<sup>1</sup>, I. Hoffmann<sup>2</sup>, A. Radulescu<sup>3</sup>, S. Förster<sup>1</sup>, R. Biehl<sup>1</sup>

<sup>1</sup>Jülich Centre for Neutron Science JCNS and Institute of Biological Information Processing IBI, Forschungszentrum Jülich GmbH, Jülich, Germany;

<sup>2</sup>Institut Max von Laue-Paul Langevin (ILL), Grenoble, France; <sup>3</sup>Jülich Centre for Neutron Science (JCNS) at MLZ, Forschungszentrum Jülich GmbH, Garching, Germany

The structure and dynamics of polyelectrolytes in dilute to semidilute conditions were examined using dynamic light scattering, neutron spin echo spectroscopy, small angle neutron scattering and pulse field gradient NMR, revealing a decoupling of local chain dynamics from interchain interactions. We find that hydrodynamic interactions are not fully screened between chains and that the segment dynamics is that of a neutral chain with internal friction.

### Unscreened charges expand polyelectrolytes

Polyelectrolytes (PE) are polymeric macromolecules in aqueous solution characterized by their chain topology and intrinsic charge in a neutralizing fluid (see Fig. 1). The structure and dynamics are related to several characteristic screening length scales determined by electrostatic, excluded volume and hydrodynamic interactions. We examine PE structure and dynamics in dilute to semidilute conditions where chains already overlap for different salt concentrations from 0 to 1M NaCl in the solution [1]. The intrinsic charge of the PE leads to a more extended chain configuration for low salt compared to high salt, as observed by small angle scattering using neutrons (at KWS-2) and X-rays. For high salt the chain collapses as the larger ion concentration screens the intrinsic charge on the chain and reduces repulsion between segments.

### But local dynamics is like a neutral chain with internal friction

Dynamic light scattering (DLS) reveals the collective diffusion coefficient at lowest  $Q$  while neutron spin echo spectroscopy (NSE) is also sensitive to local motions of the chains at larger  $Q$ , as depicted in Fig. 1. Pulsed field gradient NMR measures the self-diffusion on larger length scales. We describe collective diffusion within a colloidal picture, including electrostatic and hydrodynamic interactions. The segment dynamics of the polymer is characterized by the classical Zimm model of a neutral chain retarded by internal friction which dominates chain modes on shorter length scales, respectively larger  $Q$ . For intermediate  $Q$ , the chain dynamics follows the Zimm prediction of a neutral chain ( $D_{\text{eff}} \sim Q$ ) that is expanded due to repulsion between charged monomers. The observations reveal a decoupling of local chain dynamics from interchain interactions. Hydrodynamic interactions between chains are not fully screened and are essential to understand the relation between collective diffusion, self-diffusion and segment dynamics. The internal friction within the chain increases with increasing ion condensation on the chain. The source of internal friction seems to be related to counter ion condensation.

[1] E. Buvalaia et al., *Interchain Hydrodynamic Interaction and Internal Friction of Polyelectrolytes*, *ACS Macro Lett* 22, 1218 (2023)

DOI: 10.1021/ACSMACROLETT.3C00409.

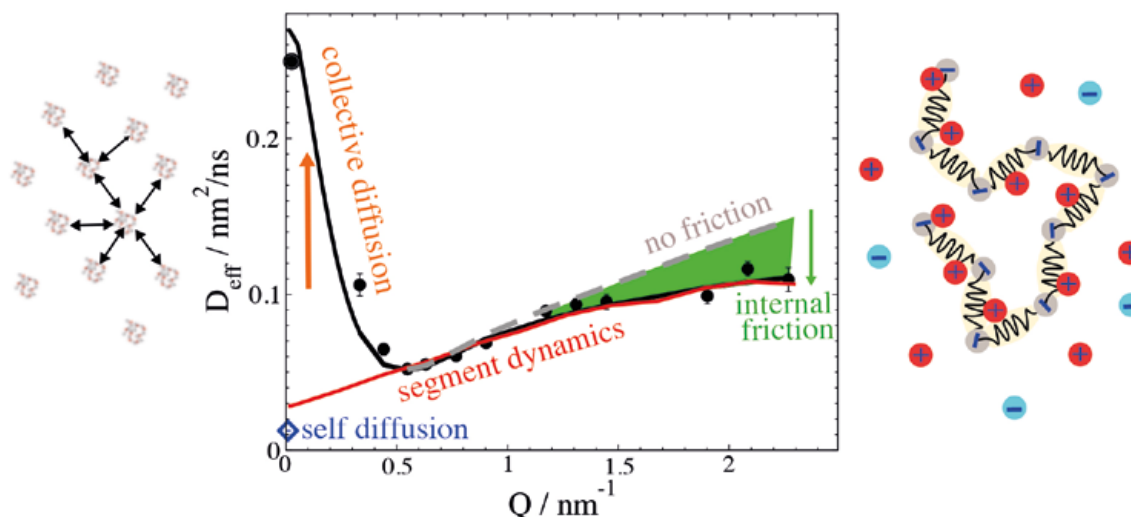


Figure 1: Effective diffusion  $D_{\text{eff}}$  for PSSH 39k without salt (dots) as extracted from NSE and DLS. The Zimm model (dashed + low  $Q$  red line) describes segment dynamics starting from self-diffusion (blue, PFG-NMR). Internal friction slows down segment dynamics at larger  $Q$  (green area) because of friction between neighboring monomers (right illustration). Interchain interactions (left illustration) increase  $D_{\text{eff}}$  at low  $Q$  showing collective chain diffusion (black line).

## Critical dynamics in quasi-binary fluids without and with 2-dimensional confinement

H. Frielinghaus<sup>1</sup>, P.S. Dubey<sup>1</sup>, B. Wu<sup>1</sup>, O. Holderer<sup>1</sup>, S. Förster<sup>2</sup>, T. Heiden-Hecht<sup>1</sup>

<sup>1</sup>Jülich Centre for Neutron Science (JCNS) at MLZ, Forschungszentrum Jülich GmbH, Garching, Germany;

<sup>2</sup>Jülich Center for Neutron Scattering JCNS-1, Jülich, Germany

Complex fluids containing ions are highly interesting in battery/electrolyte research and for fuel/electrolyzer cells. A binary mixture of 3-methyl pyridine (3MP) and heavy water was studied that is close to the phase boundary. Additionally, we added the antagonistic salt sodium tetraphenylborate (NaBPh<sub>4</sub>) that acts as a surfactant and imposes a 2-dimensional confinement on the binary critical composition fluctuations through charge density waves.

### Results in brief

We observed criticality in the structure and dynamics of a three-dimensional (3D) and two-dimensional (2D) Ising system consisting of 3MP/D<sub>2</sub>O without and with antagonistic salt using neutron and X-ray scattering and complementary methods [1] (data collected at SNS, HANARO, TUM and from KWS-X). We were able to describe both dynamic criticalities by the Kawasaki crossover function. The dynamic critical exponent was  $z = 0.063 \pm 0.020$  and  $0.005 \pm 0.019$  for three and two dimensions, which confirms earlier observations in the 3D case and confirms expectations in the 2D case. The amplitudes of the critical dynamics are governed by the bare viscosities experimentally, and by the coefficient  $R$  theoretically [the latter is proportional to  $(4-d)^{-1}$  with the dimensionality  $d$ ]. This finding is in accordance with the lubrication effect, which is also connected to lamellar systems of

the Brazovskii criticality. This lubrication effect is tightly connected to a laminar flow enforced by the domain structure, and it also holds for our 2D Ising system.

### The master curves

The scaled diffusion constant obtained by dynamic light scattering ( $Q\xi < 1$ ) and neutron spin echo spectroscopy ( $Q\xi > 1$ ) is summarized in Fig. 2. For each dimensionality we get a single curve that is constant for  $Q\xi < 1$  indicating whole domain diffusion and an inclination for  $Q\xi > 1$  indicating the domain “wall” fluctuations. The latter expresses a slope of  $(1+z)$  yielding the critical exponent  $z$  that confirms earlier measurements/considerations. The vertical shift of the two curves is due to the different bare viscosity  $\eta_0$ . While theories connect this difference to a coefficient  $R \sim (4-d)^{-1}$  rather exactly, a microscopic understanding is missing at this stage. The viscosity measurements and the understanding of the lubrication effect for 2-dimensional fluids (low viscosity) compared to unconfined fluids finally explain the findings much better. This result is highly important for applications when confinement occurs due to charged molecules at solid walls such as electrodes or scaffold materials.

[1] H. Frielinghaus et al., *Experimental critical dynamics of 3-methyl pyridine/D<sub>2</sub>O mixtures without and with antagonistic salt*, *Phys. Rev. Research* 5, 023053 (2023)

DOI: 10.1103/PhysRevResearch.5.023053



Figure 1: The current research topic brought many people from the soft-matter-group at MLZ (whole group on image) and international scientists from Korea and USA together.

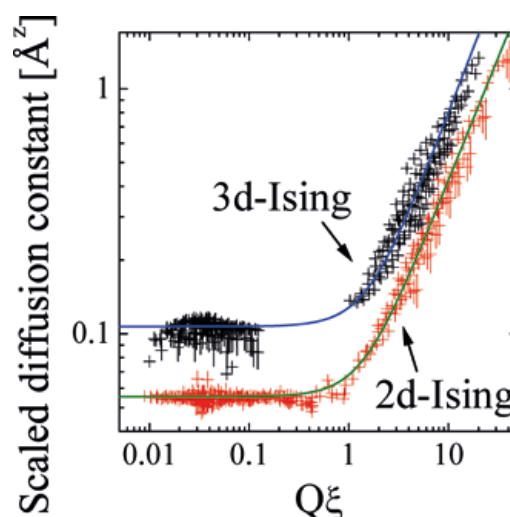


Figure 2: The scaled diffusion constant  $D_{\text{scal}} = \xi^{1+z} D \eta_0 / (k_B T)$  as a function of the dimensionless length scale  $Q\xi$  is described by a master curve for each dimensionality. The scaling was done with the measured correlation length  $\xi$ , the diffusion constant  $D$ , the bare viscosity  $\eta_0$  and the thermal energy  $k_B T$ .

## Internal structure of small unilamellar vesicles of mixed surfactants TDMAO/LiPFO

A. F. Hörmann<sup>1</sup>, A. Feoktystov<sup>2</sup>, T. Narayanan<sup>3</sup>, J. Gummel<sup>3</sup>, M. Gradzielski<sup>1</sup>

<sup>1</sup>Stranski-Laboratorium für Physikalische und Theoretische Chemie, Institut für Chemie, Technische Universität Berlin, Berlin, Germany; <sup>2</sup>Jülich Centre for Neutron Science (JCNS) at MLZ, Forschungszentrum Jülich GmbH, Garching, Germany; <sup>3</sup>European Synchrotron Radiation Facility, Grenoble, France

The mixed surfactant system tetradecyldimethylamine oxide (TDMAO) and lithium perfluorooctanoate (LiPFO) is known to spontaneously self-assemble into well-defined small unilamellar vesicles. Complementary studies point to two main findings: the vesicles formed contain a much higher mole fraction of TDMAO than the bulk sample and the vesicle bilayer is asymmetric with a higher fraction of LiPFO on the outside.

### Structure of vesicles with surfactant

The study of self-assembled small unilamellar vesicles is of relevance for the development of applications like an encapsulation of active agents and, ultimately, drug delivery. In order to control vesiculation for this purpose, it is important to understand both the self-assembly process and its final state. In our study [1] we have chosen a surfactant mixture, where the use of a perfluorinated surfactant (LiPFO) allows for a detailed investigation of the relative location of the individual surfactants within a bilayer. Based on the predictions from the regular solution theory for the expected composition of the vesicles ( $x_{\text{TDMAO}} = 0.46$ ), a significant lack of forward SAXS intensity is observed. This discrepancy must arise from a lower volume fraction of vesicles and means that a much smaller fraction of the surfactant must be aggregated, where, in particular, the high contrast LiPFO must be missing.

### Contrast variation reveals details

To determine the mole fraction of both surfactants in our aggregates, we employed contrast variation in SANS at the KWS-1. The higher fraction of TDMAO in the vesicles,  $x_{\text{TDMAO}} = 0.61$ , as determined from SANS requires more LiPFO to be present as unimers, which is confirmed by electrical conductivity measurements and detailed modeling of the SAXS data. With the correct volume fraction, composition, and background, the question of analyzing the structural properties of the small unilamellar vesicles can be addressed quantitatively, with the aim of deducing detailed information regarding the internal structure of the bilayers. Using simple but constrained geometric models, we find an asymmetric scattering length density profile with more LiPFO in the outer layer and, therefore, a more negatively charged outer surface. The result of an asymmetric bilayer is supported by theories based on curvature considerations and molecular packing theories. This was the first experimental analysis to address bilayer asymmetry using these methods and in such detail, and is therefore important for an enhanced understanding of self-assembled bilayer systems.

[1] A. F. Hörmann et al., *High unimer concentration and asymmetric bilayer observed in small unilamellar vesicles of mixed surfactants TDMAO/LiPFO*, *J. Chem. Phys.* **158**, 214901 (2023)

DOI: 10.1063/5.0150223

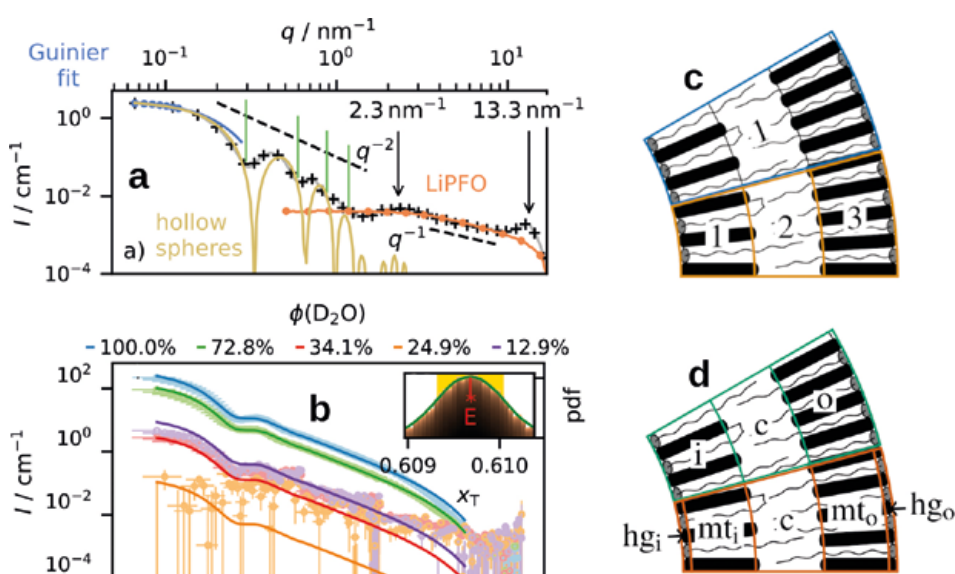


Figure 1: a) Guinier approximation at low  $q$ , hollow sphere form factor and the positions of the local minima (green vertical lines). Contribution from LiPFO unimers is shown by orange line. b) SANS data and hollow spheres with the best-fit values for mole fraction of TDMAO. c) blue: homogeneous spherical shell model; light orange: three-shell model. d) green: three-shell model with inner (i), central (c), and outer (o) shells; dark orange: five-shell model.

## Neutron crystallography combined with QM/MM calculations of bilin reductase PcyA mutants reveal substrate and catalytic residue protonation states

M. Unno<sup>1,2</sup>, T. Joutsuka<sup>1,2</sup>, M. Sugishima<sup>3</sup>, K. Wada<sup>4</sup>, Y. Hagiwara<sup>5</sup>, N. Yano<sup>6</sup>, K. Kusaka<sup>7</sup>, A. Ostermann<sup>8</sup>

<sup>1</sup>Graduate School of Science and Engineering, Ibaraki University, Hitachi, Japan; <sup>2</sup>Frontier Research Center for Applied Atomic Sciences, Ibaraki University, Tokai, Japan; <sup>3</sup>Department of Medical Biochemistry, Kurume University School of Medicine, Kurume, Japan; <sup>4</sup>Department of Medical Sciences, University of Miyazaki, Miyazaki, Japan; <sup>5</sup>Department of Biochemistry and Applied Chemistry, National Institute of Technology, Kurume College, Kurume, Japan; <sup>6</sup>Structural Biology Division, Japan Synchrotron Radiation Research Institute, Sayo-Cho, Japan; <sup>7</sup>Centre for the Promotion of Neutron Industrial Applications, Comprehensive Research Organization for Science and Society, Shirakata, Japan; <sup>8</sup>Heinz Maier-Leibnitz Zentrum (MLZ), Technical University of Munich, Garching, Germany

**P**cyA is an enzyme that biosynthesizes phycocyanobilin used in photosynthesis and photosensing. PcyA mutants in complex with the substrate biliverdin show altered electronic absorption spectra. In this study, the protonation states of two mutants were successfully determined and proved the hypothesis that differences in their spectra reflect differences in the protonation states of the biliverdin.

### Mutants of PcyA and their absorption spectra

Bilin pigments act as photosensors to control leaf coloration, defoliation, and flowering, and act as photosynthetic pigments, playing an important role in the survival of photosynthetic organisms. The enzyme, phycocyanobilin:ferredoxin oxidoreductase (PcyA), catalyzes the production of phycocyanobilin by selectively and sequentially providing two electrons and two protons (H<sup>+</sup>) each to two distant sites (D- and A- rings) of biliverdin (BV). We noticed an unusual feature of the I86D mutant of PcyA. In the absorption spectrum of the complex of the I86D mutant and the substrate BV (I86D-BV), the absorption peak around 730 nm, corresponding to the second absorption peak of the wild-type

PcyA-BV, is greatly increased, while the peak around 660 nm is clearly reduced. Although results from computational chemistry suggest that BV is present in the protonated form as BVH<sup>+</sup>, this hypothesis has not yet been confirmed, even with high-resolution X-ray diffraction at 1.05 Å resolution. We therefore performed a neutron crystal structure determination of I86D-BV at the instrument BIODIFF to visualize the hydrogen atoms. As a control, the neutron crystal structure of the mutant D105N (D105N-BV) whose absorption spectrum shows no peak around 730 nm was determined.

### Protonation states of the BV in the PcyA mutants

The neutron structures of I86D-BV and D105N-BV were obtained at a resolution of 2.0 Å and 2.1 Å respectively [1]. The protonation states of the respective BVs were clearly different: In I86D-BV, all four pyrrole nitrogen atoms of the BV were protonated, whereas in D105N-BV the C-ring nitrogen atom was unprotonated (see Fig. 1). In I86D-BV, the catalytic active Asp105 was of the acidic -COO<sup>-</sup> type, while Asp86 interacting with Asp105 was of the neutral -COOH type. In D105N-BV, the conformation of Asn105 is uniquely fixed by hydrogen bonding of the -NH<sub>2</sub> group to the main chain -C=O of Leu86. Unlike aspartate, asparagine cannot transfer H<sup>+</sup> to or from the BV. The side chain O atom of Asn105 forms a hydrogen bond with the hydrogen atom bound to the B-ring pyrrole nitrogen atom of the BV. In order to check the influence of the protonation state of the BV on the corresponding absorption spectra, spectra were calculated using the QM/MM method based on the neutron structures of wild-type PcyA-BV and the two mutant structures obtained in this work. The calculated absorption spectra of the two mutants and wild-type PcyA-BV showed qualitative consistencies with the experimental results, thereby explaining why the absorption spectrum of the wild-type PcyA-BV has two peaks in the visible region.

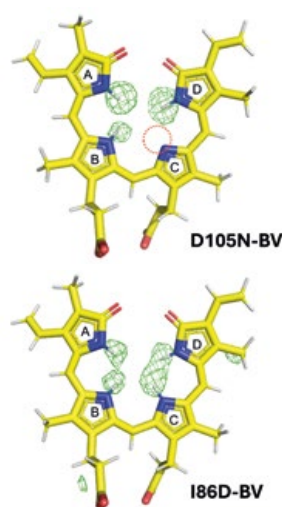


Figure 1: Neutron crystal structures of two mutants of PcyA revealed the protonation states of the substrate biliverdin. Three pyrrole rings of biliverdin were protonated in D105N-BV and four in I86D-BV. The protonation site of the C-ring is marked with a red circle. The green meshes are the  $F_o - F_c$  neutron scattering length density maps at 3.6 $\sigma$  contour level calculated excluding hydrogen (deuterium) atoms bound to N atoms in the pyrrole rings.

[1] T. Joutsuka et al., *Neutron crystallography and quantum chemical analysis of bilin reductase PcyA mutants reveal substrate and catalytic residue protonation states*, *J. Biol. Chem.* 299, 102763 (2023)  
DOI: 10.1016/j.jbc.2022.102763

## Dynamic structure evolution of extensively (de-)lithiated high voltage spinel

N. M. Jobst<sup>1</sup>, N. Paul<sup>2</sup>, P. Beran<sup>3,4</sup>, M. Mancini<sup>1</sup>, R. Gilles<sup>2</sup>, M. Wohlfahrt-Mehrens<sup>1</sup>, P. Axmann<sup>1</sup>

<sup>1</sup>Accumulators Materials Research (ECM), ZSW Centre for Solar Energy and Hydrogen Research, Ulm, Germany; <sup>2</sup>Heinz Maier-Leibnitz Zentrum (MLZ), Technical University of Munich, Garching, Germany; <sup>3</sup>Nuclear Physics Institute CAS, Rez, Czech Republic; <sup>4</sup>European Spallation Source ERIC, Lund, Sweden

High voltage spinel  $\text{Li}_{1+x}\text{Ni}_{0.5}\text{Mn}_{1.5}\text{O}_4$  is a promising cobalt-free cathode for lithium ion battery applications. In fact, additional Li can be introduced into the structure in an extended voltage range to 1.50 V. Although this leads to a significant increase in the specific energy, it also results in rapid capacity fading. Using operando XRD and neutron diffraction (ND), we identify a third 'distorted' phase and predict where lithium ions are located.

### Low voltage behavior of $\text{Li}_x\text{Ni}_{0.5}\text{Mn}_{1.5}\text{O}_4$

The structural evolution of  $\text{Li}_x\text{Ni}_{0.5}\text{Mn}_{1.5}\text{O}_4$  high voltage spinel cathode during battery operation in the range of  $0 < x < 2.5$  was investigated in order to understand what happens in the low voltage region, which shows two distinct deviations from the voltage plateaus expected from a two-phase reaction mechanism: (i) an additional voltage step at (a)  $\sim 2.10$  V during lithiation and (ii) at  $\sim 3.80$  V during delithiation. Another goal was to locate the sites of lithium ions in this cathode for  $x > 2$ .

### Correlation of structure with voltage profile

With operando XRD measurements, we were able to find evidence for the evolution of a second tetragonal phase (T2)  $\text{Li}_{2.5}\text{Ni}_{0.5}\text{Mn}_{1.5}\text{O}_4$  that evolves kinetically favored when the average lithium content is in the range of  $1.6 < x < 2$ . Consequently, the coexistence of three phases (C1, T1, T2) leads to a deviation from the voltage plateau that was

defined by a two-phase reaction mechanism and a voltage step at 2.10 V can be observed in the galvanostatic voltage profile. The evolution of a third phase is supported by the increase in the configurational entropy.

A lithiation beyond  $x = 2$  leads to the formation of an over-lithiated tetragonal phase with constantly increasing  $c/a$  ratio and strong changes in the entropy. Analysis of ND data indicates that the lithium ions are inserted into the tetrahedral 4a sites when all octahedral sites are being occupied.

Evaluation of the weight ratio of the transformation to the cubic phase during delithiation shows a nonlinear evolution of C1. Supported by a strong increase in the configurational entropy it is likely that an additional intermediate phase is present during delithiation, which causes the shoulder at  $\sim 3.80$  V in the voltage profile. The slope of the evolution of the cubic phase indicates a composition of  $\text{Li}_{1.5}\text{Ni}_{0.5}\text{Mn}_{1.5}\text{O}_4$  of the phase C1\*, with additional lithium ions on octahedral 4a sites in the  $\text{P4}_3\text{32}$  crystal system. The necessity for  $\text{Mn}^{3+}$  ions in a C1\* phase with this composition explains the  $\sim 3.80$  V step, which is close to the  $\text{Mn}^{3+}$  contribution observed in nonstoichiometric or disordered nickel manganese spinel.

[1] N. M. Jobst et al., *Dynamic Structure Evolution of Extensively Delithiated High Voltage Spinel  $\text{Li}_{1+x}\text{Ni}_{0.5}\text{Mn}_{1.5}\text{O}_4$ ,  $x < 1.5$* , *J. Am. Chem. Soc.* 145, 8, 4450, (2023)  
DOI: 10.1021/jacs.2c09621

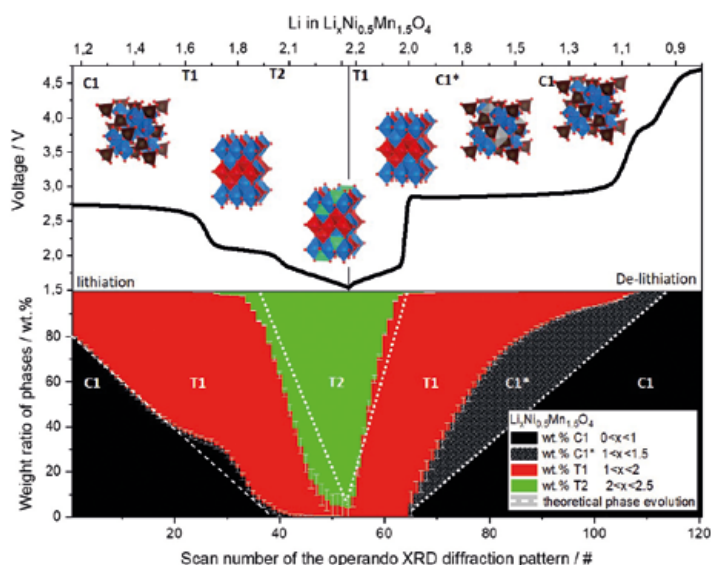


Figure 1: Galvanostatic voltage profile of  $\text{Li}_{1+x}\text{Ni}_{0.5}\text{Mn}_{1.5}\text{O}_4$  during discharge (lithiation) and charge (delithiation) and weight ratio of the different phases C1, T1, T2, and C1\* as obtained by Rietveld refinement of the operando recorded diffraction patterns (Mo  $\text{K}\alpha 1$   $\lambda = 0.709$  Å).

## Mechanism for the combined Li–Na ionic conductivity in sugilite ( $\text{Fe}_2\text{Na}_2\text{K}[\text{Li}_3\text{Si}_{12}\text{O}_{30}]$ )-type compounds

S. Park<sup>1</sup>, C. Paulmann<sup>2</sup>, M. Hoelzel<sup>3</sup>, R. Hochleitner<sup>4</sup>

<sup>1</sup>Department of Geo- and Environmental Sciences, Section of Crystallography, Ludwig-Maximilians-Universität München (LMU), Munich, Germany;

<sup>2</sup>Department of Earth System Sciences, Institute of Mineralogy and Petrography, University of Hamburg, Hamburg, Germany, <sup>3</sup>Heinz Maier-Leibnitz Zentrum (MLZ), Technical University of Munich, Garching, Germany; <sup>4</sup>Mineralogische Staatssammlung München (SNSB), Munich, Germany

In exploring prototype structures for combined Li and Na ionic conductors, this study explains the ionic conductivity in the mineral sugilite ( $\text{Fe}_2\text{Na}_2\text{K}[\text{Li}_3\text{Si}_{12}\text{O}_{30}]$ ) by resolving the charge transport mechanisms of both Li and Na cations over 2-dimensional (2D) pathways using synchrotron X-ray single-crystal and neutron powder diffraction techniques.

### The Search for Sustainable Batteries

Combined Li–Na ionic conductors with a high number of charge carriers are of interest for their potential application as solid electrolytes in all-solid-state batteries. In this respect, among Li–Na-containing milarite-type cyclosilicates exhibiting a high chemical flexibility and a thermal stability, sugilite-type compounds are highly interesting for the highest Li and Na contents and higher ionic conductivity.

### A Smart Combo of Neutron and X-ray Diffraction

To explain the mechanisms of the ionic conductivity, neutron diffraction data were collected on a powder sample of sugilite-type compound  $\text{Fe}_2\text{Na}_2\text{K}[\text{Li}_3\text{Si}_{12}\text{O}_{30}]$  at the neutron powder diffractometer SPODI up to 973 K while X-ray dif-

fraction studies were carried out on a small single crystal at beamline F1 (DESY, Hamburg) up to 1023 K. The data were analyzed to study the evolution of structural parameters, in particular anharmonic thermal displacement parameters as a function of temperature. Diffraction data analysis precisely revealed thermally activated hopping mechanisms for both Li and Na cations over the several interstitial sites commonly present in the (a–b) plane (Fig. a). Bond-valence sum values and isosurface energy landscape maps of Li and Na cations evaluated with the refined structure models at each measured temperature strongly support the 2D charge transport routes of Li (Fig. b) and Na cations (Fig. c) hopping toward the common direction parallel to the (a–b) plane in the sugilite framework (Fig. a). The structural parameters and bulk ionic conductivities obtained are compared to those of other Li and Na ionic conductor cyclosilicates to comprehend subtle structure-property relationships. This crystallographic study is dedicated to designing combined Li–Na-ionic conductors [1]

[1] S. Park et al., *Mechanism for the Combined Li–Na Ionic Conductivity in Sugilite ( $\text{Fe}_2\text{Na}_2\text{K}[\text{Li}_3\text{Si}_{12}\text{O}_{30}]$ )-Type Compounds*, *Minerals* 13, 620 (2023)

DOI: 10.3390/min13050620

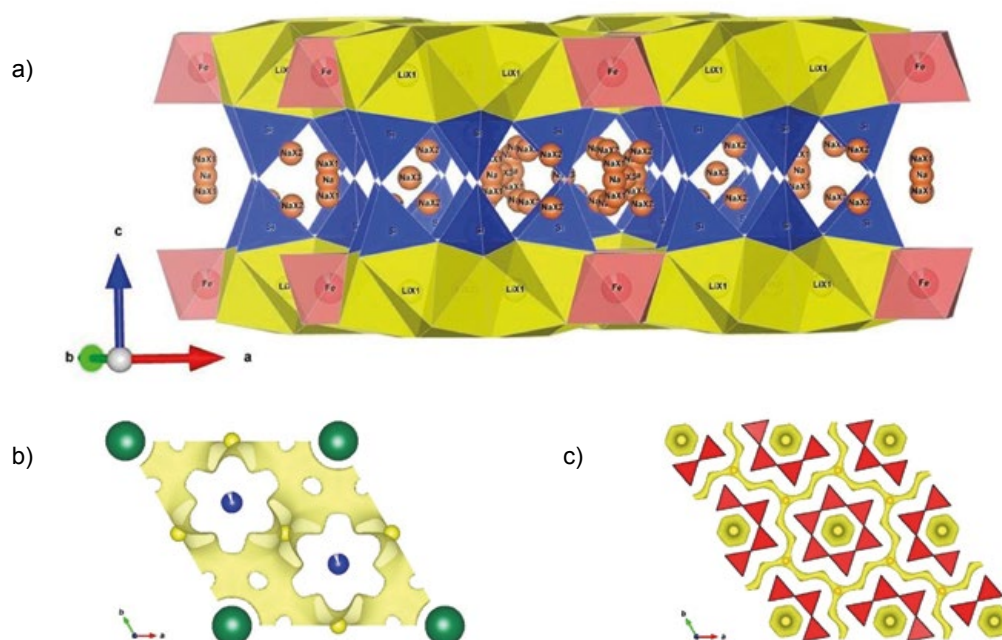


Figure 1: Li (yellow) and Na (orange) interstitial networks in sugilite (a). Isosurface of Li<sup>+</sup> (b) and Na<sup>+</sup> (c) with a potential threshold  $\Delta V = 0.5$  v. u., based on BVS calculations with the structure model refined with 1023 K XSD data of a sugilite single crystal sample ( $\text{KNa}_2(\text{Fe}_{1.7}\text{Mn}_{0.1}\text{Al}_{0.1}\text{Mg}_{0.1})[\text{Li}_3\text{Si}_{12}\text{O}_{30}]$ ). Li and Na are presented by large spheres in pale yellow and small spheres in yellow, respectively. This isosurface BVS landscape maps support the presence of 2D Li- and Na-interstitial networks over which Li<sup>+</sup> and Na<sup>+</sup> can move fast.

G. Das Adhikary<sup>1,2</sup>, P. Punetha<sup>1,2</sup>, R. Prakash Singh<sup>1</sup>, V. Dwij<sup>3</sup>, V. Sathe<sup>3</sup>, A. Senyshyn<sup>4</sup>, P. Nukala<sup>2</sup>, R. Ranjan<sup>1</sup>

<sup>1</sup>Department of Materials Engineering, Indian Institute of Science, Bangalore, India; <sup>2</sup>Center for Nanoscience and Engineering, Indian Institute of Science, Bangalore, India; <sup>3</sup>UGC-DAE Consortium for Scientific Research, University Campus, Indore, India; <sup>4</sup>Heinz Maier-Leibnitz Zentrum (MLZ), Technical University of Munich, Garching, Germany

In contrast to other Pb-free ferroelectrics, the covalency effect associated with the  $6s^2$  lone pair of  $Bi^{+3}$  at the A-site and  $Ti^{+4}$  at the B-site in the tetragonal phase of  $K_{1/2}Bi_{1/2}TiO_3$  (KBT) makes it a unique material possessing a negative and/or near zero thermal expansion (ZTE). The effect was purposefully tuned in a solid solution series  $K_{1/2}Bi_{1/2}TiO_3-Na_{1/2}Bi_{1/2}TiO_3$ . The system shows abrupt vanishing of ZTE above a critical composition  $x=0.58$  due to sudden weakening of the covalency effect caused by the onset of octahedral tilt distortion.

### The Complex Thermal Expansion of Ferroelectrics

A series of  $(1-x)KBT-(x)NBT$  (KBT-NBT) specimens were synthesized using the conventional solid-state reaction method and characterized for their structural behavior. Looking at the evolution of the lattice parameters (Fig. 1a–d), one can identify three characteristic regions with a positive volume thermal expansion (PTE), negative thermal expansion (NTE), and nearly zero thermal expansion (ZTE). Fig. 1e summarizes the thermal expansion behavior of KBT-NBT in the composition-temperature space. Although the abrupt change in the thermal expansion behavior for  $x > 0.58$  suggests a qualitative change in the lattice property, X-ray powder diffraction (XRD) failed to reveal any structural change; the diffraction pattern of  $x=0.58$  (showing NTE and ZTE) is

the same (tetragonal) as that of  $x=0.60$  (exhibiting neither NTE nor ZTE). However, the tetragonality ( $c/a - 1$ ) exhibits an abrupt drop at  $x=0.60$  (Fig. 1f), thus suggesting the onset of a subtle structural order, whose signature cannot be identified by the XRPD technique.

### Surprising Insights from Neutron Powder Diffraction

Contrary to  $x=0.50$  (a composition showing NTE and ZTE behavior), the electron diffraction patterns of  $x=0.60$  (showing no NTE and ZTE behavior) displays  $1/2\{00e\}$  type of superlattice reflections, suggesting in-phase octahedral tilt distortions on the local scale. This was further confirmed by high-resolution neutron powder diffraction (NPD) on SPODI. Detailed structural analysis using these NPD data suggests that the prevalence of the NTE and ZTE behavior for  $x < 0.60$  is associated with a subtle synergy between the covalency effects between the A-site (primarily the  $Bi^{+3}$   $6s^2$  lone pair) and B-site cations, manifested via the difference in the  $Ti-O1$  and  $Ti-O3$  bonds parallel to the  $c$  axis. The abrupt decrease of this parameter above the critical composition,  $x > 0.58$ , confirms sudden weakening of the A site contribution to this synergy due to the onset of octahedral tilt.

[1] G. Das Adhikary et al., Negative and zero thermal expansion in  $K_{0.5}Bi_{0.5}TiO_3$ , *Phys. Rev. B* 108, L140104 (2023)  
DOI: 10.1103/PhysRevB.108.L140104

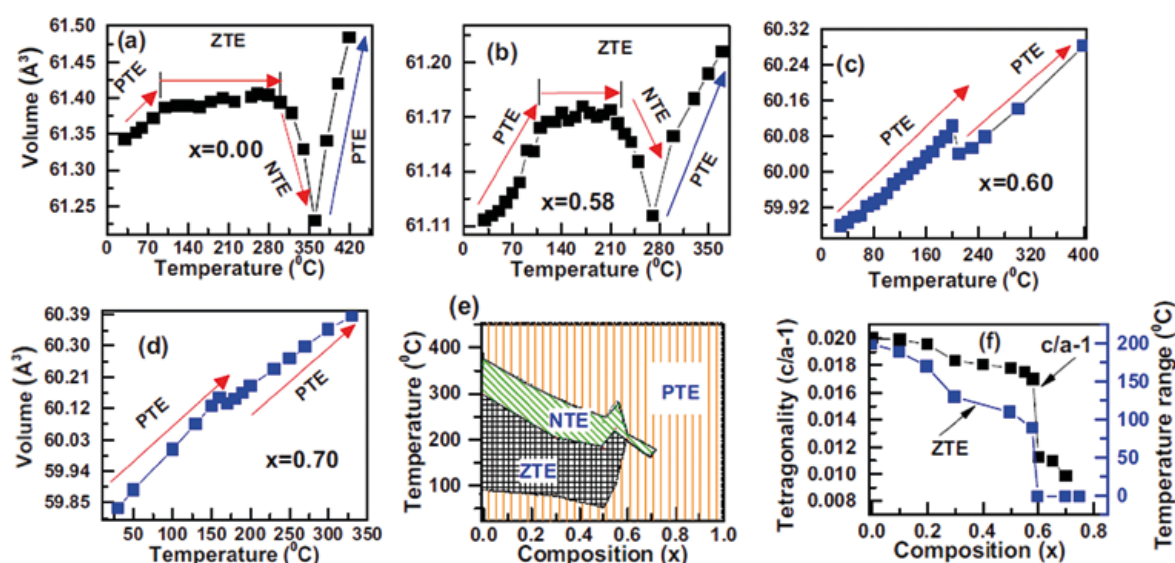


Figure 1: Temperature evolution of unit-cell volume of tetragonal (P4mm) phase in  $(1-x)K_{1/2}Bi_{1/2}TiO_3 - (x)Na_{1/2}Bi_{1/2}TiO_3$  [ $(1-x)KBT - (x)NBT$ ]: (a)  $x = 0.00$ , (b)  $x = 0.58$ , and (c)  $x = 0.60$ ; (d) Composition dependence of temperature range in which ZTE and NTE occur with collapse at  $x = 0.60$ . Phase diagram of (e) KBT-(x)NBT highlighting temperature ranges for ZTE, NTE, and PTE. (f) Tetragonality and ZTE temperature range as a function of KBT-(x)NBT composition  $x$ .

## Combined X-ray and neutron powder diffraction study on *B*-site cation ordering in $\text{La}_2(\text{Al}_{1/2}\text{MgTa}_{1/2})\text{O}_6$

Y. J. Sohn<sup>1</sup>, V. Baran<sup>2,3</sup>, R. Gilles<sup>2</sup>, G. Roth<sup>4</sup>, R. Vaßen<sup>1</sup>

<sup>1</sup>Institute of Energy and Climate Research, Materials Synthesis and Processing (IEK-1), Forschungszentrum Jülich GmbH, Jülich, Germany;

<sup>2</sup>Heinz Maier-Leibnitz Zentrum (MLZ), Technical University of Munich, Garching, Germany; <sup>3</sup>Deutsches Elektronen-Synchrotron (DESY), Hamburg, Germany; <sup>4</sup>Institute of Crystallography, RWTH Aachen University, Aachen, Germany

$\text{La}_2(\text{Al}_{1/2}\text{MgTa}_{1/2})\text{O}_6$  crystallizes in a monoclinic unit cell at room temperature. Owing to little scattering contrast between the neighboring elements Mg and Al of the periodic table, its *B*-site cation ordering could not be resolved by X-ray powder diffraction alone. Applying a combined Rietveld analysis on the X-ray and neutron powder diffraction data simultaneously, a more detailed crystal structure analysis was successfully carried out.

### Lifetime of Perovskites under Heat

Complex rare-earth perovskites with the general formula  $\text{A}(\text{B}'\text{B}'')\text{O}_3$  are among the promising candidates for thermal barrier coating (TBC) materials due to their high melting points as well as their high thermal expansion coefficient values. Great efforts have been made to increase gas turbine engine efficiency, for which a higher inlet temperature is inevitable. In addition, higher operation temperatures lead to a lower  $\text{CO}_2$  production. Recently, a considerably prolonged thermal cycling lifetime was reported with such a complex perovskite  $\text{La}_2(\text{Al}_{1/2}\text{MgTa}_{1/2})\text{O}_6$  (LAMT) as a TBC topcoat.

### The Benefits of Using Neutron Powder Diffraction

So far, the crystal structure of LAMT at room temperature has been reported using only X-ray powder diffraction. Since Mg and Al as neighboring elements of the periodic table bring little scattering contrast in the case of X-ray diffraction, a full description of the exact *B*-site cation ordering was not possible. Hence, a complementary diffraction study was performed on the high-resolution neutron powder diffractometer (NPD) SPODI at MLZ.

### What We Have Learned

After localizing the heavy element Ta unambiguously on the  $2d$ -Wyckoff position through X-rays, two different crystal structure models of the space group symmetry  $P2_1/n$  were refined using both the X-ray and neutron powder diffraction data simultaneously: (1) full occupancy of Mg and (2) half occupancy of Mg on the  $2c$ -Wyckoff position. The NPD data here responded sensitively to the *B*-site cation ordering due to the substantially different coherent scattering lengths of

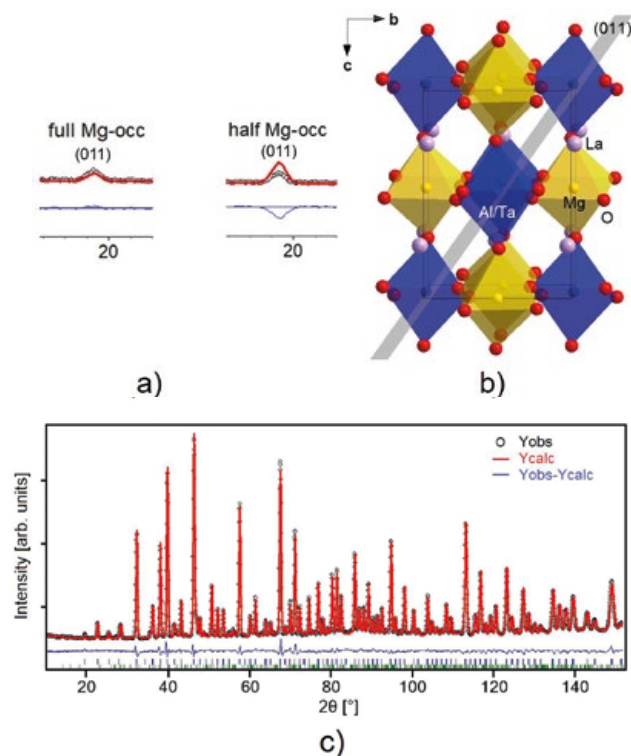


Figure 1: a) Discrepancy of the (110)-Bragg peak intensity on the NPD data between the full and half Mg occupancy. b) (011)-plane in the monoclinic unit cell. Isotropic displacement parameters are visualized at the 50% probability level. c) Rietveld refinement of NPD data. Bragg peak positions are indicated as vertical lines below the difference curve, LAMT in blue,  $\text{La}_3\text{TaO}_7$  in green.

Mg and Al for thermal neutrons. A notable discrepancy between the observed and the calculated Bragg peak intensities was evidenced for each structure model, and a full occupancy of Mg on the  $2c$ -Wyckoff position could also be pinned down (Fig. 1).

In this specific configuration of the heterogeneous *B*-cations, only the strategy of a combined Rietveld analysis using both the X-ray and NPD data simultaneously succeeded in the end, allowing us to achieve a more detailed crystal structure analysis of this complex perovskite system [1].

[1] Y. J. Sohn et al., *Combined X-ray and Neutron Powder Diffraction Study on B-site Cation Ordering in Complex Perovskite  $\text{La}_2(\text{Al}_{1/2}\text{MgTa}_{1/2})\text{O}_6$* , *Solids* 4, 87 (2023)  
DOI: 10.3390/solids4010006

## Orthorhombic symmetry and anisotropic properties of rutile TiO<sub>2</sub>

N. Gonzalez Szwacki<sup>1</sup>, P. Fabrykiewicz<sup>2,3</sup>, I. Sosnowska<sup>1</sup>, F. Fauth<sup>4</sup>, E. Suard<sup>5</sup>, R. Przeniosło<sup>1</sup>

<sup>1</sup>Faculty of Physics, University of Warsaw, Warsaw, Poland; <sup>2</sup>Institute of Crystallography, RWTH Aachen University, Aachen, Germany;

<sup>3</sup>Jülich Centre for Neutron Science (JCNS) at MLZ, Forschungszentrum Jülich GmbH, Garching, Germany; <sup>4</sup>CELLS-ALBA, Cerdanyola del Vallès, Barcelona, Spain; <sup>5</sup>Institut Laue-Langevin, Grenoble, France

**W**e demonstrate by both experimental results and numerical simulations that the actual symmetry of the rutile phase of TiO<sub>2</sub> is orthorhombic with space group *Pn*nm, in contrast to the common belief that rutile TiO<sub>2</sub> has a tetragonal symmetry with space group *P4*<sub>2</sub>/*mnm*. This symmetry lowering has a small but significant influence on the elastic, vibrational, and optical properties of rutile TiO<sub>2</sub>.

### Rutile and its properties

Rutile TiO<sub>2</sub> is a very chemically resistant compound. It is used as a white pigment and photocatalyst. It has interesting electronic and optical properties like birefringence with a high refractive index of about 2.5 to 3.0 in the visible light range, which can be applied in rutile polarizing cubes, prisms, and optical isolators.

### Neutron and synchrotron radiation diffraction

We performed neutron and synchrotron radiation powder diffraction experiments on rutile TiO<sub>2</sub>. After correcting the instrumental resolutions, both diffraction patterns show the same *hkl*-dependent zig-zac pattern of peak widths versus *Q* vectors. Peaks with *h* = *k* are narrower than those with *h* ≠ *k*. Our Rietveld refinements showed that the actual symmetry of the rutile phase of TiO<sub>2</sub> is orthorhombic, described with space group *Pn*nm, a subgroup of the tetragonal space group *P4*<sub>2</sub>/*mnm*, which is commonly assumed for rutile TiO<sub>2</sub>.

### First-principles calculations

Our first-principles calculations confirmed the symmetry lowering of rutile TiO<sub>2</sub>. We have tested several exchange-correlation functionals and the best agreement with the experimental data was obtained using a meta-GGA functional. We determined that the total energy profile of rutile-

type TiO<sub>2</sub> has two minima, corresponding to the *P4*<sub>2</sub>/*mnm* and *Pn*nm symmetries, but with the lower minimum in energy for *Pn*nm-TiO<sub>2</sub>, making it, therefore, the global minimum.

The lowering of the symmetry affects the elastic, vibrational, and optical properties of rutile TiO<sub>2</sub>. Our calculations show that the elastic and optical responses differ along each orthorhombic axis. For the refractive indices, the relative relationship is *n*<sub>c</sub> > *n*<sub>a</sub> > *n*<sub>b</sub> although the difference between *n*<sub>a</sub> and *n*<sub>b</sub> is rather modest. The A<sub>2g</sub> mode, which is neither Raman-active nor infrared-active in the *P4*<sub>2</sub>/*mnm* symmetry, becomes Raman-active in the *Pn*nm symmetry; therefore, this mode may serve as the fingerprint of the rutile TiO<sub>2</sub> symmetry lowering.

[1] N. Gonzalez Szwacki et al., *Orthorhombic Symmetry and Anisotropic Properties of Rutile TiO<sub>2</sub>*, *J. Phys. Chem. C* 127, 19240 (2023)

DOI: 10.1021/acs.jpcc.3c04573

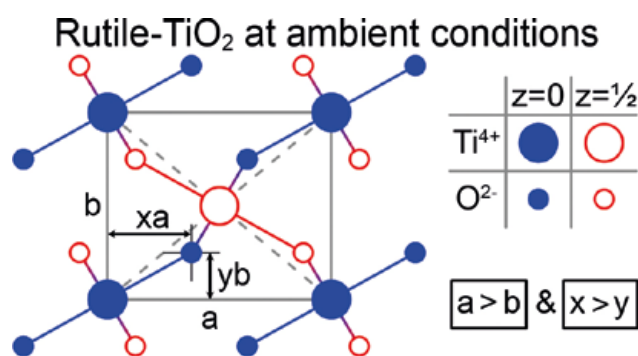


Figure 1: The orthorhombic rutile crystal structure. Big and small circles represent Ti<sup>4+</sup> and O<sup>2-</sup> ions, respectively. Full and empty circles represent the positions of ions at sites located at the *z* = 0 and *z* = 1/2 planes, respectively. Please note the correlation between the elongation of the lattice parameter and the shift of the oxygen positions (with respect to the tetragonal model).

## Spin reorientation in hcp-cobalt

P. Kozłowski<sup>1</sup>, P. Fabrykiewicz<sup>2,3</sup>, I. Sosnowska<sup>1</sup>, F. Fauth<sup>4</sup>, A. Senyshyn<sup>5</sup>,  
E. Suard<sup>6</sup>, D. Oleszak<sup>7</sup>, R. Przeniosło<sup>1</sup>

<sup>1</sup>Faculty of Physics, University of Warsaw, Warsaw, Poland; <sup>2</sup>Institute of Crystallography, RWTH Aachen University, Aachen, Germany; <sup>3</sup>Jülich Centre for Neutron Science (JCNS) at MLZ, Forschungszentrum Jülich GmbH, Garching, Germany; <sup>4</sup>CELLS-ALBA, Cerdanyola del Vallés, Barcelona, Spain; <sup>5</sup>Heinz Maier-Leibnitz Zentrum (MLZ), Technical University of Munich, Garching, Germany; <sup>6</sup>Institut Laue-Langevin, Grenoble, France; <sup>7</sup>Faculty of Materials Science and Engineering, Warsaw University of Technology, Warsaw, Poland

The crystal structure of the hexagonal close packed phase of bulk cobalt (hcp-Co) was investigated using neutron diffraction (SPODI@MLZ, D2B@ILL) and synchrotron radiation diffraction (BL04-MSPD@CELLS-ALBA). As a result, the crystal structure and the magnetic ordering model are described with the monoclinic magnetic space group  $C2'/m'$ , i. e. in lower symmetry than the hexagonal  $P6_3/mmc$  space group commonly assumed for hcp-Co.

The gradual ferromagnetic spin reorientation transition (SR) in hcp-Co between 230°C and 330°C was reported for a Co single crystal with hexagonal structure by Bertaut in the 1960-ies. SR transitions are allowed in monoclinic symmetry but in general not in hexagonal symmetry. This motivated us to perform neutron powder diffraction and synchrotron radiation powder diffraction experiments on hcp-Co samples.

### Monoclinic symmetry of hcp-Co

The analysis of diffraction data confirms the monoclinic  $C2/m$  crystal structure of hcp-Co, i. e. a lower symmetry than the hexagonal  $P6_3/mmc$  space group commonly assumed for hcp-Co. In this monoclinic crystal structure (see Fig. 1), the former hexagonal [001] and [010] axes form an angle equal to  $\alpha \approx 90.10(1)^\circ$ , while the angle between the in-plane axes [100] and [010] equals to  $\gamma \approx 120.11(1)^\circ$ . We confirmed the presence of SR in hcp-Co, but our studies also show that in powder SR occurs in two times broader ranges of temperatures (from  $\sim 100^\circ\text{C}$  to  $\sim 300^\circ\text{C}$ ) than in single crystals.

### Lattice mismatch and anisotropic strains

A lattice mismatch of about 0.5% between the hexagonal layers in hcp-Co and face centered cubic cobalt (fcc-Co) is well known. But, to the best of our knowledge, we report here for the first time a one order of magnitude smaller lattice mismatch in the hexagonal planes between hcp-Co and fcc-Co than the mismatch between layers. Our William-

son-Hall analysis shows that microstrains are larger inside hexagonal planes than along the stacking faults direction. Moreover, a higher content of the fcc-Co phase reduces microstrains in hcp-Co.

Up to now, most cobalt structure studies have focused on a proper description of the stacking faults. Our results shed new light on the hcp-Co structure, highlighting a monoclinic distortion of nominally hexagonal planes which are stacked one on another with small in plane shifts due to the monoclinic symmetry. Also, our study shows that in-plane microstrains are significant and that the structure of the nearest and next nearest Co neighbours is different in monoclinic symmetry from that in the hexagonal one. Thus, stacking faults models of hcp-Co should be revised.

[1] P. Kozłowski et al., *Monoclinic symmetry of the hcp-type ordered areas in bulk cobalt*, *Phys Rev. B* 107, 104104 (2023)  
DOI: 10.1103/PhysRevB.107.104104

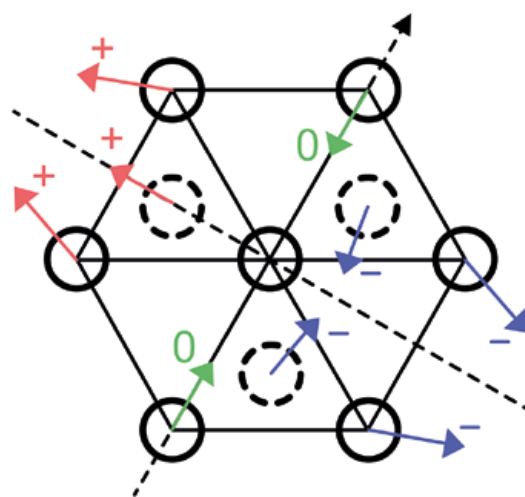


Figure 1: Arrangement of the Co atoms (circles). The layer of dashed atoms is above the layer of solid atoms. The arrows indicate the small shifts of the Co positions by passing from the hexagonal to the monoclinic lattice. The symbols '+', '0' and '-' next to the distortion vectors show if the vector points below or above the layer. Magnetic moments are perpendicular to the unique monoclinic axis represented by the dotted arrow.

Incommensurate antiferromagnetic order in  $\text{CePtAl}_3$ 

M. Stekiel<sup>1,2</sup>, P. Čermák<sup>1,3</sup>, C. Franz<sup>1,4</sup>, W. Simeth<sup>5</sup>, S. Weber<sup>2</sup>, E. Ressouche<sup>6</sup>, W. Schmidt<sup>7</sup>,  
K. Nemkovski<sup>1,8</sup>, H. Deng<sup>1,9</sup>, A. Bauer<sup>2,10</sup>, C. Pfleiderer<sup>2,10,11</sup>, A. Schneidewind<sup>1</sup>

<sup>1</sup>Jülich Centre for Neutron Science (JCNS) at MLZ, Forschungszentrum Jülich GmbH, Garching, Germany; <sup>2</sup>Physics Department, Technical University of Munich, Garching, Germany; <sup>3</sup>Charles University, Faculty of Mathematics and Physics, Department of Condensed Matter Physics, Prague, Czech Republic; <sup>4</sup>Heinz Maier-Leibnitz Zentrum (MLZ), Technical University of Munich, Garching, Germany; <sup>5</sup>Paul Scherrer Institut, Villigen, Switzerland; <sup>6</sup>University Grenoble Alpes, French Alternative Energies and Atomic Energy Commission (CEA), Interdisciplinary Research Institute of Grenoble (IRIG), Modeling and Exploration of Materials (MEM), Magnetism and Neutron Diffraction (MDN), Grenoble, France; <sup>7</sup>JCNS at Institut Laue-Langevin (ILL), Forschungszentrum Jülich GmbH, Grenoble, France; <sup>8</sup>ISIS Neutron and Muon Source, Science and Technology Facilities Council (STFC) Rutherford Appleton Laboratory, Oxon, United Kingdom; <sup>9</sup>Institute of Crystallography, RWTH Aachen at MLZ, Garching, Germany; <sup>10</sup>Center for Quantum Engineering (ZQE), Technical University Munich, Garching, Germany; <sup>11</sup>Munich Center for Quantum Science and Technology (MCQST), Technical University Munich, Garching, Germany

**M**odern day electronics: spintronics, magnonics, polaronics, identified complex types of magnetic ordering as prospective platforms for spin manipulation and transport, making new types of devices possible and allowing for technological advancement. In light of these technological prospects, we are searching for materials hosting non-collinear, modulated, or topological types of long-range magnetic order, and investigate their evolution under applied field.

### Components for the complex magnetic order

We considered  $\text{CePtAl}_3$ , a member of the rare-earth intermetallics family, as a potential platform to host exotic magnetic order. In these systems the long-range magnetic order arises from indirect exchange interactions between localized  $4f$ -electrons mediated by the  $d$ -electrons from the conduction band. This gives rise to interactions of oscillating ferro- and antiferromagnetic character with increasing distance between magnetic ions. In addition, the  $4f$ -electrons reside in a strongly anisotropic environment caused by the crystal-electric field. The combination of these effects gives rise to modulated types of magnetic order, as evidenced by related  $\text{CeTAl}_3$  compounds.

### Characterization of magnetic order in $\text{CePtAl}_3$

We found an incommensurate magnetic modulation vector  $k=(0.676\ 0\ 0)$  from measurements at DNS. We measured the intensities of magnetic reflections at POLI and PANDA. The data suggest a non-collinear type of magnetic order; however, measurements at zero field were not able to differentiate between a multi- $k$ , twinned, and a single- $k$  magnetic structure. We conducted final measurements at the D23 diffractometer at the Institute Laue Langevin. Two magnetic reflections shown in Fig. 1 behave differently under applied field and prove that  $\text{CePtAl}_3$  exhibits a single- $k$  multi-domain state. We can follow the population of two domains by rescaling the reflections' intensities, as shown in Fig. 1c. There, around 2.5 T, an unexpected repopulation of magnetic domains takes place. As we collected large datasets and selected fields, we were able to perform magnetic struc-

ture refinement and identify the arrangement of magnetic moments. We found that, below 2.5 T,  $\text{CePtAl}_3$  hosts a cycloidal arrangement of magnetic moments. At 2.5 T there is a magnetic transition which seems to confine the moments to a collinear structure oriented along the applied field.

Further details on the magnetic structure and its potential connection to the structural disorder of  $\text{CePtAl}_3$  characterized in our study are available in our publication.

[1] M. Stekiel et al., *Incommensurate antiferromagnetic order in  $\text{CePtAl}_3$* , *Phys. Rev. Research* 5, 013058 (2023)  
DOI: 10.1103/PhysRevResearch.5.013058

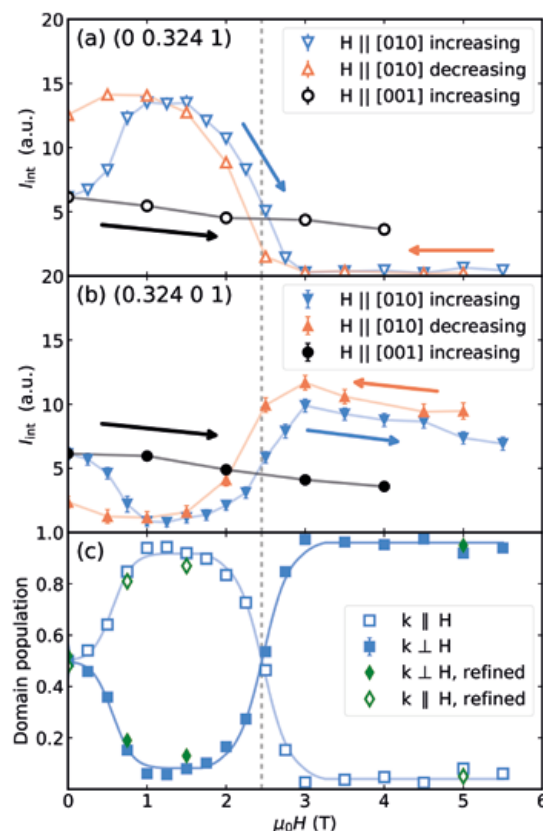


Figure 1: Signatures of the magnetic order in  $\text{CePtAl}_3$ . Intensities of the (a)  $(0\ 0.324\ 1)$  and (b)  $(0.324\ 0\ 1)$  reflections measured with the field applied along the  $[010]$  direction (triangles) and the  $[001]$  direction (squares) with increasing field (black and blue) and decreasing field (orange). (c) Evolution of magnetic domain populations under field. Green diamonds show results population from the structural refinement.

## Near-surface SANS: Probing nanoscale magnetic correlations in reduced sample dimensions

Grace L. Causer<sup>1</sup>, A. Chacon<sup>1</sup>, A. Heinemann<sup>2</sup>, C. Pfeleiderer<sup>1,3,4</sup>

<sup>1</sup>Physics Department, Technical University of Munich, Garching, Germany; <sup>2</sup>Heinz Maier-Leibnitz Zentrum (MLZ), Technical University of Munich, Garching, Germany; <sup>3</sup>Centre for Quantum Engineering (ZQE), Technical University of Munich, Garching, Germany; <sup>4</sup>Munich Center for Quantum Science and Technology (MCQST), Technical University of Munich, Garching, Germany

**A** new methodology to measure long-wavelength magnetic correlations in materials of reduced sample dimensions was recently developed on SANS-1 at the MLZ. The near-surface SANS method capitalizes on negligible refraction effects at shallow angles of incidence just above a material's critical angle of reflection in order to improve the signal-to-noise of scattering from thin films or microstructured bulk samples as compared to conventional transmission SANS.

### SANS and thin films

Magnetic small-angle neutron scattering (SANS) is ideally suited to providing direct reciprocal-space information on nanoscale magnetic modulations, such as helicoids, solitons, merons or skyrmions. However, SANS of such structures in thin films or microstructured bulk samples is greatly limited by the tiny scattering volume and the prohibitively high background scattering of the substrate and support structures. This has intensified interest in how to optimize the SANS signal-to-background ratio for materials of reduced sample dimension.

### The near-surface SANS method

A rather elegant configuration that meets this requirement may be achieved in grazing-incidence SANS (GI-SANS), where the neutrons form an evanescent wave in the top-most layer of the sample. However, this calls for GI-SANS to be a purely surface sensitive method. Furthermore,

the GI-SANS scattering condition depends sensitively on material-specific details that cannot be met in many systems of interest. It is nonetheless possible to improve the signal-to-background ratio considerably close to, but slightly above, the critical angle of reflection. This near-surface SANS (NS-SANS) geometry allows one to probe the full volume of the sample while minimizing scattering contributions from the substrate, and results in scattering patterns that are essentially identical to those of a transmission measurement, facilitating easy and unambiguous data analysis.

### Method's proof-of-principle

To prove the principle of the method, NS-SANS was performed on thinned bulk MnSi which has a well-documented phase diagram consisting of nanoscale helical, conical and skyrmion lattice phases. Measurements were performed at an incidence angle of  $\alpha_i = 0.3^\circ$  slightly above the critical angle of MnSi ( $\alpha_c = 0.076^\circ$ ) at a neutron wavelength of 5.5 Å in the NS-SANS regime. This experiment demonstrated that scattering patterns obtained in the NS-SANS geometry are essentially identical to those obtained in transmission, albeit with the addition of specular scattering, as shown in Fig. 1 in the helical phase of MnSi.

[1] G. L. Causer et al., *Small-angle neutron scattering of long-wavelength magnetic modulations in reduced sample dimensions*, *J. Appl. Cryst.* 56, 26 (2023)

DOI: 10.1107/S1600576722010755

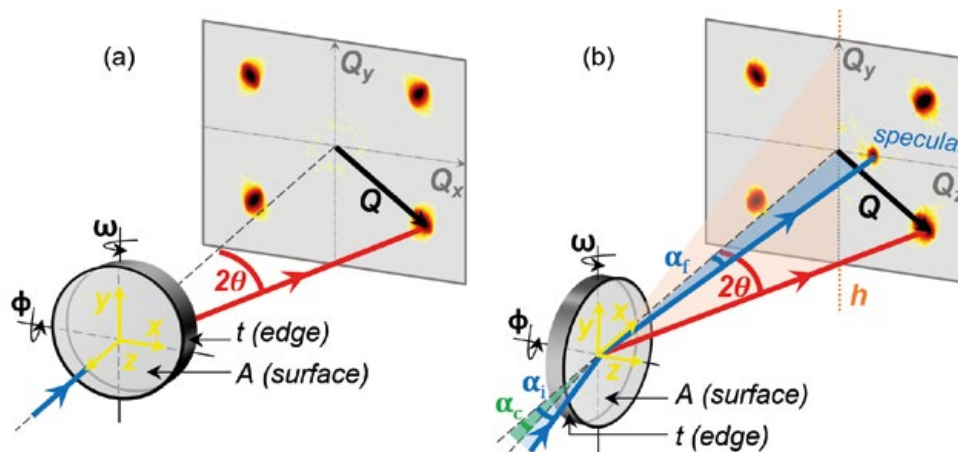


Figure 1: Comparison of (a) transmission and (b) NS-SANS geometries measured in the helical phase of MnSi. In the NS-SANS geometry, the neutron beam is directed at a shallow incidence angle ( $\alpha_i$ ) with respect to the sample surface, above the material-specific critical angle of reflection ( $\alpha_c$ ). The resulting scattering pattern is identical to the transmission measurement, albeit with the addition of specular scattering.

## Temperature-driven transition into vortex clusters in low-kappa intertype superconductors

A. Backs<sup>1,2</sup>, A. Al-Falou<sup>3,4</sup>, A. Vagov<sup>5</sup>, P. Böni<sup>4</sup>, S. Mühlbauer<sup>3</sup>

<sup>1</sup>Department of Mechanical Engineering Sciences, Lund University, Lund, Sweden; <sup>2</sup>European Spallation Source ERIC, Lund, Sweden;

<sup>3</sup>Heinz Maier-Leibnitz Zentrum (MLZ), Technical University of Munich, Garching, Germany; <sup>4</sup>Physics Department E21, Technical University of Munich, Garching, Germany; <sup>5</sup>Institute of Theoretical Physics III, University of Bayreuth, Bayreuth, Germany

**C**lose to the type-I/type-II crossover in conventional superconductors, vortices show a non-monotonic interaction. We perform molecular dynamics simulations of vortex matter in the intertype regime in a field cooled approach, where we find the transition of a homogeneous vortex lattice into a domain structure. The results show extraordinary stability of the transition against vortex pinning and a strong dependence on the external magnetic field.

### The intermediate mixed state

Conventionally, vortex interactions are either attractive or repulsive, which corresponds to type-I and type-II superconductivity. However, a non-monotonic interaction is possible close to the type-I/type-II crossover, which is labeled as intertype superconductivity. One of the vortex matter states found there is the intermediate mixed state (IMS), which exhibits a domain structure of vortex lattice (VL) and flux free Meissner state.

### Simulating the IMS

Experimentally, it is challenging to obtain microscopic bulk information about the IMS. Therefore, we used 2D molecular dynamics simulations to study the transition into the IMS on a field cooling path. The simulations are based on a temperature dependent, non-monotonic vortex interaction derived in the extended Ginzburg-Landau formalism. This interaction defines a temperature dependent optimal

separation of neighboring vortices. A transition into the IMS is possible below the temperature  $T_{\text{IMS}}$ , where the optimal separation drops below the VL lattice parameter  $a_{\text{VL}}$  defined by an external magnetic field. For modeling samples of varying quality, we have included vortex pinning in the form of individual randomly distributed pinning centers, defined by the density  $\rho_p$  of pinning sites and the strength  $v_p$  of their interaction.

### Vortex pinning in the IMS

A systematic study of  $\rho_p$  and  $v_p$  showed four distinct regions. No effect of pinning is observed for small  $\rho_p$  and  $v_p$ . The initial (stable) vortex lattice breaks apart into a domain structure with large domains (5–10  $\mu\text{m}$ ) below  $T_{\text{IMS}}$ . With decreasing temperature,  $a_{\text{VL}}$  decreases, as described by the vortex interaction, while the domain morphology does not change notably. Increasing  $v_p$  leads to individual pinning of single vortices, while increasing  $\rho_p$  leads to collective pinning of the VL. Both cases result in smaller domains with increasing pinning parameters. For too large  $\rho_p$  and  $v_p$ , the VL become disordered above  $T_{\text{IMS}}$ . Furthermore, we have found differences in the field dependence of the transition temperature, structure size and morphology for the different pinned cases.

[1] A. Backs et al., *Temperature-driven transition into vortex clusters in low-kappa intertype superconductors*, *Phys. Rev. B* **107**, 174527 (2023)

DOI: 10.1103/PhysRevB.107.174527

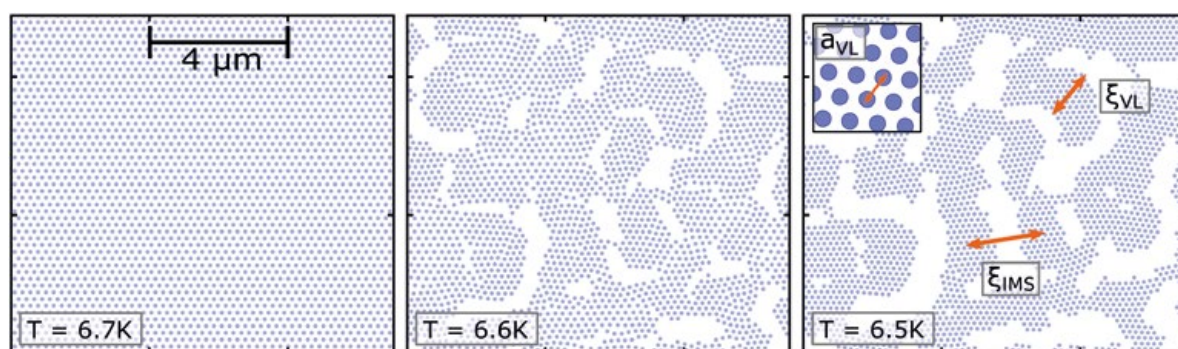


Figure 1: Exemplary simulation results of the IMS transition without pinning. Each dot represents a vortex, which is initially arranged in a hexagonal lattice. The third panel indicates the VL lattice parameter  $a_{\text{VL}}$ , and two length scales characteristic of the domain morphology.

## Magnetic structure of the magnetoelectric material $\text{Ba}_2\text{MnGe}_2\text{O}_7$

A. Sazonov<sup>1</sup>, H. Thoma<sup>2</sup>, R. Dutta<sup>2</sup>, M. Meven<sup>2</sup>, A. Gukasov<sup>3</sup>, R. Fittipaldi<sup>4</sup>, V. Granata<sup>5</sup>, T. Masuda<sup>6</sup>, B. Náfrádi<sup>7</sup>, V. Hutanu<sup>2</sup>

<sup>1</sup>European Spallation Source ERIC, Lund, Sweden; <sup>2</sup>Institute of Crystallography, RWTH Aachen University and Jülich Centre for Neutron Science (JCNS) at Heinz Maier-Leibnitz Zentrum (MLZ), Garching, Germany; <sup>3</sup>Laboratoire Léon Brillouin, CEA-CNRS, CE-Saclay, Gif-sur-Yvette, France; <sup>4</sup>CNR-SPIN c/o University of Salerno, Fisciano, Italy; <sup>5</sup>Department of Physics “E. R. Caianiello”, University of Salerno, Fisciano, Italy; <sup>6</sup>Institute for Solid State Physics, The University of Tokyo, Chiba, Japan; <sup>7</sup>École Polytechnique Fédérale de Lausanne, Laboratory of Nanostructures and Novel Electronic Materials, Lausanne, Switzerland

A detailed study of  $\text{Ba}_2\text{MnGe}_2\text{O}_7$  was performed in its low-temperature magnetoelectric state, combining neutron diffraction with magnetization measurements on single crystals. Crystal and magnetic structures were determined using unpolarized neutron diffraction and magnetic symmetry analysis. Polarized neutron diffraction was used to probe the magnetic anisotropy. Distinct differences to other melilite-type multiferroics were found.

Members of the melilite family have been found to exhibit static and dynamic magnetoelectric effects, host remarkable optical properties, and adopt a wide variety of low-temperature magnetic structures. We performed a detailed study of  $\text{Ba}_2\text{MnGe}_2\text{O}_7$ , which has a number of important differences from other melilite-type multiferroics.

### Antiferromagnetic order

In the antiferromagnetic state, at 2.5 K, the magnetic structure of  $\text{Ba}_2\text{MnGe}_2\text{O}_7$  was accurately refined based on the magnetic symmetry analysis and single-crystal neutron diffraction data from HEIDI at MLZ. The results indicate the orthorhombic symmetry of the magnetic structure with either  $C_2mc2_1$  or  $P_212_12_1$  magnetic space group (Fig. 1a), which is impossible to distinguish with unpolarized neutron diffraction because of the equally populated 90°-type magnetic

domains (Fig. 1b). In both models, the spin pattern shows a square-lattice in-plane antiferromagnetic order. At zero magnetic field the magnitude of the averaged ordered magnetic moment of  $\text{Mn}^{2+}$  ions is found to be about  $3.24 \mu_B$ . Small canting (minor antiferromagnetic component) in the  $ab$  plane perpendicular to the primary antiferromagnetic moment is allowed by symmetry and found to be relatively small.

### Local susceptibility

In the paramagnetic phase of  $\text{Ba}_2\text{MnGe}_2\text{O}_7$ , at 10 K, the field-induced magnetization was precisely refined from polarized neutron diffraction measurements on VIP at LLB. The results indicate no clear anisotropy in the local susceptibility tensor, which is in agreement with the expectation from electron spin resonance and our magnetization measurements.

The detailed parameters for the nuclear and magnetic orders and the reported magnetic phase diagram of  $\text{Ba}_2\text{MnGe}_2\text{O}_7$  can serve as an important experimental basis for developing microscopic models describing the multiferroic nature and peculiar magnetoelectric phenomena in melilites.

[1] A. Sazonov et al., *Magnetic structure of the magnetoelectric material  $\text{Ba}_2\text{MnGe}_2\text{O}_7$* , *Phys. Rev. B* 108, 094412 (2023)  
DOI: 10.1103/PhysRevB.108.094412

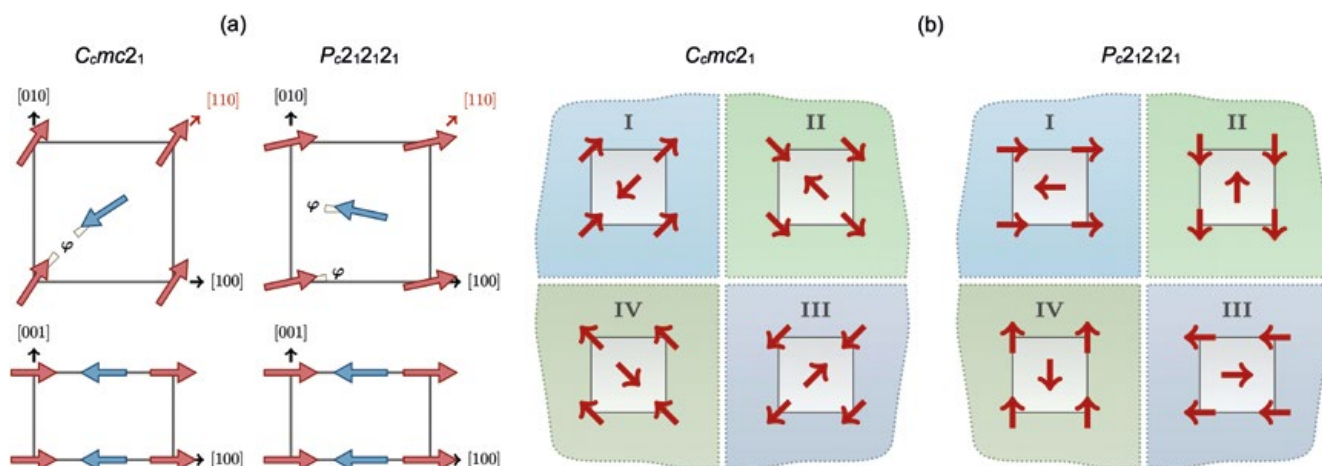


Figure 1: (a) Possible in-plane magnetic structures of  $\text{Ba}_2\text{MnGe}_2\text{O}_7$  in the  $C_2mc2_1$  and  $P_212_12_1$  models, according to our neutron diffraction data at 2.5 K. Angle  $\phi$  denotes in-plane canting of magnetic moments allowed by symmetry. (b) Schematic view of the possible magnetic domains in  $\text{Ba}_2\text{MnGe}_2\text{O}_7$  for both  $C_2mc2_1$  and  $P_212_12_1$  models. A single layer along the  $[001]$  direction is shown for simplicity.

# Magnetic structure of the two-dimensional XY antiferromagnet $\text{Sr}_2\text{CoSi}_2\text{O}_7$ studied using single-crystal neutron diffraction

R. Dutta<sup>1,2</sup>, H. Thoma<sup>1,2</sup>, A. Sazonov<sup>3</sup>, B. Náfrádi<sup>4</sup>, M. Meven<sup>1,2</sup>, A. Gukasov<sup>5</sup>, V. Kocsis<sup>6,7</sup>, U. Zeitler<sup>8</sup>, A. Puri<sup>8,9</sup>, Y. Tokunaga<sup>6,10</sup>, Y. Taguchi<sup>6</sup>, Y. Tokura<sup>6,11,12</sup>, S. Bordács<sup>13</sup>, I. Kézsmárki<sup>14</sup>, V. Hutanu<sup>1,2</sup>

<sup>1</sup>Institute of Crystallography, RWTH Aachen at MLZ, Garching, Germany; <sup>2</sup>Jülich Centre for Neutron Science (JCNS) at MLZ, Garching, Germany; <sup>3</sup>European Spallation Source ERIC, Lund, Sweden; <sup>4</sup>EPFL, Laboratory of Nanostructures and Novel Electronic Materials, Lausanne, Switzerland; <sup>5</sup>Laboratoire Léon Brillouin, CEA-CNRS, CE-Saclay, Gif-sur-Yvette, France; <sup>6</sup>RIKEN Center for Emergent Matter Science (CEMS), Wako, Saitama, Japan; <sup>7</sup>Leibniz Institute for Solid State and Materials Research IFW Dresden, Dresden, Germany; <sup>8</sup>High Field Magnet Laboratory (HFML-EMFL), Radboud University, Nijmegen, The Netherlands; <sup>9</sup>CNR-IOM-OGG c/o ESRF-The European Synchrotron, Grenoble, France; <sup>10</sup>Department of Advanced Materials Science, University of Tokyo, Kashiwa, Japan; <sup>11</sup>Quantum-Phase Electronics Center, Department of Applied Physics, University of Tokyo, Tokyo, Japan; <sup>12</sup>Department of Applied Physics, University of Tokyo, Hongo, Tokyo, Japan; <sup>13</sup>Department of Physics, Institute of Physics, Budapest University of Technology and Economics, Budapest, Hungary; <sup>14</sup>Department of Experimental Physics V, University of Augsburg, Augsburg, Germany

**M**elilite-type multiferroic  $A_2MB_2O_7$  ( $A = \text{Ca}, \text{Sr}, \text{Ba}$ ;  $M = \text{Co}, \text{Mn}, \text{Cu}, \text{Fe}$ ; and  $B = \text{Ge}, \text{Si}$ ) compounds are interesting potential candidates for studying exotic low-dimensional quantum phenomena including magnetic, electronic and structural correlations along with the magnetoelectric effect. In the last few decades, the true symmetry of the nuclear and magnetic structure of multiferroic germanates has been studied via single crystal neutron and synchrotron X-ray diffraction. Compared to germanates, silicate family members  $(\text{Ba}, \text{Sr}, \text{Ca})_2\text{CoSi}_2\text{O}_7$  have not been well explored except for a few of them which show quite complex magnetic structure completely different from germanates. For example,  $\text{Ba}_2\text{CoSi}_2\text{O}_7$  shows a quasiohedral monoclinic  $C2/c$  structure with magnetic wave vector  $(1/2, 1/2, 1/2)$  and  $\text{Ca}_2\text{CoSi}_2\text{O}_7$  was described within orthorhombic  $P2_1'2_1'2_1'$  with magnetic wave vector  $(1/3, 1/3, 1)$ , but there has been no report on the refined magnetic structure of  $\text{Sr}_2\text{CoSi}_2\text{O}_7$  below  $T_N \sim 6.5$  K.

## Experimental structure determination

Here, we have taken a significant step towards the understanding of the magnetic structure using single crystal neutron diffraction at 2.3 K on the hot-neutron four-circle diffractometer (HEiDi) at the FRM II reactor, Heinz Maier-Leibnitz Zentrum (MLZ), Germany. Additionally, we have carried out spin polarized flipping ratio (FR) measurements using polarized neutron diffraction on the Very Intense Polarized (VIP) diffractometer at the Orphée reactor at the Laboratoire Léon Brillouin (LLB) in Saclay, France to understand the magnetic spin anisotropy in the paramagnetic phase. Fig. 1: (a–c) shows nuclear and magnetic structural refinement carried out below and above the  $T_N$ , respectively. In zero magnetic field, an equal population of all four domains is expected for both magnetic space group  $Cm'm2'$  and  $P2_1'2_1'2_1'$ , making them indistinguishable from a refinement point of view. Fig. 1: (d, e) displays the refined asymmetry values for both data sets with magnetic field along the [551] and [115]

directions and overall fit qualities. The magnetic moment obtained along the [551] and [115] directions is  $0.61(2)$  and  $0.39(8) \mu_B/\text{Co}$ , respectively. Nevertheless, our bulk magnetization (not shown here) and FR measurements reflect the magnetic anisotropic character nicely, between the  $ab$  plane and  $c$  axis of the crystal [1]. This could in principle reflect the similar value of magnetic single-ion anisotropy in both compounds  $\text{Sr}_2\text{CoSi}_2\text{O}_7$  and  $\text{Ba}_2\text{CoGe}_2\text{O}_7$ .

## Conclusion

In summary, we have presented a detailed unpolarized neutron diffraction study on the magnetic structure of a  $\text{Sr}_2\text{CoSi}_2\text{O}_7$  single crystal at 2.3 and 15 K combined with polarized neutron diffraction FR measurements in its paramagnetic phase and bulk magnetization measurements [1]. Surprisingly,  $\text{Sr}_2\text{CoSi}_2\text{O}_7$  does not align with its sister compounds like  $\text{Ba}_2\text{CoSi}_2\text{O}_7$  and  $\text{Ca}_2\text{CoSi}_2\text{O}_7$ ; Rather, the magnetic structure and the refined structural parameters of  $\text{Sr}_2\text{CoSi}_2\text{O}_7$  are very close to the values found in  $\text{Ba}_2\text{CoGe}_2\text{O}_7$ .

[1] R. Dutta et al., *Magnetic structure of the two-dimensional XY antiferromagnet  $\text{Sr}_2\text{CoSi}_2\text{O}_7$  studied using single-crystal neutron diffraction*, *Phys. Rev. B* **107**, 014420 (2023)

DOI: 10.1103/PhysRevB.107.014420

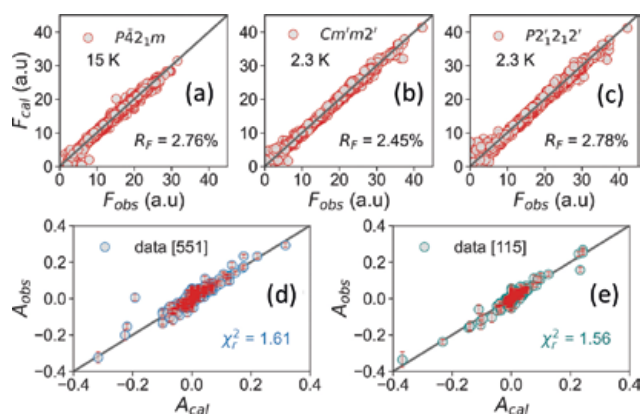


Figure 1: (a–c) Observed and calculated structure factors. (d, e) Calculated and observed asymmetry ( $A$ ) is plotted for data measured with field applied along [551] and along [115].

## Gamma In Addition to Neutron Tomography (GIANT) at the NECTAR instrument

R. Kumar<sup>1</sup>, L. Sommer<sup>2</sup>, A. S. Tremsin<sup>3</sup>, A. S. Losko<sup>2</sup>

<sup>1</sup>German Engineering Materials Science Centre (GEMS) at MLZ, Helmholtz-Zentrum hereon GmbH, Garching, Germany; <sup>2</sup>Heinz Maier-Leibnitz Zentrum (MLZ), Technical University of Munich, Garching, Germany; <sup>3</sup>Space Sciences Laboratory, University of California, Berkeley, USA

**N**ECTAR is a fast neutron imaging instrument, which also gives access to thermal neutrons and gamma-rays present as inevitable by-products of fast neutron production. These three modes of imaging have been combined to develop multi-modal imaging using one setup by changing the combination of beam filters and scintillators. This opens avenues for multi-modal imaging of large and dense objects like concrete, hydrogen storage tanks, etc.

The NECTAR instrument provides access to thermal neutrons directly from the reactor core and fast neutrons from a thermal-to-fast neutron converter, which are suitable for non-destructive inspection of large and dense objects. It is known that the combination of multiple probes often provides complementary information that can result in a better insight into the sample composition. Gamma-rays are inevitable by-products of neutron production at NECTAR. We demonstrate how these gamma-rays, previously treated as beam contamination, can be used as a complementary probe.

### Concept of multimodal imaging at NECTAR

We present a multimodal imaging technique employing thermal, fast neutrons and gamma-rays using one setup but varying the combination of scintillator and beam filters. This has been implemented at NECTAR as Gamma in Addition to Neutron Tomography (GIANT), which involves:

1. Fast neutron imaging utilizing a PP/ZnS:Ag scintillator with Cd-B filter (to suppress thermal neutrons)
2. Thermal neutron plus gamma-ray imaging with a Gadox scintillator without Cd-B filter
3. Gamma-ray imaging, using the Gadox scintillator with Cd-B filter

Thermal neutron images are obtained by subtracting the gamma-ray contribution from images obtained by a combination of thermal and gamma-ray imaging.

### Feasibility study and applications of multimodal imaging

To demonstrate multimodal imaging, step wedges made of polyethylene, aluminium, steel, copper, and lead were imaged using this approach. Fig. 1 shows a picture of the different step wedges and radiographs obtained by different modes. It can be seen that different modes give rise to different contrasts for the same material. With a single mode, the differentiation of all materials is not possible, but combining the different modes evidently enhances elemental sensitivity. This is a unique technique with many potential applications ranging from hydrogen storage materials, concrete characterization to Li-ion batteries etc., extending the capabilities of cold neutrons combined with X-rays for small samples (<1 cm) to thermal and fast neutrons in combination with gamma-rays for imaging of large objects (>1 cm).

[1] R. Kumar et al., *Gamma In Addition to Neutron Tomography (GIANT) at the NECTAR instrument*, *Sci Rep* 13, 20120 (2023)  
DOI: 10.1038/s41598-023-47237-y

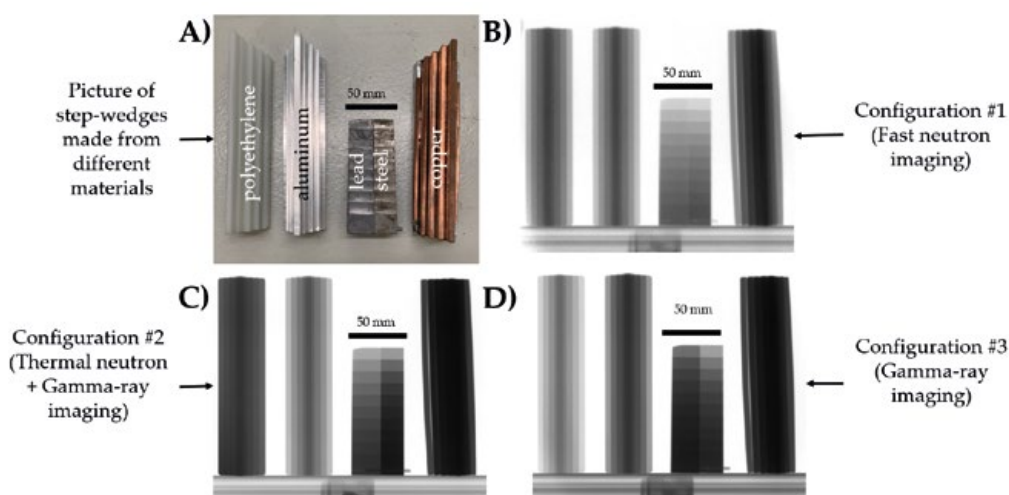


Figure 1: A) Picture of step wedges made of different materials that have been marked. Normalized radiograph of the step wedges obtained using the different imaging modalities, B) Fast neutron, C) Thermal neutron + Gamma-ray, D) Gamma-ray.

## A new multi leaf collimator for the fission neutron therapy facility at FRM II

L. B. Sommer<sup>1,2,3</sup>, T. Chemnitz<sup>3</sup>, S. Kampfer<sup>1,2</sup>, D. Bausenwein<sup>3</sup>, A. Beimler<sup>3</sup>, M. Kellermeier<sup>3</sup>, R. Schütz<sup>3</sup>, J. J. Wilkens<sup>1,2</sup>, F. M. Wagner<sup>3</sup>

<sup>1</sup>Technical University of Munich, TUM School of Medicine and Klinikum rechts der Isar, Department of Radiation Oncology, Munich, Germany;

<sup>2</sup>Technical University of Munich, TUM School of Natural Sciences, Physics Department, Garching, Germany; <sup>3</sup>Heinz Maier-Leibnitz Zentrum (MLZ), Technical University of Munich, Garching, Germany

**A** newly designed, electronically operated multi leaf collimator was introduced at the fission neutron therapy facility MEDAPP. The design of the collimator was optimized to increase dose output and to allow patient positioning closer to the collimator. A re-calibration of the ionization chambers used at FRM II was performed. The new collimator will enable more conformal dose delivery and help to reduce healthy tissue damage.

After a long period of in-house construction, in 2019 a new motorized multi leaf collimator (MLC) was implemented at the fission neutron therapy facility MEDAPP [1]. The ionization chambers used in the two-chamber method for neutron dosimetry were re-calibrated in 2018.

### The multi leaf collimator

The new MLC shown in Fig. 1 consists of two leaf banks with 19 upper and 19 lower leaves. Individual leaf movement can be performed in the vertical up and down direction in order to shape irregular treatment fields. The consecutive selection of different field shapes is possible, thereby shortening the set-up time for treatment. The leaf design accounts for the effective spatial extension of  $150 \times 150 \text{ mm}^2$  of the converter plates that serve as the radiation source. The leaves consist of a sequence of steel, boron enriched polyethylene, and aluminum selected for an optimal attenuation of the mixed neutron-gamma beam.

### Beam characteristics

Dosimetry measurements for the new MLC were compared to measurements from the initial dosimetric characterization of MEDAPP from 2008 for the old MLC. All dose measurements were performed in a water phantom. The depth dose curves of the neutron and the gamma components measured in January 2020 with the new MLC for a square field of side length 82 mm were compared with results for the old MLC with a side length of 90 mm. The neutron-over-gamma dose ratio in 50 mm depth in the phantom in 2020 was found to be comparable to the ratio measured in 2008 for the slightly larger field. Whereas no significant change in the beam quality was found with the new MLC, a much steeper lateral gradient is reported as compared to fields with comparable size shaped by the former MLC.

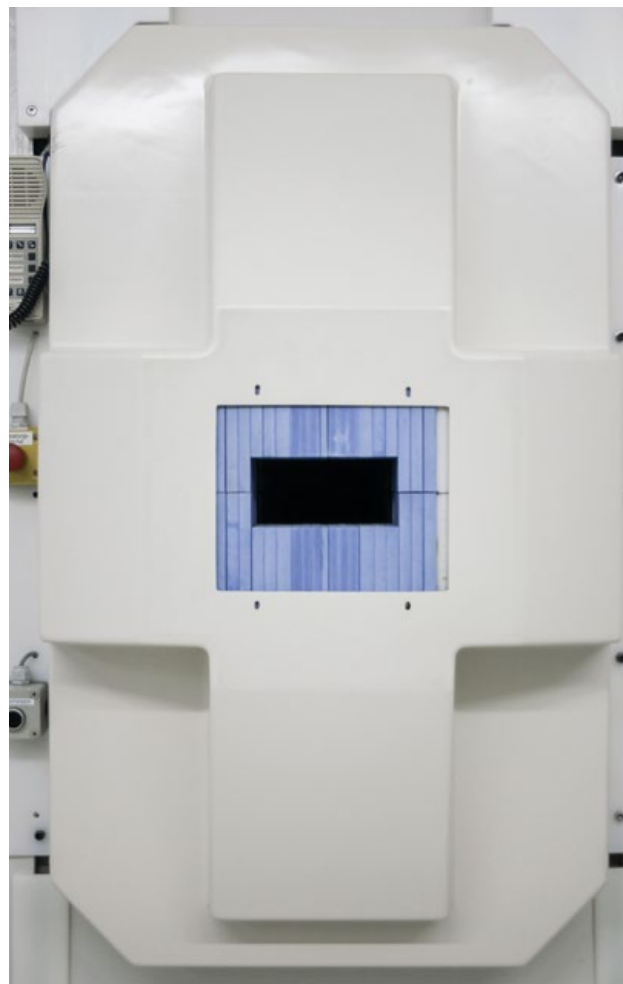


Figure 1: Front view of the new MLC with a rectangular field of size  $146 \times 82 \text{ mm}^2$ .

Thus, the measured beam profiles show clearly that the irradiation conditions have greatly improved with the new MLC.

As a result of the consistent beam quality and the improvements in the beam profiles measured in water, a dose distribution with a higher degree of conformity to the target volume within the patient will be possible.

[1] L. B. Sommer et al., A new Multi Leaf Collimator for the fission neutron therapy facility at FRM II, *Nucl. Instrum. Methods Phys. Res., Sect. A* 1057, 168717 (2023)  
DOI: 10.1016/j.nima.2023.168717

## Imaging low-energy positron beams in real-time with unprecedented resolution

M. Berghold<sup>1</sup>, V.V. Burwitz<sup>1</sup>, L. Mathes<sup>1</sup>, C. Hugenschmidt<sup>1</sup>, F. Guatieri<sup>1</sup>

<sup>1</sup>Heinz Maier-Leibnitz Zentrum (MLZ), Technical University of Munich, Garching, Germany

Low-energy positron beams such as NEPOMUC are a powerful tool of investigation in material science and of particular interest would be the deployment of micrometer-sized beams. Unfortunately, positron beams have very low brightness; the world's brightest, NEPOMUC, consists of  $10^9 e^+/s$ , while source-based beams are four orders of magnitude less intense. Prior to this work, online monitoring of low-energy low-brightness particle beams was not possible, which hindered the deployment of positron microbeams. To overcome this difficulty, we tested the novel approach of modifying a smartphone camera sensor to detect the positron beam.

### Direct imaging of the beam

We imaged positrons at the source-based Lab-beam maintained through our collaboration ( $6 \cdot 10^4 e^+/s$ ) using modified commercial CMOS image sensors (Sony IMX219). We modified the sensors by removing the Bayer filter and microlens array from their surface; and then either left the sensor surface bare or coated it with a  $70 \mu\text{m}$  thick layer of EJ-600 ZnS:Ag phosphor powder. In both cases, the sensor can detect the particle beam, with different performance.

We assessed the resolution of the sensor through the shadow projected onto it by tungsten wires. The phosphor-coated sensor proved a resolution better than  $20 \mu\text{m}$ , while the bare sensor detects individual positrons with a resolution of less than  $1 \mu\text{m}$ , which is unprecedented for real-time positron detectors. We proceeded by determining the sensitivity of the detector. With long exposure times, the coated sensor can detect positron beams of any energy and fluxes as low as  $35 \text{ particles/s/mm}^2$ . The uncoated sensor becomes sensitive at an implantation energy of  $6 \text{ keV}$ , its detection efficiency increasing with the implantation energy up to  $92\%$  at  $15 \text{ keV}$ .

### Conclusions

We have proven that, by modifying modern commercial CMOS sensors, we can achieve exceptional performance in the detection of low-energy positron beams. We foresee the use of CMOS technology as a staple of low-energy positron beam handling in the near future.

[1] M. Berghold et al., *Imaging low-energy positron beams in real-time with unprecedented resolution*, *Sci Rep* 13, 18526 (2023)

DOI: 10.1038/s41598-023-45588-0

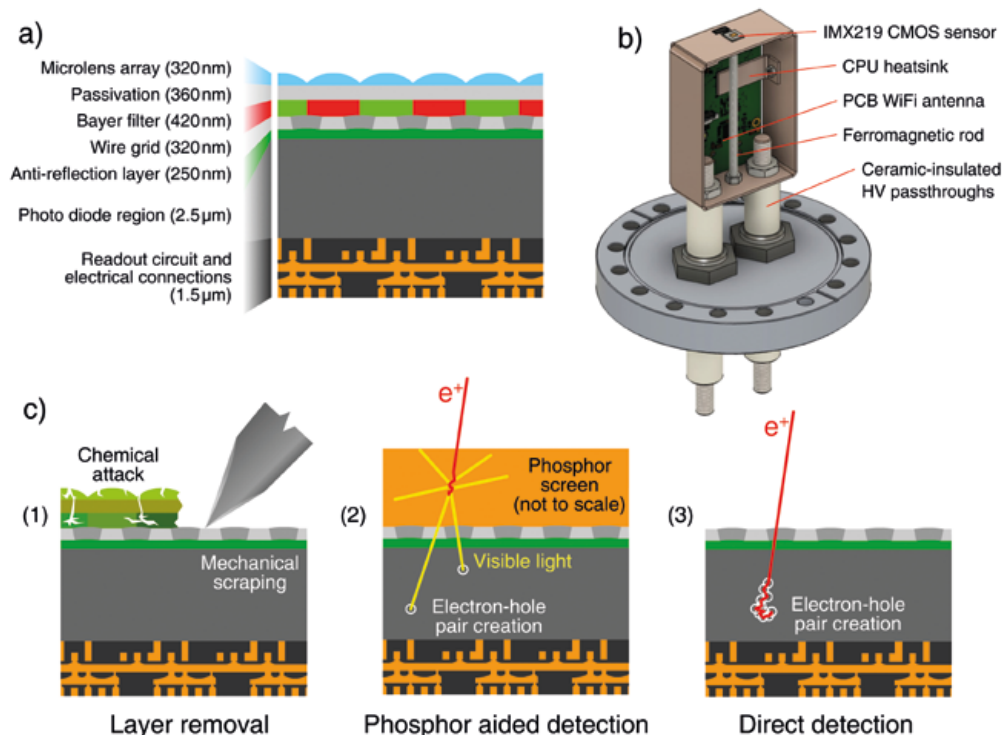


Figure 1: a) The composition of the CMOS sensor, shown in section. b) The apparatus used to read out the CMOS sensor while biasing it up to  $15 \text{ kV}$  c) Preparation and working principle of the sensor: (1) Removal of the Bayer filter and microlens array (2) phosphor-mediated imaging of positrons (3) unmediated imaging of positrons.

## Combined remoderation-drift scheme for positron injection into a magnetic trap

U. Hergenbahn<sup>1,2</sup>, J. Horn-Stanja<sup>1</sup>, S. Nißl<sup>1,3</sup>, H. Saitoh<sup>1,4</sup>, M. Singer<sup>1,3</sup>, T. Sunn Pedersen<sup>1,5</sup>, C. Hugenschmidt<sup>3</sup>, E. V. Stenson<sup>1</sup>

<sup>1</sup>Max Planck Institute for Plasma Physics, Garching and Greifswald, Germany; <sup>2</sup>Fritz-Haber-Institut der Max-Planck-Gesellschaft, Berlin, Germany;

<sup>3</sup>Heinz Maier-Leibnitz Zentrum (MLZ), Technical University of Munich, Garching, Germany; <sup>4</sup>Graduate School of Frontier Sciences, The University of Tokyo, Kashiwa, Chiba, Japan; <sup>5</sup>Institute of Physics, The University of Greifswald, Greifswald, Germany

**R**emoderation (in a solid) and steering with ExB drifts (by biasing nearby electrodes) are established ways to change the velocity distribution and trajectory, respectively, of a positron ( $e^+$ ) beam. A proof-of-principle experiment successfully combined these in the same spatial region, with an overall efficiency of  $15(\pm 1)\%$ . Trajectory simulations facilitated an accounting of losses and identification of strategies to improve future implementations.

### Motivation for a hybrid scheme

The efficient transfer of a magnetically guided  $e^+$  beam into a region of closed magnetic ( $B$ ) field lines is nontrivial. It is, however, a necessity for the APEX Collaboration, whose goal is to create and study magnetically confined “pair plasmas”, made of half matter ( $e^-$ ) and half antimatter ( $e^+$ ). This unusually simple, symmetric plasma is the subject of many theoretical and numerical predictions, some of which we aim to test experimentally. The  $e^+$  portion of the plasma will be provided by NEPOMUC at FRM II.

Previously, we used an ExB-drift technique to inject 5- to 20-eV positrons from NEPOMUC into the confinement region of Proto-APEX, our dipole trap being based on a supported permanent magnet. However, this technique might be challenged by the stronger  $B$  fields of next-generation traps. We may also need or want to use higher-energy incoming positrons; this would necessitate reducing their energy at our setup – e. g., using remoderation (in a material with a negative  $e^+$  work function).

### 2017 experiments + 2022 simulations

During a beam time in 2017, we briefly tested remoderating NEPOMUC’s 400-eV primary beam in a SiC crystal installed just outside the confinement region of Proto-APEX, in 15–25 mT (3–5x the NEPOMUC guide field). The reemitted low-energy positrons were then drift-injected. The tests were successful, with an overall efficiency of up to  $15(\pm 1)\%$ , yet we could not experimentally disentangle

the losses in the different steps of the process (steering of the beam onto the SiC, remoderation fraction, and drift injection efficiency).

Five years later, we simulated of order  $10^7$   $e^+$  trajectories with various initial conditions and experiment settings. This allowed us to conclude that 85–90% of the incoming positrons hit the SiC crystal, and up to 45% of reemitted positrons could be drift-injected, implying a respectable remoderation efficiency of 36–41%. These insights will help us to decide when to use the hybrid scheme in future experiments, as well as how to improve the efficiency in those implementations.

[1] U. Hergenbahn *et al.*, *Combined remoderation-drift scheme for positron injection into a magnetic trap*, *Phys. Rev. Research* 5, 023172 (2023)

DOI: [10.1103/PhysRevResearch.5.023172](https://doi.org/10.1103/PhysRevResearch.5.023172)

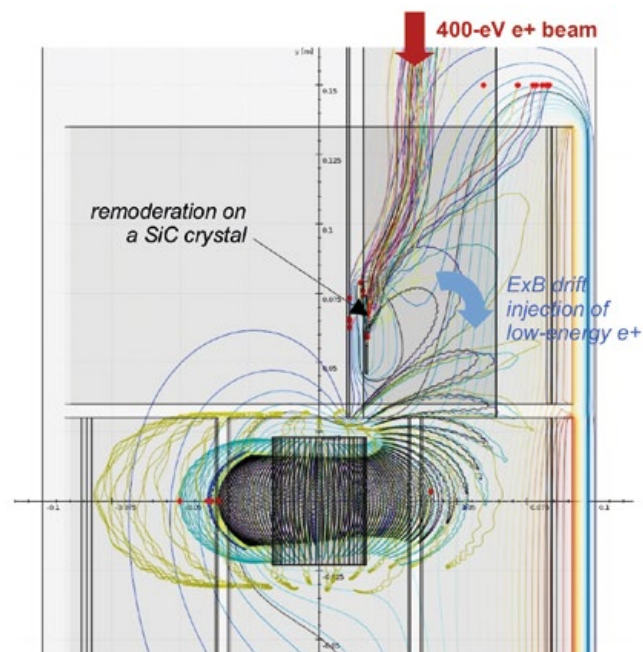


Figure 1: Simulated trajectories for a set of positrons from the NEPOMUC 400-eV primary beam, incident on a thin SiC crystal (viewed edge-on). A few cm below is a permanent magnet (cylinder), whose dipole magnetic field (not drawn) confines low-energy positrons (up to some tens of eV). Remoderated positrons (reemitted from the SiC) have energies just 1–2 eV above the SiC bias, allowing some to be steered into the dipole trap via electrode biases.

## Development of a magnetic sample environment for polarized neutron imaging of metal sheets

A. Backs<sup>1,2</sup>, S. Sebold<sup>3</sup>, M. Busi<sup>4</sup>, W. T. Lee<sup>2</sup>, M. Strobl<sup>4,5</sup>, D. Orlov<sup>1</sup>

<sup>1</sup>Mechanical Engineering Sciences, Lund University, Lund, Sweden; <sup>2</sup>Science Directorate, European Spallation Source (ESS), Lund, Sweden; <sup>3</sup>Heinz Maier-Leibnitz Zentrum (MLZ), Technical University of Munich, Garching, Germany; <sup>4</sup>Laboratory for Neutron Scattering and Imaging, Paul Scherrer Institut (PSI), Villigen, Switzerland; <sup>5</sup>Niels Bohr Institute, University of Copenhagen, Copenhagen, Denmark

**P**olarized neutron imaging (PNI) is capable of analyzing bulk magnetic properties with good spatial resolution which, however, imposes high requirements on the magnetic environment. Using finite element and ray tracing simulations, we have designed a magnetic sample environment that permits the study of ferromagnetic metals in an applied magnetic field. Here we show an analysis of its performance based on simulations and first experimental results.

### Depolarization problems with magnetic samples in PNI

Ferromagnetic metal sheets are a common material for the magnetic cores of electric motors or transformers. Polarized neutron imaging offers a unique method to study their local bulk magnetic domains during magnetization with spatial resolution. However, the technique imposes high requirements on the magnetic environment.

In our experiments, there are two main challenges. First, our sample has a strong magnetic response. It is magnetized by the required guide field which in turn gets distorted. Second, to optimally observe the Larmor-spin precession of neutrons due to the sample's magnetism we require a sample magnetization field perpendicular to the guide field defining the polarization. Both issues are avoided by creating a confined zero field region for the sample and magnetizing field to decouple both from the guide field. To avoid

losing neutron beam polarization, the two nested fields have to be narrow in beam direction, homogeneous and exhibit sharp transitions.

### A compact nested-coil solution

Our solution is a setup similar to a Mezei-spin flipper, consisting of two flat solenoids inside each other with the sample at the centre. The outer coil provides a vertical field to compensate the guide field and create a zero field region. The inner coil is oriented horizontally to magnetize the sample. The full setup is only 10mm wide in beam direction and the transition between field regions is given by the wire layers of 1–2 mm. In the design process, we simulated the full beamline to evaluate our setup. This included determining the magnetic field with finite element calculations and using the results to simulate the PNI measurements with Monte Carlo ray tracing.

### Success and challenges in experiments

Experiments have confirmed the success of our approach to compensate the guide field for measurements in zero field. With an applied magnetization field, however, large areas showed a loss of the spin rotation signal. We could recreate this effect with refined simulations which are currently used for improvements of the setup.

[1] A. Backs et al., *Development and first results of a magnetic sample environment for polarized neutron imaging of thin metal sheets*, *EPJ Web Conf.* 286, 05003 (2023)

DOI: 10.1051/epjconf/202328605003

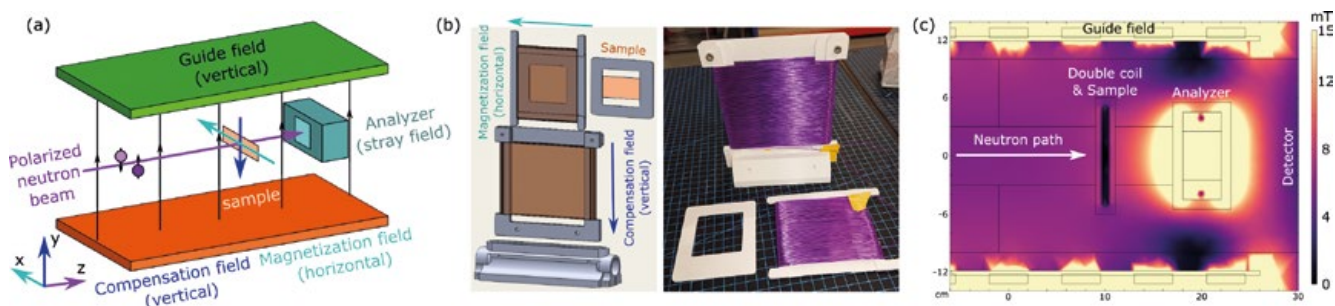


Figure 1: (a) Sketch of the relevant components in the experimental setup. The double-coil-setup has been omitted, showing only the additional fields created by it. (b) 3D-design and photo of the double-coil-setup. The sample, inner coil and outer coil form a nested compact sample environment with easy access to the sample. (c) Magnetic field distribution as calculated using COMSOL with fully compensated guide field.

## Joint PGAA analytical workflow development at the BNC and FRM II

L. Szentmiklósi<sup>1</sup>, Z. Révay<sup>2</sup>, J. Östör<sup>3</sup>, B. Maróti<sup>1</sup>

<sup>1</sup>Centre for Energy Research, Budapest Neutron Centre, Hungary; <sup>2</sup>Heinz Maier-Leibnitz Zentrum (MLZ), Technical University of Munich, Garching, Germany; <sup>3</sup>HyperLabs Software Ltd., Budapest, Hungary

The analysis protocol for Prompt Gamma Activation Analysis (PGAA) used at the PGAA and NIPS-NORMA facilities of the Budapest Neutron Centre, as well as the PGAA station at the FRM II/Heinz Maier-Leibnitz Zentrum, has undergone a comprehensive overhaul to enhance productivity and optimize spectroscopic performance. A collaborative effort for improvement on the part of these leading European PGAA centers aimed at establishing a common baseline for streamlining the analytical workflow, ensuring interoperability and seamless data exchange among each other, as well as applying a common, updated release of the PGAA spectroscopic database.

These PGAA facilities can now acquire data in unattended batch mode using computer-controlled sample changers. Automation extends to collimators, slits, shutters, and bookkeeping. PGAA spectra are taken at both facilities using a Compton-suppressed HPGe detector connected to a state-of-the-art digital spectrometer, specifically the ORTEC DSPEC 502A. This model, with its 64k histogram channels, offers improved numerical conditions for peak fitting, alongside enhanced peak shape and energy resolution. The digital Compton suppression mode may replace outdated NIM modules, accommodating both suppressed and unsuppressed forms of spectra, and thereby enabling the identification of escape peaks. The higher useful count rate range compared to traditional electronics allows the same counting statistics to be acquired in shorter beamtime.

### New analysis software

The evaluation of PGAA spectra, which used to take up to an hour by an experienced analyst, has been significantly shortened. A new version of the Hyperlab software package was developed to analyze the 64k and/or dual spectra efficiently. The nuclear database of the software, efficiency, nonlinearity, and peak width calibrations, as well as its evaluation algorithms, were fine-tuned for PGAA requirements. The updated Hyperlab release features a more appropriate FWHM model function and energy-dependent calibration of peak shape parameters, resulting in improved automatic fits with fewer user adjustments. A fully automated batch evaluation module facilitates the processing of multiple spectra of the same kind. An output template was created to export data to the ProSpeRo concentration calculation utility, using an enhanced PGAA data library where cross-section data were re-determined for several important elements with higher precision and consistency.

### Improved workflow in operation

Extensive testing demonstrated backward compatibility with the old methodology used to process over 25,000 spectra, while it was found to perform adequately at BNC under conditions beyond our previous operation boundaries as well. The new features have already been utilized in several joint experiments as part of the BNC LENS beam time offer, while others are planned at FRM II after the restart of the neutron source.

[1] L. Szentmiklósi et al., *Improved analytical workflow for prompt-gamma activation analysis*, *J. Radioanal. Nucl. Chem.* (2023)

DOI: 10.1007/s10967-023-09071-4

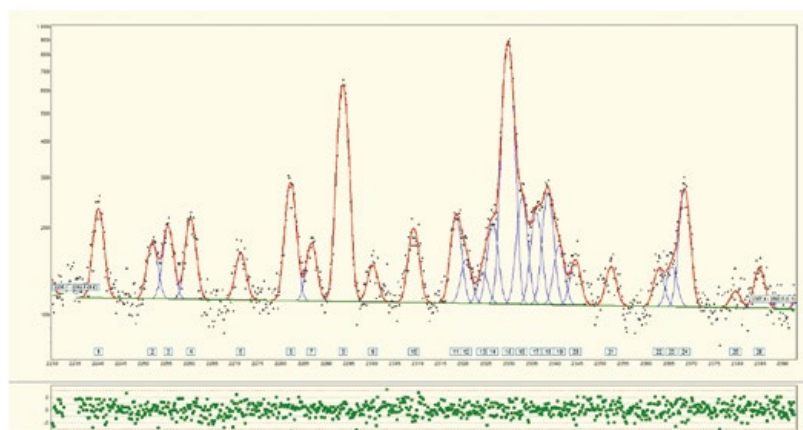


Figure 1: Successful fit of multiplets in a PGAA spectrum using the new Hyperlab gamma spectroscopy software package.

## Documenting previous knowledge and the results of Bayesian analysis: best practice for reflectometry

A. R. McCluskey<sup>1</sup>, A. J. Caruana<sup>2</sup>, C. J. Kinane<sup>2</sup>, A. J. Armstrong<sup>2</sup>, T. Arnold<sup>1</sup>, J. F. K. Cooper<sup>2</sup>, D. L. Cortie<sup>3</sup>, A. V. Hughes<sup>2</sup>, J.-F. Moulin<sup>4</sup>, A. R. J. Nelson<sup>3</sup>, W. Potrzebowska<sup>5</sup>, V. Starostin<sup>5</sup>

<sup>1</sup>European Spallation Source ERIC, Lund, Sweden; <sup>2</sup>ISIS Neutron and Muon Source, Rutherford Appleton Laboratory, Didcot, Oxfordshire, United Kingdom; <sup>3</sup>Australian Nuclear Science and Technology Organisation, New South Wales, Australia; <sup>4</sup>German Engineering Material Science (GEMS) at MLZ, Helmholtz-Zentrum hereon GmbH, Garching, Germany; <sup>5</sup>Institute of Applied Physics, University of Tübingen, Tübingen, Germany

**B**ayesian methods are gaining popularity in the field of reflectometry as they help to incorporate prior knowledge to solve the phase problem. Guidelines are proposed to improve reproducibility and transparency in the reporting of experiment analysis, emphasizing the need for detailed documentation of the refinement procedures, prior knowledge encoding, and likelihood function choices.

### A better approach to data analysis

Neutron and X-ray reflectometry are crucial for analyzing thin layers and interfaces, but they face the phase problem, where multiple matter distributions yield identical scattering patterns. Addressing these issues requires exploiting prior knowledge, which is made easy through Bayesian statistical methods. These methods update prior knowledge with experimental evidence, producing a posterior probability distribution function (pdf) for model parameters, rather than just parameter values and uncertainties.

### The challenges of rich statistical models

In recent years, several implementations of Bayesian data analysis software focused on reflectometry have been developed and the number of publications using these methods is steadily increasing. However, this growth brings challenges, notably the need for detailed descriptions of refinement procedures, initial parameter selection, and prior knowledge encoding to ensure transparency and reproducibility.

### Suggested guidelines for presenting reflectometry results

A group of experienced users and instrument scientists recommends guidelines to enhance analytical reproducibility and result quality in reflectometry experiments. Central to data evaluation is the likelihood function, which assesses fit quality by comparing observed data against model predictions. Reflectometry uses different likelihood function versions (based e.g on  $R(q)$ ,  $R(q).q^4$  or  $\log R(q)$ ) to focus on specific data regions, necessitating clear methodology documentation.

Prior knowledge is incorporated as a pdf, constraining parameter values within certain ranges or indicating some values as more likely. Documenting the former's basis is essential, whether through mathematical functions or alternative sampling methods. For the latter, the complete sampling chain must be reported.

The posterior, a product of the prior and likelihood, is also a pdf. Describing individual and correlated parameter pdfs is best achieved with corner plots (Fig. 1). This approach ensures that analytical processes in reflectometry are both transparent and reproducible, enhancing the field's overall utility and quality.

[1] A. R. McCluskey et al., *Advice on describing Bayesian analysis of neutron and X-ray reflectometry*, *J. Appl. Cryst.* **56**, 12 (2023)

DOI: [10.1107/S1600576722011426](https://doi.org/10.1107/S1600576722011426)

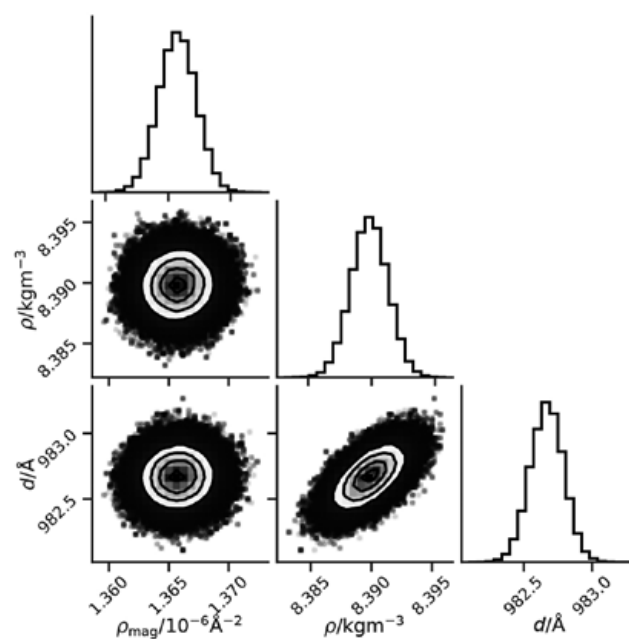


Figure 1: An example of a graphical depiction of the unthinned posterior as a corner plot (produced using the `corner.py` package; Foreman-Mackey, 2016), representing a three-dimensional probability distribution showing the posterior distribution for the parameters of nickel magnetic scattering length density, nickel mass density and nickel layer thickness, from the analysis of a nickel layer on a silicon block (Caruana & Kinane, 2022).

## ANTARES detector technology for neutron imaging facilities at 100 W reactor VR-1 in Prague and 250 kW RA-6 in Bariloche

J. Matoušková<sup>1</sup>, L. Sklenka<sup>1</sup>, T. Jünger<sup>2</sup>, T. Neuwirth<sup>2</sup>, B. Schillinger<sup>2</sup>, S. Sebold<sup>2</sup>, J. Marin<sup>3</sup>

<sup>1</sup>Czech Technical University in Prague, Prague, Czech Republic; <sup>2</sup>Heinz Maier-Leibnitz Zentrum (MLZ), Technical University of Munich, Garching, Germany; <sup>3</sup>Centro Atómico Bariloche, San Carlos de Bariloche, Argentina

At MLZ/FRM II, newly developed compact high-resolution astronomy cameras were combined with a new detector concept with external shielding and 3D-printed housings to adapt to the specific needs of two smaller reactors. In addition, the professional distributed control software used at the ANTARES facility was downscaled to run standalone on a single laptop and motor controller to create professional low-cost, but high-quality neutron computed tomography facilities at both reactors.

Neutron imaging detectors typically use a cooled CCD camera looking at a neutron-sensitive screen via a mirror. Heavy lead shielding against gamma radiation created in the sample is often included in the detector housing, making it bulky and inflexible. Recently developed cooled CMOS cameras for astronomy are so compact that they can be placed in small detector housings with the shielding stacked externally. In addition, the section of the detector box housing the mirror and neutron screen is made as a detachable part that can be exchanged for various sizes and fields of view. The ANTARES neutron imaging group developed several versions of neutron imaging detectors, the more recent version in 3D printed housings that can be adapted to the specific needs of a facility.

### World record for low-power neutron CT in Prague

At the Czech Technical University (CTU) in Prague, a custom setup was installed at the VR-1 reactor with a nominal power of only 100W, which can be increased to 500W for a limited time per year. This reactor was previously considered unsuited for neutron computed tomography, but after modification of the imaging beamline, the new detector proved so sensitive that computed tomography was possible within twelve hours of irradiation time. [1]

### Special detector for Argentina

The RA-6 reactor in Bariloche, Argentina, had unsuitable conditions with a steel beam tube with only a 6 cm sideways opening at the top. The strong background of gamma

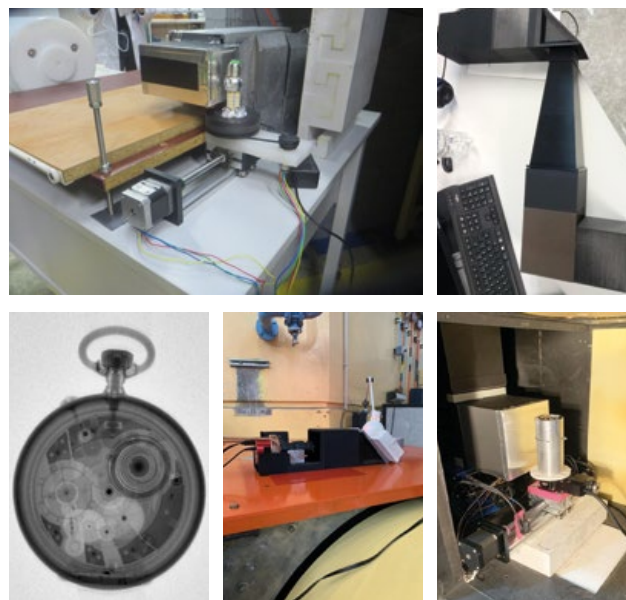


Figure 1: Clockwise from top left: First setup in Prague, Periscope for Bariloche, top and bottom of the setup in Bariloche, neutron radiography of a watch.

radiation inside the steel tube made it impossible to use a single mirror camera system to look inside the beam tube towards a neutron screen, as a camera directly at the small opening would immediately suffer radiation damage. To adapt to this situation, a double-mirror periscope system was developed in collaboration of CTU and MLZ that had parts mechanically connected through the 6 cm opening for a precise adjustment. The given geometry required putting the camera in 1.2m total distance from the screen with a tele lens, which lost a lot of recordable light intensity, but produced images of excellent quality for computed tomography. [2]

[1] J. Matoušková, et al., *New Neutron Imaging Facility NIFFLER at Very Low Power Reactor VR-1*, *J. Imaging* 9, 15 (2023)

DOI: 10.3390/jimaging9010015

[2] J. Matoušková et al., *New detector design of STORNI neutron imaging facility at RA-6 research reactor*, *Nucl. Instrum. Methods Phys. Res., Sect. A* 1056, 168594 (2023)

DOI: 10.1016/j.nima.2023.168594.



# News from the instruments



# Update from the instruments

W. Lohstroh<sup>1</sup>, T. Chemnitz<sup>1</sup>, H. Frielinghaus<sup>2</sup>, C. Garvey<sup>1</sup>, R. Georgii<sup>1</sup>, D. Gorkov<sup>3,6</sup>, C. Hauf<sup>1</sup>, M. Hofmann<sup>1</sup>, M. Hölzel<sup>1</sup>, C. Hugenschmidt<sup>1</sup>, J. Jochum<sup>1</sup>, T. Keller<sup>4,6</sup>, A. Koutsioumpas<sup>2</sup>, A. Losko<sup>1</sup>, S. Mattauch<sup>2</sup>, M. Meven<sup>2,5</sup>, A. Mutschke<sup>1</sup>, J. Park<sup>1</sup>, S. Pasini<sup>2</sup>, M. Skoulatos<sup>1</sup>, J. Voigt<sup>2</sup>, M. Wolf<sup>1</sup>

<sup>1</sup>Heinz Maier-Leibnitz Zentrum (MLZ), Technical University of Munich, Garching, Germany; <sup>2</sup>Jülich Centre for Neutron Science (JCNS) at MLZ, Forschungszentrum Jülich GmbH, Garching, Germany; <sup>3</sup>Institute of Physics II, University of Cologne, Germany; <sup>4</sup>Max-Planck-Institute for Solid State Research, Stuttgart, Germany; <sup>5</sup>Institute of Crystallography, RWTH Aachen at MLZ, Garching, Germany; <sup>6</sup>Heinz Maier-Leibnitz Zentrum (MLZ), Garching, Germany

In 2023, instrument developments and further sample environment options became available that will extend the experimental capabilities when the user operation at MLZ restarts. Most significantly, the installation work of the new instruments in the Guide Hall East, as well as of the two instruments transferred from Berlin, is progressing. Instruments already in user operation also received some upgrades and new sample environments to broaden the range of applications.

## New Instruments – getting ready for commissioning

POWTEX and SAPHIR are two of the additional powder diffraction instruments currently under construction, the latter dedicated to experiments under extreme pressure and temperature conditions. Installation is ongoing in the Guide Hall East, and the shielding structures, the instrument equipment and the surrounding infrastructure are appearing in the hall step by step. The detectors for POWTEX have been externally tested and are awaiting their final installation in the POWTEX detector vessel. For the fundamental physics beamline PERC/MEPHISTO, also a constituent part of the new instruments in the Guide Hall East, preparations for the cooling system installation are progressing for the first cooling test of the PERC magnet on-site. An initial trial setup of the guide housings of MEPHISTO in the experimental hall was performed to confirm construction prior to their final installation in 2024. The area in the experimental hall was cleared and is now ready to receive the neutron guides and corresponding shielding that will connect the new instruments to the reactor source.

Among the new instruments in the Guide Hall East is also the latest addition to the MLZ spectrometer suite, the thermal direct time-of-flight spectrometer TOPAS. It can use neutrons up to 200 meV in energy and hence extends the dynamical range that can be probed at the MLZ to higher energies. The main components of the instrument, the 75 m<sup>3</sup> vessel, which provides the evacuated flight path from sample to detector to resolve the neutron energy by time-of-flight analysis, and the 16 m<sup>2</sup> <sup>3</sup>He detector are among the first big installations in the Guide Hall East. The factory acceptance test of the chopper system, including two fast spinning Fermi choppers and a disk chopper, necessary to



Figure 1: The instrument TOPAS: outer shielding and the chopper system (front) in the neutron Guide Hall East.

provide narrow pulses of high energy neutrons, took place in Jülich in summer 2023. It will be installed in line with the installation of the instrument shielding. Over the last year, the spectrometer housing has been enclosed by polyethylene shielding to provide excellent background conditions for the instrument. The hardware for instrument control is ready for delivery to Garching. At the same time, PLC and instrument control software, as well as data acquisition and reduction based on the Mantid framework is progressing, all to be ready for the commissioning of the instrument in 2024.

The other new diffractometers under construction are located in the Experimental Hall. The high-efficiency diffractometer ERWIN is currently built-up at the beam port SR8b in the experimental hall. ERWIN is characterized by the large two-dimensional wire chamber detector, CHARM, with a virtually seamless angular coverage of 135° (in 2θ) and a vertical angle range of 15°. ERWIN will allow the characterization not only of powder samples and textured bulk samples but also single crystals, and the beam optics can be chosen accordingly. However, we expect the foremost advantage of ERWIN to be the rapid data collection that allows for time-resolved measurements, parametric studies and investigations on small samples. In its first expansion stage, ERWIN will utilize the monochromator setup of the former single crystal diffractometer RESI (using a vertically focusing Ge 511 monochromator with a monochromator angle of 90°, corresponding to a wavelength of 1.54 Å.) The

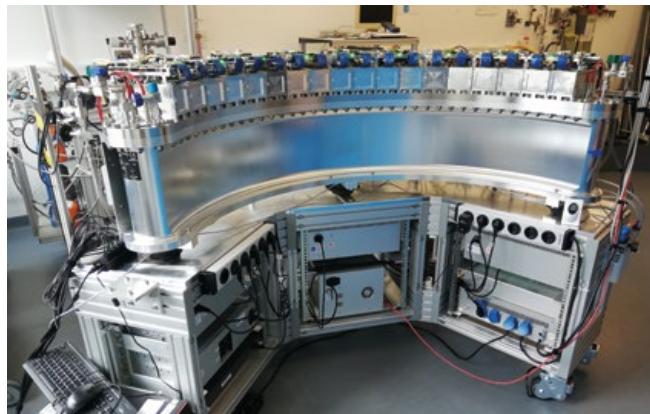
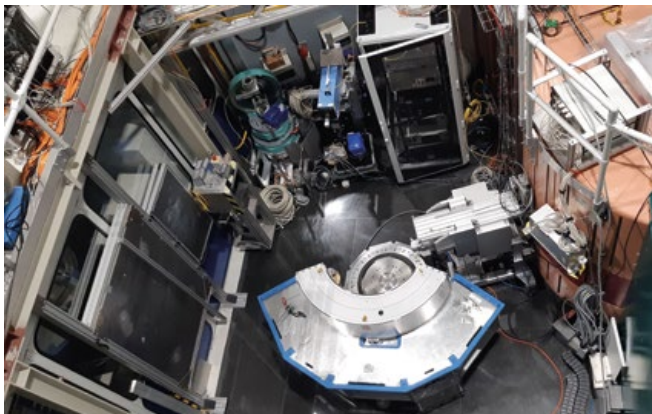


Figure 2: The instrument ERWIN (left), almost ready to accept the CHARM detector (right).

neutron optics for the monochromatic beam, the heavy-load sample table as well as the support for detector and radial collimator have already been installed and aligned with the CHARM detector ready for installation and commissioning.

On the neighboring SR8 channel, the new high throughput powder diffractometer FIREPOD is commencing installation, to complete the suite of thermal monochromatic powder diffractometers at MLZ. FIREPOD is one of the two instruments that were transferred from Helmholtz-Zentrum Berlin (HZB) to have a second lease of life at the MLZ. Initially, FIREPOD will be sharing a monochromator with SPODI. At a later stage, the entire primary neutron optic and shielding at SR8 will be renewed and updated, to allow for a simultaneous operation of both instruments.

The former FLEXX is the second instrument that was transferred from Berlin to Garching and it will serve as the backbone of the new instrument LADIFF at the neutron guide NL6 at MLZ. Currently, the original shielding has been adapted to be fit for the new position at NL6 with approximately an order of magnitude more flux. The former FLEXX monochromator housing now gets a new inner dressing of a lead and polyethylene (PE) sandwich construction to comply with the requirements for LADIFF, as determined by Monte Carlo simulations of the radiation field.

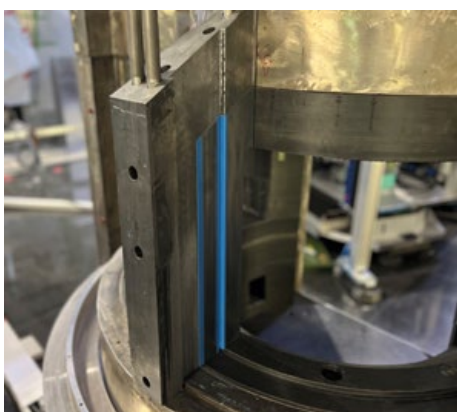


Figure 3: Adaption of the monochromator shielding for LADIFF: one of the new shielding elements comprised of a sandwich structure of lead and polyethylene (blue).



Figure 4: The arrival of the new small angle detector tank for RESEDA.

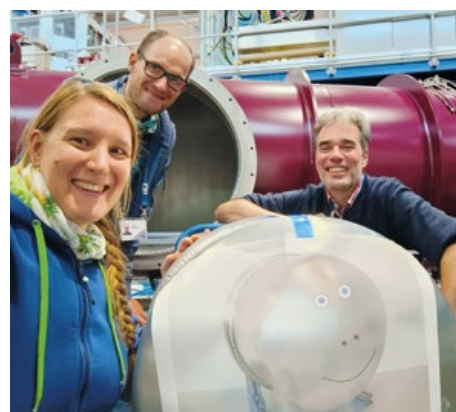


Figure 5: Smiling faces accompany the new detector at RESEDA.

### New opportunities – Recent instrument upgrades and preparation for thermal operation

In 2023, the new small angle detector tank for the resonant spin echo spectrometer RESEDA arrived, followed by the refurbished CASCADE detector, now fitted with a vacuum compatible housing. At this juncture, the BMBF Project MIASANS came to a successful conclusion. Placing the CASCADE detector inside its vacuum proof housing into the small angle detector tank will reduce background scattering while providing a higher Q-resolution and more flexibility in the Q-range covered during experiments at RESEDA.

At the three axis spectrometer KOMPASS, the finalization of the polarization analysis options is ongoing. In particular, the implementation of the Cryogenic Polarization Analysis Device (CryoPAD) for spherical polarization analysis (SPA) was pursued, which is one of the polarization analysis methods implemented at KOMPASS. By means of SPA, it becomes possible to determine the rotation of the neutron polarization and to unambiguously separate the nuclear, magnetic, nuclear-magnetic interference and chiral contributions in the scattered signal and thus solve the most sophisticated magnetic structures and excitations. First cooling of the CryoPAD and its final commissioning in the presence of experts from the ILL is foreseen for 2024. The second polarization method available at KOMPASS is longitudinal



Figure 6: The fully polarized triple axis spectrometer KOMPASS and the CryoPad installed on the sample table.

polarization (LPA). A new set of compact Helmholtz-coils is currently in production at the FZJ. The new LPA-setup has been adapted for the compact KOMPASS geometry and allows a strong and homogeneous guide field at the sample position necessary to maintain large flipping-ratios to be produced. In addition, a specially designed rotatable base allows for automatized turning of the coils to avoid depolarizing regions for all accessible scattering angles.

A number of projects is ongoing at the small angle instruments KWS-1, KWS-2 and KWS-3 to achieve higher capacity and new possibilities, but also in anticipation of operation without the cold source. The redesigned tilt-table for the neutron velocity selector at KWS-1 allows for a 20% greater range of neutron velocities, doubling the intensity and making shorter 3 Å wavelengths possible, beneficial both for analyzing larger Q vectors in proteins structures and also a shift towards the peak of the thermal spectrum to compensate for intensity losses expected for the operation without the cold source. In addition, more flexibility in the beam aperture (and of the beamstop in front of the detector) leads to an optimized resolution and intensity for larger samples, with an expected 6.3-fold increase in intensity in comparison to typical 1 x 1 cm<sup>2</sup> samples. The new second sample position at KWS-3 is fully operational, and the construction of the detector tube for the second, wide angle detector at KWS-2 is progressing.

In the aftermath of the implosion of the neutron guide at the reflectometer MARIA in 2022, the reconstruction of the neutron optics, i. e. the construction of a new RF flipper vacuum enclosure together with the new neutron guide have now been completed. The design of the new RF pin-ball machine has also been completed, while the fabrication of the housing has begun. An extra highly curved elliptical guide at the exit of the collimation system will boost the flux at the sample by almost 50%. Further intensity gains can be expected when supplementing the current velocity selector

with a resolution relaxed 20% selector. This will also help to partially compensate for the expected flux losses in thermal operation. The ex-situ commissioning of a Pulsed Laser Deposition (PLD) system has been resumed. The system is especially designed for MARIA, enabling in-situ studies of PLD grown samples by neutron reflectometry. This sample environment complements the already existing Molecular Beam Epitaxy (MBE) transfer chamber. This provides a unique tool set for the investigation of thin films and magnetic heterostructures during their deposition.

In the Experimental Hall, the instrument PUMA is being prepared for the installation of the new parabolic nested mirror optics (NMO). As part of the NMO4PUMA project, the NMO is expected to arrive in 2024. It will allow for beam spot sizes as small as 5 mm x 5 mm at the sample, while maintaining 50% of the neutron flux, leading to an 8-fold increase in intensity for small samples compared to the standard 20 mm x 20 mm beam spot size.

At the single crystal diffractometer HEiDi, the development and introduction of an area detector is ongoing. On the one hand, an area detector will enhance overall efficiency by faster sample orientation and easier detection of possible superstructure reflections. On the other hand, detector resolution and efficiency must comply with the requirements of operations with hot neutrons and smallest samples (< 1 mm<sup>3</sup>), especially in high pressure cells. After various tests and taking different detector technologies into account, a scintillation area detector based on <sup>6</sup>Li-Glass, based on the SoNDe activities of JCMS, was selected. In the final configuration, the detector uses a 2 mm thick <sup>6</sup>Li glass for a significantly increased sensitivity of >60% at 0.55 Å, and 50 mm x 50 mm multi-anode photomultipliers with a four times higher resolution (3 mm x 3 mm pixels) compared to standard photomultipliers, which guarantees a sufficient resolution. By lining up the individual modules, a total area of 250 mm x 150 mm is achieved. In collaboration with the construction and manufacturing department at FZJ/ZEA-1, the production of the detector housing has already begun. In parallel, the load capacity of the HEiDi diffractometer unit has been adjusted.

The SR10 beamport houses two irradiation rooms, MEDAPP, the fission neutron treatment facility, and NECTAR, the fast neutron imaging instrument. MEDAPP applies a mixed neutron-gamma irradiation field for the treatment of malignant tumors. In the course of the INGRAMM project, a new imaging system is currently being installed at MEDAPP to allow for neutron as well as gamma radiography. The system consists of two amorphous silicon flat panel detectors with a detector area of 410 mm x 410 mm each. The detector for gamma radiography is equipped with a Gadox scintillator,

whereas the detector for neutron imaging can be flexibly equipped with scintillators of different materials. The system aims for advances in patient positioning as well as an improvement in dose delivery monitoring. The experimental data acquisition is thereby accompanied by simulations using the recently in-house developed dose planning system. The detector system is currently being installed and the testing of the gamma-sensitive detector is taking place at the university hospital Klinikum rechts der Isar.

To further increase the options for the fast neutron imaging instrument NECTAR, the translation system that was successfully designed and constructed in recent years, is now positioned on a rail support directly embedded in the concrete floor of the NECTAR instrument. This adds about 250 mm of additional working distance in height for large, heavy and complex samples or sample environments. In addition, the first module of a collimator/scrapper system arrived to improve beam divergence and background in the NECTAR chamber. These modules can be positioned inside the MEDAPP chamber upon operation of NECTAR, but they are fully removable for use in the MEDAPP facility.

#### News from NEPOMUC and positron beam experiments – already on the move

In the near future, the positron beam instrumentation will move to its new dedicated space in the Guide Hall East. Thus, new beamline components to feed the positrons from the NEPOMUC source to the experimental stations have been constructed and set up. Two of the instruments had already been removed from the Experimental hall in order to free the area for the new shielding necessary to connect the instrument in the Guide Hall East. As part of the new beamline setup, monitoring of the beam position, size and intensity is of utmost importance to ensure reproducible measurements at the instruments. In order to minimize the time required to set up the beam, a novel kind of Faraday cup-like detector was developed, specifically designed to aid the

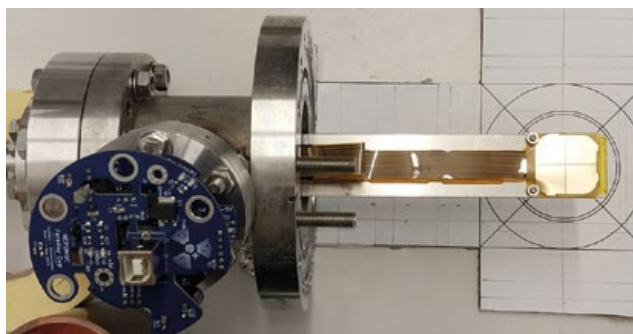


Figure 7: Faraday cup like beam monitor for fast and efficient positron beam alignment. The design consists of four pickup electrodes printed on a gold-on-kapton flexible PCB, on the back of which we mounted a preamplifier. Inserted in the path of the positron beam, the current induced onto each of the electrodes (four quadrants on the right side) is measured with a precision up to 1.8 fA. Imbalances in this current signal indicate a lack of beam centering and the direction of its misalignment.

centering of a charged particle beam with an intensity lower than 1 pA. By reading out the four quadrants electrodes, the centering of the NEPOMUC beam can be determined with a measurement time of 6 ms. This facilitates the execution of automated closed-loop beam optimization procedures with fast iteration times, which is fundamental for the transport of the beam to the instruments.

Another addition to the new beamline will be the installation of a buffer-gas trap as an optional beam conditioning device. Buffer gas traps are invaluable for high-resolution studies of matter-antimatter interactions, antihydrogen research, and positronium laser spectroscopy. They are variants of Penning traps that exploit resonant inelastic interactions with nitrogen molecules to efficiently capture positrons from a continuous beam. A multi-stage electrostatic potential minimum is generated by a series of cylindrical electrodes to axially confine the charged particles. Differential pumping produces a large pressure gradient along the trap and the asymmetric electrostatic potential ensures that the positrons cool towards the region of lowest pressure. This simultaneously maximizes the scattering rate in stage-1 whilst minimizing the annihilation rate in stage-3. The BGT was assembled at IPP Garching and successfully tested using an electron beam with a similar intensity and energy spread to the remoderated NEPOMUC beam. The BGT system is expected to extend the capabilities of the NEPOMUC by offering dense, pulsed positron beams with very narrow energy spreads (<100 meV). The device is a vital component within the APEX (A Positron Electron eXperiment) collaboration, which aims to produce a low-energy electron-positron pair plasma.

#### Hot, cold – and some pressure: new sample environment capabilities

The sample environment pool received some considerable expansion with new advanced equipment for low temperature experiments. For the first time, the new Adiabatic Demagnetization Refrigerator (ADR) arrived at MLZ. This technology, in combination with a closed-cycle-refrigerator pre-cooling system allows for continuous operation between temperatures of 300 K and 300 mK in a single system. Likewise, through the one-shot operation mode, a temperature of 200 mK can be reached. In addition, an automatic sample loading system makes sample change possible in just a few minutes, minimizing precooling times – and opening up the pathway for further automation. The special design of the ADR system for neutron scattering experiments includes the stage in the aluminum tail with a diameter of 180 mm and 360 deg neutron access. This new technology will provide a revolutionary new and simple way to achieve temperatures below one Kelvin. Currently, MLZ has two units which are operated by TUM and JCNS. The system



Figure 8: The new ADR cryostat during commissioning activities, with its sample load lock for fast and efficient automated sample mounting.

will be available for user experiments at the start of the next reactor cycle, and at PANDA the ADR will be available as PANDA's new standard cryostat.

To extend the temperature interval of 8T magnet at the POLI instrument to the mK range, an additional  $^3\text{He}$ - $^4\text{He}$  dilution insert was added. During preliminary tests of the Kelvinox JT, it reached 16 mK (without neutron beam). The system can also be used with the 12 T magnet at PANDA.

In the area of soft matter research new capabilities for humidity, temperature and hydrostatic pressure control are available. For high pressure GISANS experiments at the SANS-1 instrument, a new 2 kbar high-pressure cell with a motorized screw press manufactured by SITEC in Switzerland was delivered in 2023. The pressure cell incorporates two sapphire windows, each with a 28 mm diameter on the side for both neutron and optical access. In addition, a third optical window was integrated (90 deg orientation to the neutron beam). This window allows for the integration of advanced techniques such as optical microscopy or Raman spectroscopy at a future date. It is specifically designed for a sample size measuring 60 mm in diameter, supported on a 10 mm substrate. The motorized 2 kbar screw press empowers researchers with the ability to remotely control pressure values, providing the necessary level of precision tuning.

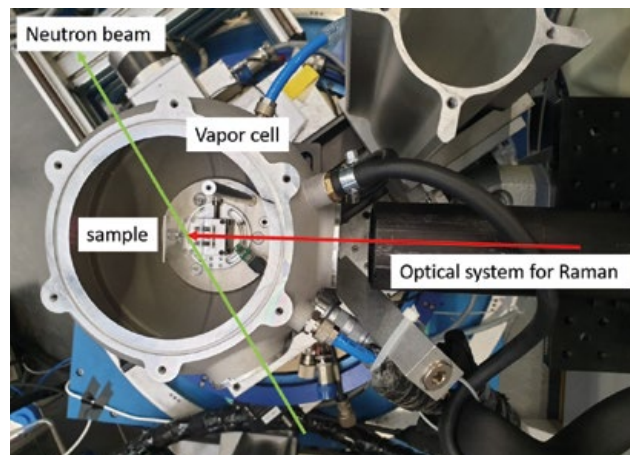


Figure 9: The new vapor chamber with additional optical access for TOFTOF.

A versatile and flexible cell based on the Flexiprobe design for controlling the gas mixtures and vapor atmosphere as well as temperature around a sample is under development, especially for use at the wide angle neutron spectrometer TOFTOF, but also for TAS and diffraction setups. Similar to the GISANS cell, an additional optical port allows for secondary characterization of the probed sample, e.g. with Raman spectroscopy. The equipment enables studies of, e.g., the effects of alcohols on lipid bilayers in fermentation, or the barrier properties of pharmaceutical excipients. First tests on the vapor controlled sample cell in combination with the already commissioned Raman spectrometer available at the instrument TOFTOF were performed with neutrons at the Paul Scherer Institut (PSI), Switzerland, with further tests planned on the IN13 backscattering spectrometer at the Institute Laue Langevin (ILL) in early 2024. Another ongoing development is the realization of a new sample holder for hydrostatic pressures up to 400 MPa for liquid samples that is realized as an insert for a standard CCR cryostat.

A further development regarding measurement in a controlled gas atmosphere and simultaneous secondary characterization is now also available at the reflectometer NREX. Hydrogen or deuterium atmospheres at pressures between 0.001 mbar and 1 bar, in a temperature range from 0.5 K to 500 K, and at magnetic fields up to 0.5 T can be applied to the thin film samples. Neutron and x-ray reflectivity can be measured in parallel to track thickness changes and depth resolved hydrogen concentrations and magnetization inside the samples. New sample holders with thin spring loaded contacts make it possible to measure electrical transport of the films during the hydrogenation process. Using lock-in amplifiers allows for very precise measurements, even in the harsh electrical environment of the guide hall. In addition, the polarization analysis at NREX is improved by a new wide area analyzer, designed by the NREX team. This analyzer covers the entire detector area (200 mm x 200 mm), corresponding to a gain factor of 40 compared to the previous analyzer (5 mm x 200 mm).

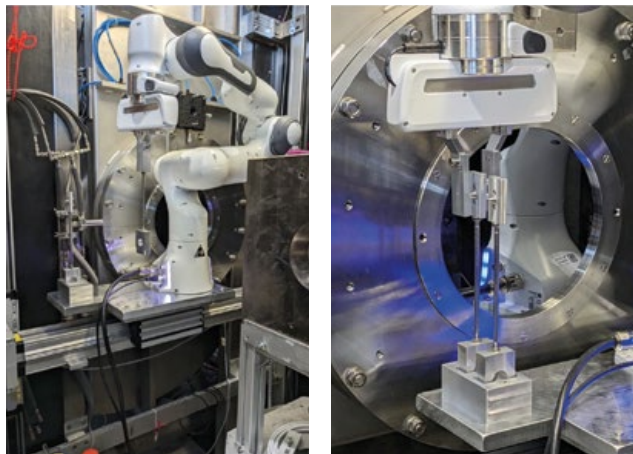


Figure 10: The non-magnetic robotic arm at KSW-1, ready to handle magnetically sensitive samples with the necessary care.

Strong emphasis is laid on the MLZ sample environment possibilities for increased automation of sample handling. After the successful integration of a robotic sample changer at the small angle instrument KWS-2, the instrument KWS-1 is also now equipped with a robotic arm for automatized sample handling. It comprises a non-magnetic robotic arm. The device is optimized for operation in combination with the 3 T magnet available at the instrument. Successful tests performed at the sample position demonstrated the robotic arm autonomously picking samples from the magazine (storage), placing them in the beam for measurement, and returning them. The new setup ensures that samples sensitive to magnetic field changes remain in a non-magnetic environment before and after measurements. Also at J-NSE, automatic sample change is making progress: a new autonomous sample changing robot has been delivered and is being tested in Jülich. It is currently integrated into the instrument control system software before the robot is delivered to MLZ at the beginning of 2024.

In the area of materials science, a couple of new devices have become operational that will enhance the ability for in-operando studies, mainly for engineering applications. For the diffractometer STRESS-SPEC, a lightweight laser furnace with a large acceptance angle for neutrons was developed and built. This furnace will be mainly used as a sample environment option for the robot sample holder at STRESS-SPEC and facilitates the investigation of samples at elevated temperatures up to 1500 K. The new control rack of the furnace was the first unit to be developed to a new MLZ standard, developed in a cooperative project between TUM and the Technikum of the Helmholtz Zentrum hereon within the framework of the BMBF project RAPtOr. The new standard is also suitable for controlling the other high temperature devices of the MLZ sample environment pool and thus facilitates the fast and easy exchange of high temperature equipment between different instruments for a smooth and fast start up of experiments during operation.

The next generation of testing machines comprises a new 100 kN testing rig for in-situ characterization. The device allows tensile, compression and fatigue tests of alloys, metals or other materials at high temperatures to be performed. Up to 100 kN can be applied to the specimen with strain rates of up to 0.05 1/s at a maximum movement speed of 150 mm/min, at temperatures up to 1500 K via resistive heating. Thin aluminum windows allow for unmitigated penetration of neutron radiation and allow for in-situ neutron scattering experiments. Currently, the application range is broadened by the implementation of laser heating that will serve for samples that cannot be heated with conventional resistance heating, e.g. due to high conductivity. Four infra-red lasers with 70 W each provide the power to heat common samples up to 1200 K. The sample chamber can be operated under vacuum ( $\sim 10^{-4}$  mbar), ambient conditions or under inert gas atmosphere. An active cooling device allows for fast temperature quenching. The new equipment thus provides a large toolset for material science research. The spatial requirements are optimized for use at the strain scanner STRESS-SPEC, however the device is freely portable and can be used at other experimental stations either at MLZ (e.g. at the powder diffractometer SPODI or the small angle instrument SANS-1) or other neutron user facilities.

#### Acknowledgement

The financial support of the German Federal Ministry of Education and Research (BMBF) for the following projects is gratefully acknowledged: POWTEX (05K19PA1, 05K22PA2), SAPHIR (05K19WCA), ERWIN (05K19VK3), HZBT (05E20WO1), MIASANS (05K16WO5), KOMPASS (05K19PK1), NMO4PUMA (05K22VK1), HEiDi (05K16PA3), INGRAMM (05K22WO6), NeutroSense (05K19WO2), EMNI (05K22WO5), RAPtOr (05K19WO1), HiMat (project number 05K19WO7).

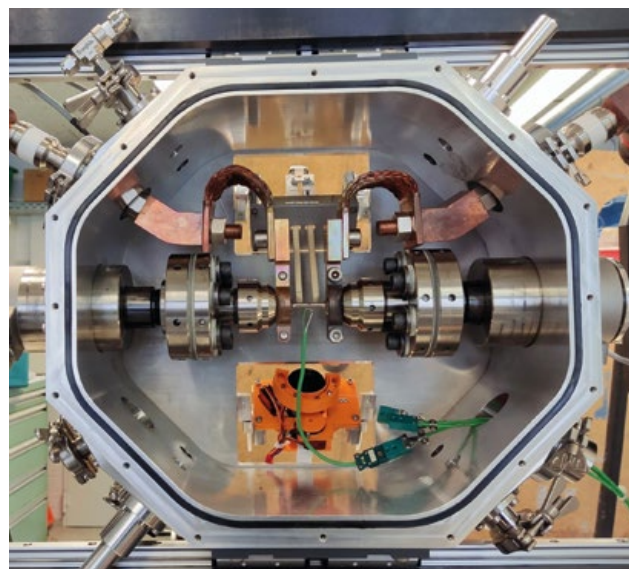
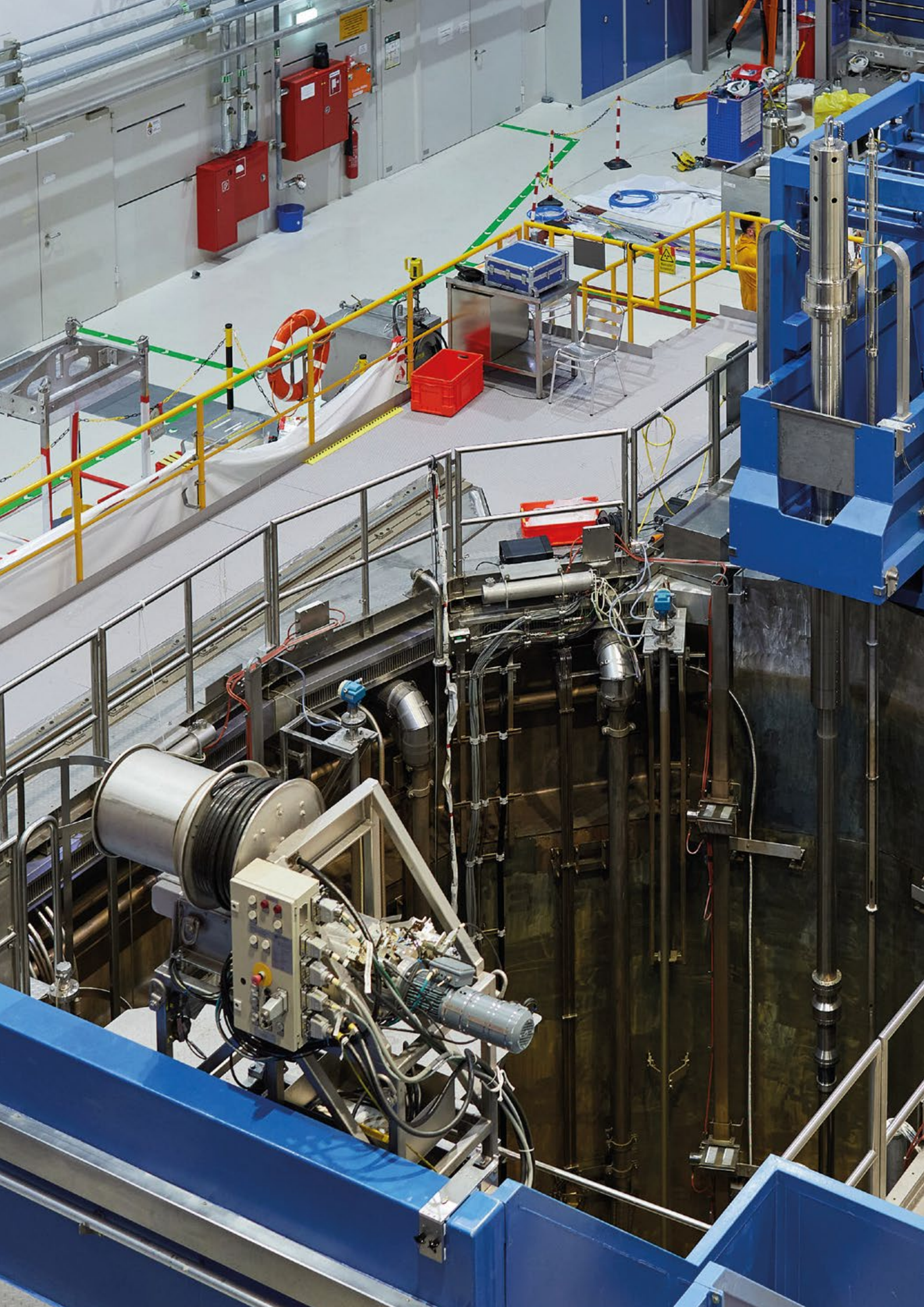


Figure 11: The new 100 kN testing machine in tensile test configuration.



# Reactor & Development



# An undesirable saga continues: more than 1300 days without neutrons, but a busy year for the FRM II

A. Pichlmaier

Forschungs-Neutronenquelle Heinz Maier-Leibnitz (FRM II), Technical University of Munich, Garching

In 2023, the FRM II was still not able to deliver any neutrons due to the continued unavailability of the “central channel” (Zentralkanal, JEC10). The manufacture of this crucial part remains challenging. Although significant progress has been made and obstacles of all kinds circumnavigated, the problem has not yet been resolved. Hence, no reactor power operation was possible in 2023 – but will hopefully be possible again soon. On the positive side: a shipment of fresh fuel to the FRM II was accomplished and the refurbishment, as well as the inspection of various crucial reactor systems, were successfully completed.

Although the main mission of the FRM II, to provide neutrons for science, medicine and industry was not fulfilled, for the reactor crew the year 2023 was arguably busier than it would have been in a “normal” year with scheduled reactor cycles smoothly delivered. Significant tasks necessary for future operation were successfully completed, both behind the scenes and in plain sight.

## Many tasks beyond regular schedule accomplished in 2023

Obviously, the main task of the reactor crews is to operate the reactor. Even in times without power operation, the reactor safety functions must be up and running at all times. To prove that this is always the case, a large test and inspection

program is carried out. This program is almost independent of power operation and in significant areas tied to the nuclear license. It includes about 1800 in-service inspections and 60 site walk-downs by the technical support organization (TSO; at FRM II the TÜV SÜD is entrusted by the regulator with the duties of the TSO) and about 40 technical modifications with formal change request requirements. The modifications can be triggered, e. g., by ageing, obsolescence, changed mode of operation or external requirements or requests. The inspections displayed beyond any doubt the excellent overall condition of the reactor systems. Some of the tasks and changes had been anticipated in order to minimize shut-down times in the future. The main renovation projects accomplished in 2023 were:

- **Refurbishment of the tertiary cooling loop (PAB/PAQ):** After years of operation, it was time for a more general overhaul. Prominent examples of this work package include the exchange or overhaul of the water conditioning systems and the cooling fans, including transmission and motors, as well as improved corrosion protection of the steel structures of the cooling towers.
- **Refurbishment of the electric and electronic components of the crane in the reactor hall (SMA10):** new normative requirements made a complete overhaul of every crane relevant for nuclear safety necessary. This long-term project started with the most prominent crane (SMA10),



Figure 1: July 2023: Fresh fuel arrives at the FRM II.

which is required for almost every task in the reactor hall, including fresh and spent fuel handling. This has not yet been completed.

- **Exchange of the polymer gaskets in the housings of the neutron detectors in the reactor pool:** After 20 years of operation under water, such an exchange became necessary. Although theoretically foreseen, this task had never been carried out before and a number of dedicated tools had to be constructed. The task is on-going.
- **Non-destructive tests in the primary cooling loop (JEA):** The primary cooling loop is inspected regularly. Most of the inspections made in 2023 are due every 5 years and include RT (x-ray testing), ET (eddy-current testing), PT (penetration testing) and VT (visual inspection).
- **Periodic safety review (PSR):** International standards require a periodic safety review to be carried out every ten years. This is in addition to the aforementioned inspections, the aim being to provide a global view of the inspection program and the status of the installation. It looks at the operational experience and lessons learned. The next PSR is due in 2024.

#### **Irradiation activities during the shut-down**

Using gamma radiation from spent fuel may be only a niche-product – yet an important one. It changes the negative connotation associated with spent fuel into a positive one, presenting it as a useful product. Gamma irradiation is important for the characterization of rock salt considered a promising candidate for a spent fuel repository or, more recently, as a cavern for H<sub>2</sub>-storage required for the energetic transition. Other applications include the creation of color centers in gem stones or the test of satellite electronics under the gamma stress in space. Even medical applications seem possible in the future. Gamma spectroscopy, in some sense related to gamma irradiation, is now also routinely offered as a service.

The shooting star of the medically used radio isotopes is doubtlessly <sup>177</sup>Lu. The FRM II started activities to significantly increase its production capabilities with the goal of making them available as soon as possible.

#### **Mission accomplished:**

##### **Transport of fresh fuel to the FRM II**

After several years of negotiations, of progress and setbacks, fresh fuel was finally shipped to the FRM II this year. The physical transport remained full of suspense until the very last moment when heavy storms, lightning and rain threatened its progress. However, leaving nothing to chance, the operation was safely concluded.

The transport question has still not permanently been solved and future transports might remain as challenging as ever. However, this first shipment in years gives some

confidence and peace of mind for reactor operation and for future transports.

#### **Central Channel (“Zentralkanal” JEC10)**

The Central channel is the root cause of the current absence of power operations at the FRM II. A new one needs to be manufactured and mounted before power operations will be able to resume. Manufacturing made good progress in 2023, although it was far from easy to accomplish: following internal difficulties with the main contractor, the whole project had to be readjusted. Nevertheless, the raw material could be successfully qualified. Other important sub-projects like the welding of the bellows were completed. More details on the overall project can be found, e. g. in last year’s MLZ-report.

#### **Manufacturing of the In-pile part of the Cold Neutron Source (CNS)**

Since the failure and removal of the in-pile section of the Cold Neutron Source (CNS), significant efforts went into its timely replacement. In the overall context however, “timely” does not mean days or weeks but several years. It was possible to purchase all major materials. Many required so called non-conformity reports (NCR) to be written by FRM II and evaluated by the TSO, since the material initially specified was no longer available on the market. A large number of procedures need to be created and evaluated for almost every step of the project. Still, the project is moving forward and some of the initial welding tests have already been completed successfully.

#### **Conversion of FRM II to fuel of low enrichment (from HEU to LEU)**

In 2023 the decision was taken to convert the FRM II to LEU. This goes far beyond the requirements of the reactor license or the conversion agreement but is the only way to secure the long-term operation of the FRM II. While it is too early to elaborate on any concrete technical steps taken at the FRM II; visible for all is the new organizational structure in the nuclear fuel laboratory and the creation of a new unit “fuel conversion” (Teilbereich 2.6 “BE Umrüstung”) within the FRM II exclusively devoted to achieving the fuel conversion.

#### **Outlook**

“Prediction is very difficult, especially about the future.”<sup>1</sup> This is particularly true in projects of nuclear procurement. However, we do what we can to make the restart of the FRM II possible again soon. While at the time of writing this task appears to be feasible, it remains challenging and will, with all its sub-projects, continuously be the most prominent task for the year 2024.

<sup>1</sup> Attributed to many including W. Churchill and N. Bohr. However, the origin of this bon mot is not quite clear, as is the future.

# Experiments to support conversion of FRM II to Low Enriched Uranium (LEU)

C. Reiter, J. P. Acuna, T. Azzouni, D. Bonete-Wiese, J. Brotz, T. Chemnitz, C. Ehrich, A. Kloh, J. Mercz, P. Salazar, L. Schirmer, T. Schlitt, R. Schönecker, K. Shehu, P. Weimer

Forschungs-Neutronenquelle Heinz Maier-Leibnitz (FRM II), Technical University of Munich, Garching, Germany

**B**oiling phenomena during transient states significantly influence nuclear research reactor operations, with safety protocols emphasizing the avoidance of uncontrolled boiling to mitigate safety risks. However, accurately assessing boiling occurrences and types during transients requires computer programs capable of capturing physical processes accurately as the calculation of different transients is a standard procedure for safety analysis. Unfortunately, modern Computational Fluid Dynamics (CFD) programs struggle to model boiling at low pressures, presenting challenges for research reactor safety assessment.

To address these challenges, new experiments under precisely defined conditions are necessary. The Technical University of Munich (TUM) has developed the TUM Loop for Obtaining Knowledge in nucleate boiling (TUM.LOKI) to investigate boiling phenomena at low pressure. TUM.LOKI facilitates the validation of CFD simulations for low-enriched U-10Mo fuel elements and makes it possible to study mechanical properties and flow restrictors crucial for LEU conversion scenarios. A state-of-the-art 3D tomography Particle Image Velocimetry (PIV) system, supported by a novel AI approach for data analysis, allows for coolant flow analysis and vibration visualization.

Additionally, the construction of a more powerful test rig, TUM.Thermal Hydraulic IoOp for research Reactors (TUM.THOR), aims to simulate realistic research reactor conditions, focusing on pressures, flow velocities, and heat fluxes.

Meanwhile, collaboration with McMaster University provides access to their experimental infrastructure, such as the McMaster Hydraulic Loop, permitting state-of-the-art measurements to support the conversion of FRM II. The McMaster hydraulic loop, renowned for its adaptability and versatility, facilitates the generation of conclusions essential for the advancement of contemporary CFD codes.

Furthermore, various transients can be conducted with the McMaster Nuclear Reactor (MNR), serving as a valuable data source for instrumented reactor cores, ultimately leading to more sophisticated conversion scenarios. This collab-

oration exemplifies a comprehensive approach to address current questions related to conversion, enhancing our understanding of nuclear reactor operations and safety.

## Norse gods for thermal-hydraulic experiments

During transient states, boiling phenomena play a crucial role in the operation of nuclear research reactors. In contrast to power reactors, where controlled boiling is sometimes intentional, the safety concept of many research reactors, such as the Forschungs-Neutronenquelle Heinz-Maier Leibnitz (FRM II), is based on avoiding boiling under all circumstances. This is crucial as uncontrolled boiling can lead to significant safety risks.

However, to adequately assess whether boiling occurs during transient states and, if so, what type of boiling occurs, the computer programs used for conversion analyses must be capable of accurately capturing the physical processes. Unfortunately, given the current state of science and technology, it is known that modern Computational Fluid Dynamics (CFD) programs used to calculate transients struggle to adequately capture boiling at low pressures. This presents a significant challenge as accurate prediction of boiling behavior under these conditions is essential for reactor safety assessment.

To develop better boiling models and improve understanding of boiling phenomena, and especially heat transfer at low pressure, new experiments under precisely defined conditions are required. The Technical University of Mu-

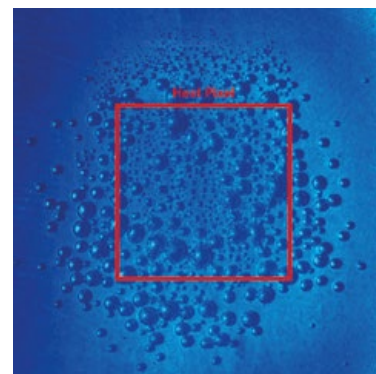


Figure 1: Image of the heated surface in TUM.LOKI taken with a high-speed camera. In this experiment only one heating pixel was installed and the covered area is marked in red. The resulting steam bubbles due to surface boiling can be seen.

nich (TUM) has already constructed and put into operation a small test rig called the TUM Loop for Obtaining Knowledge In nucleate boiling (TUM.LOKI). This test rig allows for the examination of steam bubble content and bubble detachment from the wall. TUM.LOKI is specifically designed to investigate boiling phenomena and heat transfer at low pressure and permits detailed optical data evaluation, including the use of an existing high-speed camera. So called "heating pixels" are used to heat the surface.

With the instrumented test section of TUM.LOKI, the validation of CFD simulations for a low-enriched U-10Mo fuel element can be pushed forward. Additionally, such a test section allows for the study of the mechanical properties of the fuel plates as well as the flow restrictor, which is essential for an LEU conversion scenario. Using a state-of-the-art 3D tomography Particle Image Velocimetry (PIV) system, which was purchased in 2023, the resulting coolant flows can be analyzed, vibrations of the fuel plates made visible, and the effectiveness of various designs for a flow restrictor assessed. For the analysis of the data, a novel approach based on Artificial Intelligence will be applied, which has already proven its performance in small-scale experiments. For the evaluation of the expected data volumes, an upgrade of the existing hardware was necessary, which is why a powerful Graphics Processing Unit cluster was also procured.

As a next step, a significantly more powerful test rig, TUM.THOR, will be constructed and commissioned. Through extensive integration of heating pixels, heat fluxes of up to 500 watts/cm<sup>2</sup>, as encountered in high-performance research reactors (including FRM II), will be realized. The large-scale experiment TUM.THOR aims to experimentally simulate realistic research reactor conditions, focusing on pressures, flow velocities, and heat fluxes. Within the framework of the proposed project, another hydraulic circuit will be established in a laboratory at TUM Center for Nuclear Safety and Innovation (CNSI), here, the Chair of Nuclear Engineering, allowing for the generation of a heating power profile. "Heating pixel" technology, the same as that used in TUM.LOKI, will also be employed to heat the test rig, enabling the replication of various heating profiles. Modern control software facilitates the adjustment of time-dependent heating powers and profiles, enabling, among other things, the simulation of decay heat. Although TUM.THOR is primarily designed for heat transfer phenomena without phase change, boiling can still be achieved in the test setup, thereby making possible the study of the effects of increasing steam content in the coolant water.

Several bypasses additionally permit the replication of Loss-of-Coolant-Accident (LOCA) and Loss-of-Flow-Accident (LOFA) scenarios. State-of-the-art instrumentation at

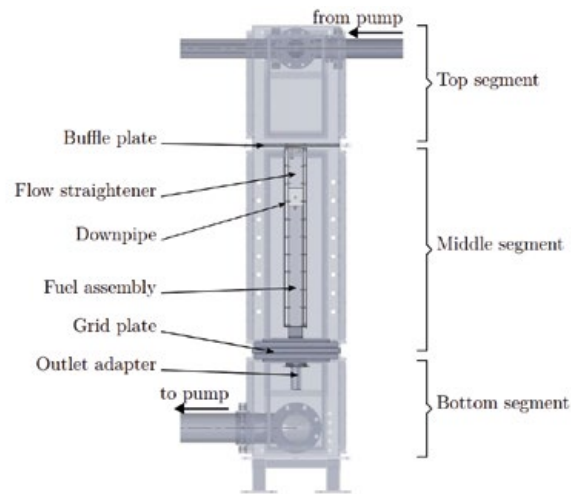


Figure 2: Schematic illustration of the McMaster university hydraulic loop test section (transparent) including the adapter structure with the relevant denomination to accommodate the flow to the desired condition.

the facility enables the acquisition of precise data during the transient events, facilitating a comparison with computer simulations conducted in Ansys CFX/Fluent and Relap 5.

### Canada is supporting the conversion

McMaster hydraulic loop, renowned for its adaptability and versatility, serves as a paramount testing platform capable of accommodating a wide array of experiments, ranging from full-scale fuel element assessments to the evaluation of intricate core-loading configurations. Empowered by cutting-edge instrumentation and advanced control software, the McMaster hydraulic test loop stands at the forefront of experimental research, facilitating the generation of indispensable conclusions pivotal to the establishment of a comprehensive verification and validation (V&V) database essential for the advancement of contemporary CFD codes.

TUM.CNSI utilizes the collaboration with McMaster university to test and further develop expertise on current questions related to conversion. Access to their experimental infrastructure, such as the McMaster hydraulic Loop, as described above, allows for state-of-the-art measurements to support the study of different conversion scenarios. Additionally, various transients can be conducted via MNR, serving as a valuable data source of the instrumented reactor core, thus generating vital experimental data. This enables not only the validation of computational programs but also, more importantly, the direct experimental verification of specific material requirements, ultimately leading to more sophisticated conversion scenarios.

### Acknowledgement

This work was supported by a combined grant (FRM2023) from the Federal Ministry of Education and Research (BMBF) and the Bavarian State Ministry of Science and the Arts (StMWK).



# Facts & Figures



## The year in pictures

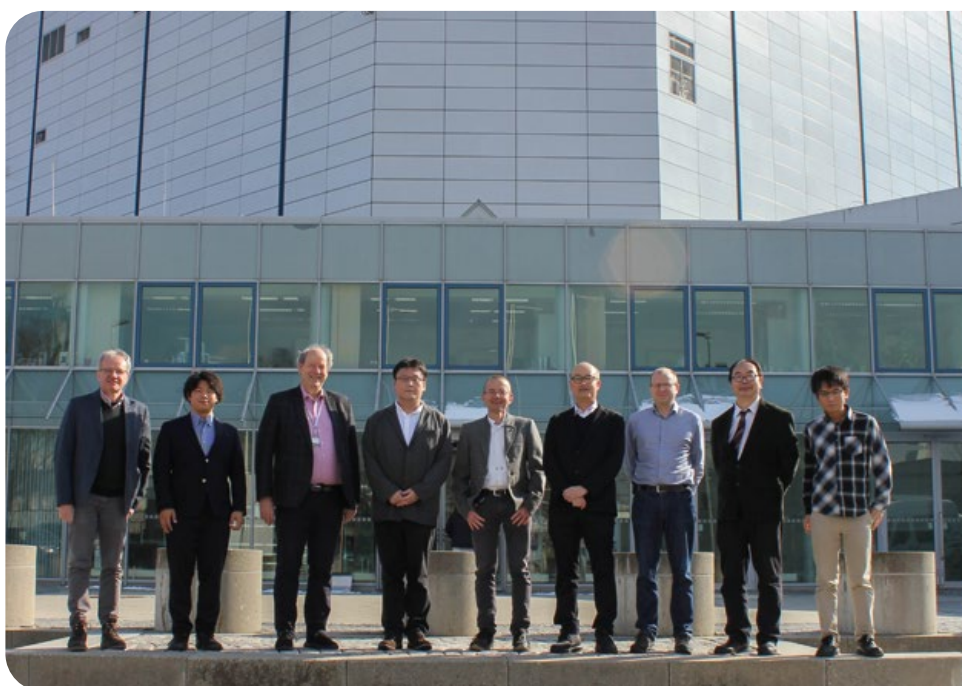


**FEBRUARY 17<sup>th</sup>**

**Insight into the reactor** – The Miesbach group of the conservative party CSU toured the neutron source.

**FEBRUARY 28<sup>th</sup>**

**From Japan to Garching** – A Japanese delegation from Kyoto university was given a tour and insights into technique and research at the FRM II und MLZ by Technical Director, Dr. Axel Pichlmaier (middle), Deputy Scientific Director, Dr. Jürgen Neuhaus (3<sup>rd</sup> from left), Prof. Dr. Christoph Hugenschmidt (left) and Florian Jeschke (3<sup>rd</sup> from right).



**MARCH 1<sup>st</sup>**

**No life without water** – Dr. Sebastian Busch from Helmholtz-Zentrum Hereon explains in his public talk for 100 visitors at the Deutsches Museum Munich, why the small molecule  $\text{H}_2\text{O}$  is so important. 17,500 have watched the video on YouTube so far.



**FEBRUARY 24<sup>th</sup>**

**Taking advantage of the maintenance break –**  
The crane in the FRM II reactor hall receives  
new control technology.



**MARCH 23<sup>rd</sup>**

**Congratulations, Prof. Dr. Martin Müller** – The League of Advanced European Neutron Sources (LENS) has elected the MLZ Director, Helmholtz-Zentrum Hereon Director and Professor at the University of Kiel as its new Chair.

**MARCH 23<sup>rd</sup>**

**From Sydney to Garching** – The MLZ was happy to host Prof. Dr. Maxim Avdeev (r.), Diffraction Group Manager at the ANSTO and Professor at the University of Sydney, during a recent visit. The MLZ Science Group “Structure Research” with its manager Dr. Anatoliy Senyshyn acted as local host.



**APRIL 18<sup>th</sup>**

**Most powerful reactor in Germany** – The commercial use of nuclear power for electricity generation in Germany has ended. This decision does not include the Research Neutron Source Heinz Maier-Leibnitz (FRM II), which now makes this the most powerful German reactor. The reactor operation team with Technical Director Dr. Axel Pichlmaier (m.) is ready to take on the challenges of the future, using the downtime to update the research reactor technically.

**APRIL 20<sup>th</sup>**

**Shortage of medical radioisotopes –**

A panel discussion with the FRM II presenting its capacity in radioisotope production in front of more than 300 nuclear medicine specialists at the conference of the German Association of Nuclear Medicine (DGN) in Leipzig.



**MAY 19<sup>th</sup>**

“The neutron source is addressing important questions as how to diagnose and treat cancer” – states Permanent Representative of the German UN Mission in Vienna, Dr. Götz Schmidt-Bremme (2<sup>nd</sup> from left) after his visit to the FRM II. Head of Nuclear Science, Theory Division (TUM.CNSI) Dr. Christian Reiter (l.) and Deputy Scientific Director Dr. Jürgen Neuhaus (2<sup>nd</sup> from right) accompanied him and his colleague, Johannes Beck, to the reactor pool.

**MAY 22<sup>nd</sup>**

**Common interest in nuclear technology –**

Visit from McMaster University with Deputy Scientific Director Dr. Jürgen Neuhaus (l.), Prof. Dr. Bastian Märkisch, TUM (3<sup>rd</sup> from left) and Dr. Christian Reiter (3<sup>rd</sup> from right) welcoming the guests from Canada (from left): Dr. Sarah Dickson-Enderson, Associate Dean at the Faculty of Engineering, Prof. Dr. Heather Sheardown, Dean of the Faculty of Engineering and Soren Harbel, strategic advisor.





**JUNE 13<sup>th</sup>**

**Recruiting young talents for nuclear technology** – Stephanie Mayr and Alexander Wunderskirchner (r.) with two prospective applicants at the FRM II booth of the jobfair KERNTec in Frankfurt am Main.

**JUNE 19<sup>th</sup>**

**Trapping matter and antimatter** – The plasma physicist Dr. Eve Stenson presents her experiments using positrons at the FRM II at a public talk called Café und Kosmos in Munich.



**JUNE 20<sup>th</sup>**

**New head of the International Group of Research Reactors (IGORR)** – FRM II Technical Director, Dr. Axel Pichlmaier (l.), is the newly elected Chairman of IGORR, following Dr. Gilles Bignan (m.). Sean O'Kelly (r.) was elected vice-chairman.

**JULY 3<sup>rd</sup>**

**Visit from the funding bodies** – Representatives of the German federal and Bavarian state ministries for science visit the FRM II and MLZ with the Chancellor of the Technical University of Munich, Albert Berger (back, 2<sup>nd</sup> from left), the MLZ and FRM II Scientific Directors Prof. Dr. Martin Müller (front, 2<sup>nd</sup> from right) and Prof. Dr. Peter Müller-Buschbaum (back, 3<sup>rd</sup> from left), Technical Director Dr. Axel Pichlmaier (front, middle) and Administrative Director Robert Rieck (back, left).



**JULY 4<sup>th</sup>**

**Hospital meets neutron source** – Scientific Director, Prof. Dr. Peter Müller-Buschbaum (front row 4<sup>th</sup> from right) welcomed nuclear medicine specialists from the University Hospital Rechts der Isar of the Technical University of Munich.

**JULY 14<sup>th</sup>**

**From south to north** – Dr. Jürgen Neuhaus (2<sup>nd</sup> from left), FRM II Deputy Scientific Director welcomes representatives from the SAFARI reactor, South Africa (from right): Deon Marais, Tatij Tjebane and Andrew Venter, who plan to build a new multi purpose reactor.



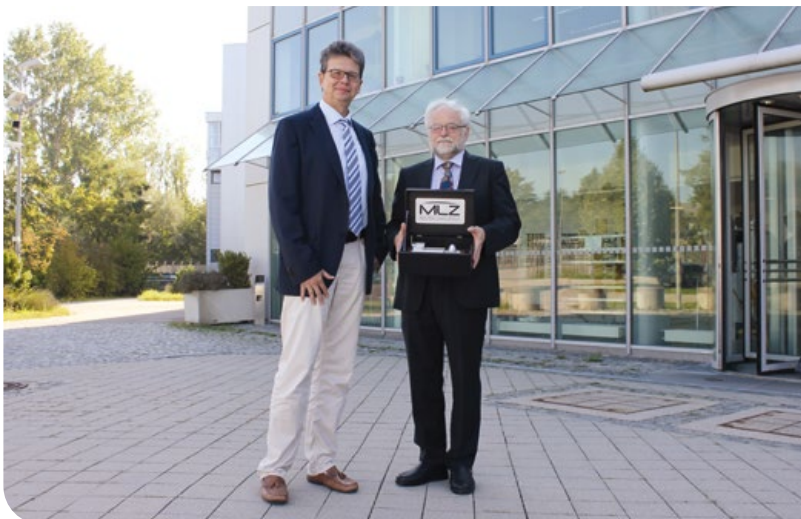


**AUGUST 3<sup>rd</sup>**

**Reliable supply of neutrons needed in Germany** – Bettina Stark-Watzinger visited the neutron source in her capacity as a member of the German parliament for the FDP and emphasized the important role of the MLZ and FRM II.

**SEPTEMBER 7<sup>th</sup>**

**Award for instrument construction** – This year's MLZ Prize for Instrumentation and Scientific Use goes to Prof. Dr. Wolfgang Schmahl from the Ludwig-Maximilians-Universität München. He has rendered outstanding services to the construction and operation of the scientific instruments RESI and SPODI.

**SEPTEMBER 26<sup>th</sup>**

**Political visit from Ahaus** – The spent fuel elements of the FRM II are to be transported to the Ahaus interim storage facility. A political delegation from the North Rhine-Westphalian city visited the neutron source and the city of Garching for the first time for an exchange.

**OCTOBER 3<sup>rd</sup>**

**Organizing team for mouse day** – Together with 16 other institutes, the FRM II led the open day for children and adults on the Germany-wide day of the "Sendung mit der Maus".





**OCTOBER 3<sup>rd</sup>**

**Open doors at the FRM II** – 270 adults booked guided tours at the research neutron source and around 5,000 visited the exhibition and hands-on activities on the campus.

**NOVEMBER 8<sup>th</sup>**

**Exactly the right position** – Our team at the Hochschulkontaktmesse, the job fair at the University of Applied Science in Munich, promoting student and permanent jobs, Master and Bachelor theses at the FRM II and MLZ booth.



**DECEMBER 18<sup>th</sup>**

**Proud of the FRM II** – are the two members of the Bavarian state parliament, Benjamin Miskowitsch (r.) and Maximilian Böttl (l.), who visited the research neutron source together with FRM II reactor physicist Dr. Christian Reiter.



**OCTOBER 17<sup>th</sup>**

**Cool towers** – The ventilation rotors, gearbox and engines inside the FRM II cooling towers have been prophylactically exchanged after a 20 year lifespan. They are permanently exposed to steam.

## In memoriam

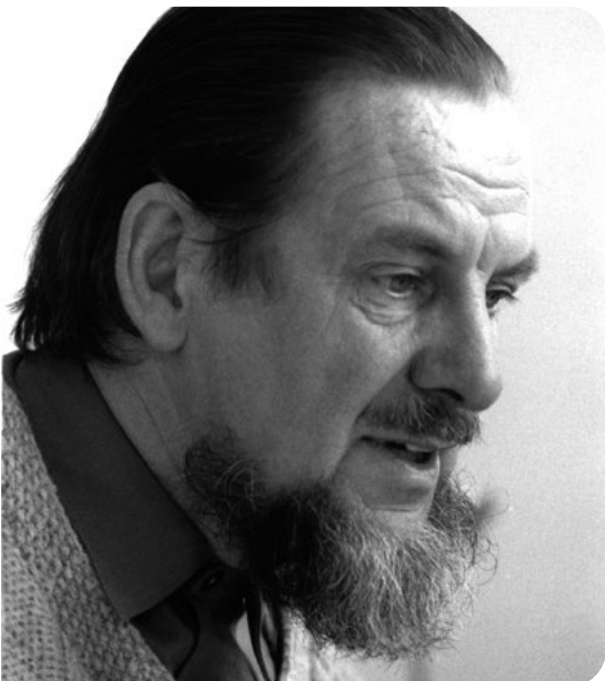


### FEBRUARY 4<sup>th</sup>

He was the successor of Heinz Maier-Leibnitz and contributed significantly to the fact that the most modern neutron source in the world is located in Garching. Prof. Dr. Wolfgang Gläser has passed away at the age of 89.

### SEPTEMBER 13<sup>th</sup>

Our much-loved and highly respected long-standing colleague, Dr. Marie-Sousai Appavou, employed first at the Technical University of Munich and then the Forschungszentrum Jülich, passed away suddenly at the age of 46.



### OCTOBER 2<sup>nd</sup>

Dr. Wolfgang Waschkowski, who was part of the project management for the construction of the FRM II for many years, has died at the age of 84. He had been awarded the Order of Merit of the Federal Republic of Germany for his commitment to the realization of the research neutron source.

# Workshops, Conferences and Schools



March 20–23: **European Conference on Neutron Scattering 2023, Garching**



April 26–27: **MORIS User Workshop, Garching**



May 3: **FullProf Workshop 2023, Garching**



May 22: **DAPHNE Workshop – Data from PHoton and Neutron Experiments**



May 10: Laboratoire Léon Brillouin (LLB)-MLZ Workshop



### MLZ internal workshop in Grainau

From 19 – 22 of June the MLZ biannual internal workshop took place in the picturesque environment of Grainau close to Garmisch-Partenkirchen. 130 participants from the Heinz Maier-Leibnitz Zentrum (MLZ), the universities TUM, Aachen, Köln and LMU, as well as the colleagues from the Max Planck Institutes and the KIT in Karlsruhe met for discussing about the science and instrumentation on the MLZ.

The program consisted in discussions in plenary and parallel sessions managed by the science groups of MLZ as well as in plenary scientific talks about particle physics with neutrons, magnetic interactions and neutrons for food. A conference dinner after a hike to the hotel at the Riessersee and an excursion to the research station in the Schneefernerhaus on the Zugspitze offered ample time for discussion with the colleagues. A very exciting evening talk by Dr. Sandra Kortner from the Max Planck Institute of Physics “revealed nature’s secrets with the Higgs boson”.



May 22–25: **MLZ Conference 2023: Neutrons for Biomaterials, Fürstenried**



June 28–30: **Workshop and hands-on Tutorial on Tools and Shells at Bilbao Crystallographic Server, Garching**



July 3–7: **F-Praktikum, Hands-on training for TUM physics students, Garching**



July 24–28: **Sino-German Forum STRESS-SPEC, Garching**



### Neutron sciences are accelerating at MLZ

Started on 1<sup>st</sup> September 2021, the GNeuS project is providing a unique space for cutting-edge research with neutrons, by recruiting 45 post docs over 3 calls, hosted by the GNeuS Partner organizations, Forschungszentrum Jülich (FZJ), the Technical University of Munich (TUM) and Helmholtz Zentrum Hereon (Hereon) and supervised by MLZ staff scientists.

The GNeuS program aims to train the next generation of neutron researchers to address global challenges in areas like environment, energy, key technologies, and life sciences. This 5-year initiative provides 45 fellowships,

each comprising a 24-month contract, co-financed by MLZ-partners and the European Commission under the Marie Skłodowska-Curie Actions (MSCA) program.

The program focuses on tailored training, encompassing neutron instrumentation, technique, and scattering, along with soft skills development and entrepreneurial skills.

Recent highlights include the 1<sup>st</sup> GNeuS Science Day (March 2023), fostering collaboration among fellows, supervisors, and partner organization directors. Fellows shared their research progress, leading to lively discussions and valuable feedback.



(COFUND EU Grant N. 101034266)

*This project has received funding from the European Union's Horizon 2020 Research and Innovation Programme under the Marie Skłodowska-Curie Grant Agreement N°101034266.*



September 4–15: **25<sup>th</sup> JCNS Laboratory Course – Neutron Scattering 2023, Jülich and Garching**



September 26–27:  
**ND 2.0 SPLENDID Workshop, Fürstenried**



September 26–27: **Workshop on Spin wave calculations with Takin, Garching**



October 6–8: **Texture School 2023, Garching**



October 9–12: **JCMS Workshop 2023 – Trends and Perspectives in Neutron Scattering: Future Instruments at Pulsed Sources, Tutzing**



October 18–20: **JANA Workshop 2023, Garching**



November 27: **Sample Environment Meeting, Garching**



November 21–24: **SR2A 2023 – 10<sup>th</sup> International Conference on Synchrotron Radiation and Neutrons in Art and Archaeology, Munich**



December 4–5: **MLZ User Meeting 2023, Munich**



### Data Evaluation Group at MLZ

The Data Evaluation Group (DEVA) is a team of scientists with many years of experience in selected neutron and X-ray methods. The group has organized several method-based one-day workshops in Garching to provide insights into neutron methods and the associated software needed for data analysis. The aim is to train a new generation of neutron researchers and to foster interdisciplinary partnerships between scientists and software providers to further develop the software accordingly. DEVA helps to ensure that valuable data do not remain unprocessed and unpublished.

Up to 15 students and scientists who were curious about applied software tools could participate in the workshops with lectures and practical exercises. The following softwares were available: FullProf, SteCa, OpenHKL, Grasp, QtiSAS, BornAgain, Anaklasis, ImageJ, MuhRec, KipTool, etc.

The DEVA group also supported the scientific groups "Structural Research" and "Quantum Phenomena" in the organization of software workshops with external speakers from other European institutions. The DEVA workshops were provided free of charge to participants from the MLZ User community and partner institutions.



- 07.12.2023: **DEVA Steca Workshop**
- 06.12.2023: **DEVA Rietveld Workshop**
- 17.11.2023: **DEVA Single crystal Workshop**
- 03.11.2023: **DEVA SANS Workshop**
- 24.10.2023: **DEVA GISAS Workshop**
- 16.10.2023: **DEVA Imaging Workshop**
- 11.07.2023: **DEVA PGAA Workshop**
- 10.05.2023: **DEVA SteCa Workshop**
- 13.04.2023: **DEVA Rietveld Workshop**

# Changing media presence

A. Voit, A. Görg

Heinz Maier-Leibnitz Zentrum (MLZ), Technical University of Munich, Garching, Germany

Despite long downtimes and declining research results, the Research Neutron Source (FRM II) and the Heinz Maier-Leibnitz Zentrum (MLZ), remain in the media spotlight. The press office maintains the extensive media coverage with a remarkable number of over 600 media articles in 2023, increased engagement on social media platforms and a diverse range of events. Over the year, the FRM II visitors' service welcomed 3,296 visitors and offered interesting tours of the reactor, further strengthening our public relations work.

## Media Coverage: The art of presence

With a total of 626 media articles in 2023, ranging from various scientific topics to risk issues, in print and online media as well as on TV and radio, they remain in the spotlight. This year, we recorded over 21 press inquiries.

The number of 119 (19%) scientific media articles covering research with neutrons at the MLZ and FRM II is mainly due to 17 press releases sent out by the Technical University of Munich and the FRM II, ITM Radioisotope GmbH and Framatome as well as MLZ partners such as KFN, Forschungszentrum Jülich and the University of Bayreuth. 497 contributions (79%) about the neutron source in 2023 deal with

## Media contributions in 2023 by topic area

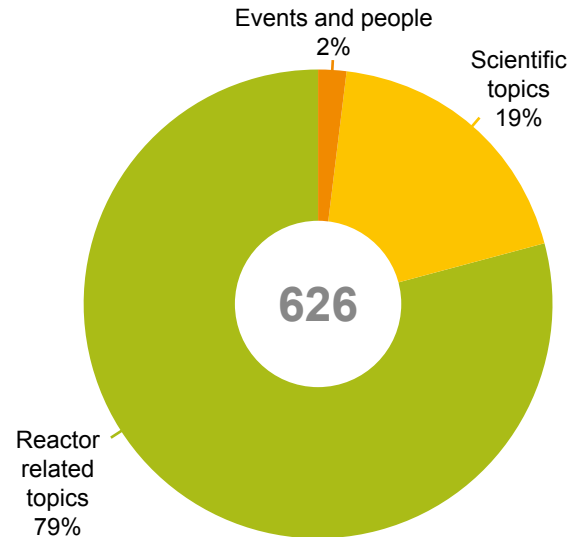


Figure 1: 19 percent of all media reports on the MLZ and FRM II in 2023 were on scientific topics. Reactor related topics include the nuclear phase-out, conversion and the future medical supply of important radioisotopes.

“reactor” topics such as the German nuclear phase-out, the restart of the research reactor, the planned conversion and the opening of the ITM production facility for lutetium 177.

As always, all 40 news items of the year can be found on our two websites [frm2.tum.de](http://frm2.tum.de) and [mlz-garching.de](http://mlz-garching.de). In addition we published three articles in the section “From Behind The Sciences”.

## Number of media articles from 2016 to 2023

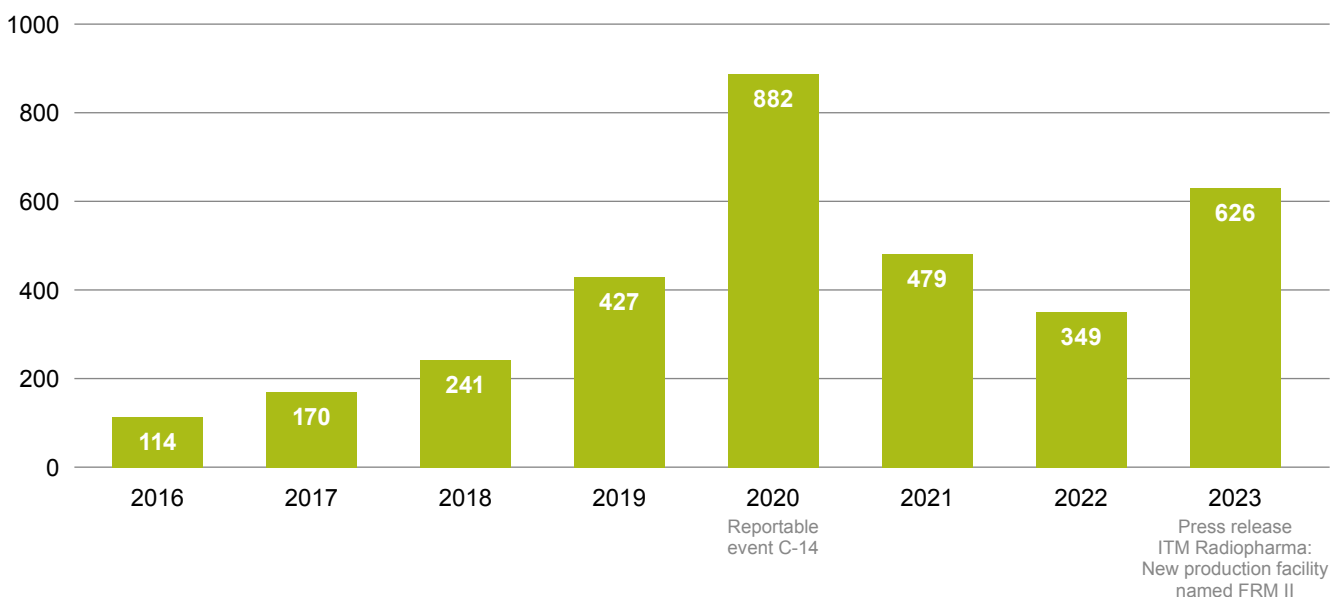


Figure 2: 626 media articles appeared in 2023 about the Research Neutron Source (FRM II) and the Heinz Maier-Leibnitz Zentrum (MLZ). This confirms the unbroken media interest that we have experienced for years despite the long shutdown of the neutron source and the lack of research results.

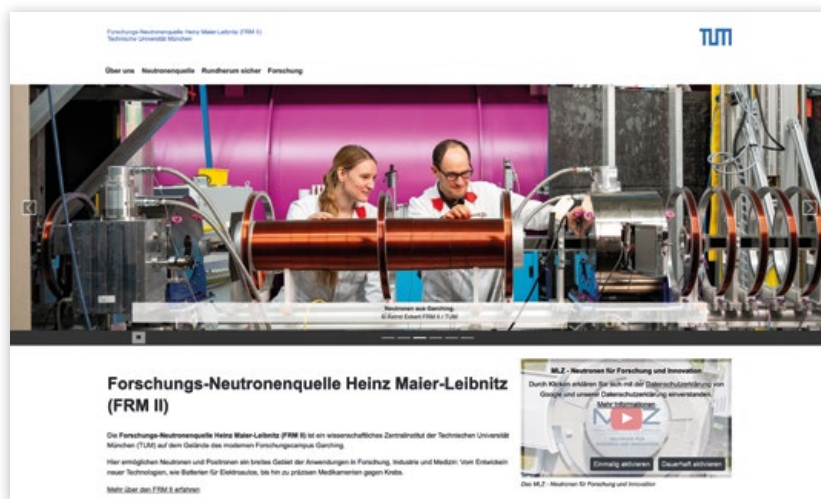


Figure 3: We are successively renewing our content on the www.frm2.tum.de website.

### New design – New content

In 2023, TUM provided an update for the Typo3 content management system. The design includes new design elements and a new layout for the homepage. As part of this, we are updating our content and adapting it to the new design.

### Accessibility = maximum user-friendliness

During the redesign, we tried to implement the basic principles of digital accessibility for our websites and digital media. With the aim, that everyone can use them easily. Every image should have a text with a description, because blind people use devices that read such texts aloud. Videos will have subtitles for people with hearing impairments and/or an audio description for visually impaired people. In order to increase the user-friendliness of our media, we are continuously working on the presentation of our content.

### Social media: The new stage for engagement

As the landscape of media consumption evolves towards social platforms, we at FRM II and MLZ have adapted by expanding our presence on these channels. While the transition from platforms such as Twitter, now known as X, has led to a decline in user engagement, we have recognized the growing importance of LinkedIn in fostering meaningful interactions. In addition, we are actively exploring the potential of visual platforms such as Instagram and YouTube to engage and connect with a younger audience.



[https://www.youtube.com/watch?v=St0PDB\\_6kuM](https://www.youtube.com/watch?v=St0PDB_6kuM)



Figure 4: The MLZ film: "Neutrons for Research and Innovation" has been on our YouTube channel since this year: [https://www.youtube.com/watch?v=St0PDB\\_6kuM](https://www.youtube.com/watch?v=St0PDB_6kuM)

## The direct line to the target groups

Events play a crucial role in engaging directly with the public to make scientific topics accessible to a wide audience. Whether through public lectures, virtual conferences or face-to-face meetings with policy makers, these are great opportunities to promote dialog with the public and raise awareness of the great research being done. We reach out to our different target groups:

### Public

*Science for Everyone:* At events like those held at the Deutsches Museum, we elucidate complex scientific concepts to the general public. Dr. Sebastian Busch's lecture on the significance of water for life garnered significant attention, with over 17,500 views on YouTube.



<https://www.youtube.com/watch?v=kqpre6Fc96s>

Welcoming several thousand science enthusiasts (children and adults) to our annual *Open Door* and *Mouse Day House* on October 3, we provided interactive experiences and engaging demonstrations, fostering curiosity and interest in our research activities. The feedback from 278 respondents to an online survey was overwhelmingly positive, so a similar day is also being planned for 2024.



Figure 5: The highlight of Mouse Day 2023 for the children: homemade ice cream!

### Users

We intensively cover prominent conferences such as the *European Conference on Neutron Scattering (ECNS)* and the *MLZ Conference*, sharing insights and updates through various social media platforms including films.

*User Meeting:* We ensure that our user community remains informed and engaged by actively participating in user meetings, facilitating discussions, and disseminating relevant information.



Figure 6: Nuclear Medicine 2023, the largest trade fair for nuclear medicine specialists in Germany. Panel discussion with the FRM II press office, patients, doctors, pharmaceutical company and a representative of the Federal Ministry of Health.



Figure 7: FRM II @ KernTec Scientific Days in Frankfurt.



Figure 8: MLZ User Meeting in December 2023, in Munich.

### Policy makers and other stakeholders

We have engaged with nuclear medicine specialists at conferences in Leipzig and Augsburg: Through presentations by the press office and discussions at these important medical conferences, we highlight the importance of our research facility in producing important medical isotopes and addressing urgent healthcare challenges.

One of the highlights of the year was the visit of the *Federal Minister of Science, Bettina Stark-Watzinger*, and the visit of the *City Council of Ahaus*: We promote constructive dialogue with political decision-makers and stakeholders, emphasizing the social impact and benefits of our research initiatives.

### Employees and potential employees

We actively participate in job fairs such as *HOKO in Munich* and *KernTec Scientific Days in Frankfurt*, showcasing employment opportunities and promoting our organization as an

attractive employer. Additionally, we provide guided tours and presentations to prospective candidates, offering insights into our research environment and career prospects.

### Conclusion

Despite the challenging circumstances caused by the continuing shutdown of the FRM II, the final shutdown of the German nuclear reactors and the dwindling research results, the FRM II and the MLZ have proven that a proactive and versatile communication strategy is crucial to stay in the media spotlight. Through continuous presence in the media, adaptation to changing trends in social media and direct interaction with the audiences, we have been able to successfully communicate our research results and explain the importance of a German neutron source to different target groups.



Figure 9: Andrea Voit & Anke Görg

# MLZ hosted the European community

I. Lommatzsch, R. Schurek

Jülich Centre for Neutron Science (JCNS-4) at MLZ, Forschungszentrum Jülich GmbH, Garching, Germany

Two events occupied the MLZ User Office this year: The European Conference on Neutron Scattering (ECNS) in March and the annual User Meeting in December. For sure, it was another year without neutrons and thus without users at the instruments, but we could hug many members of the neutron-scattering community after such a long time!

The first quarter of the year was filled with busy work preparing everything for the start of the ECNS on March 19<sup>th</sup>, 2023. For sure, rooms and lecture halls at the Campus Garching had already been booked when the European Neutron Scattering Association (ENSA), the organization behind ECNS, had chosen MLZ to host the 2023 conference some years ago. But there was a lot more to do: the programme had to be created, all participants' questions had to be answered, the catering and the choices for dinner had to be finalized, a lot of things had to be set and printed, and we even created a conference app for the event!



Figure 1: Impressions from the MLZ User Meeting 2023.

It became a huge success, as you can see from the infographic on the right. Because it was the first big neutron users' event in person after a long time, everybody enjoyed meeting colleagues again, and happy faces were everywhere!

## A User Meeting to remember

Due to the weather, this year's User Meeting on December 4<sup>th</sup> and 5<sup>th</sup> became a meeting to remember. The snow falling on December 1<sup>st</sup> and 2<sup>nd</sup> turned Munich into a beautiful white fairytale scene. Unfortunately, it also hit Munich Airport and Munich Central Station. Thus, there were only limited trains and nearly no airplanes for the following days! Participants from Austria, Hungary, and Serbia had no chance to arrive; it was very difficult for those from Spain and Italy – and even within Germany, it was nearly impossible to travel. In the end, 42 of the 250 registered participants could not make it to the venue in Munich.

On short notice, we were able to organise a kind of hybrid meeting and thus, for example, stream the plenary talks of Michael Gradzielski (TU Berlin) on ionic assembly of polyelectrolytes and surfactants and Piero Baglioni (University of Florence) on how neutrons can help to find new cleaning tools for cultural heritage artifacts. The update by the MLZ Directors was also well received online and offline, and the present scientific director of the FRM II, MLZ director and spokesperson, Peter Müller-Buschbaum, used the opportunity to introduce his successor from 2024, Christian Pfeleiderer.

A total of 63 talks and 116 posters delivered a lot of topics for discussion. The lively exchange also continued during the typical Bavarian dinner, which ended abruptly just before an icy rain started late in the evening and stopped all suburban trains in the Munich area again ...

## MLZ User Committee: Appointment prolonged

The current MLZ User Committee, Tommy Nylander, and the other members, elected normally for three years and thus active until the end of 2023, agreed to prolong their appointments until the summer of 2025. They are all eager to accompany the MLZ users during the restart of user operation.

This restart will also be a reset regarding proposals that have become outdated due to long waiting times. A new proposal round will be opened as announced during the User Meeting.

# ECNS 2023



Garching

165

talks (mostly 5 in parallel)

277

posters in total

539

participants from 27 different countries

39

sessions on 4 days



926

litre of beer were served during the conference dinner and the poster sessions

2730

small cakes, croissants, and cookies were savoured

3600

cups of coffee were consumed

1500

pretzels were eaten

# Organization

## FRM II and MLZ

The Forschungs-Neutronenquelle Heinz Maier-Leibnitz (FRM II) provides neutrons for research, industry and medicine and is operated as a Corporate Research Center by the Technical University of Munich (TUM). Scientific use of the FRM II, with around 1,200 user visits per year, is organized within the Heinz Maier-Leibnitz Zentrum (MLZ).

The chart below shows the overall network comprising the Neutron Source FRM II and the MLZ, as well as the funding bodies and the scientific users that perform experiments at the MLZ, addressing the major challenges facing present-day society.

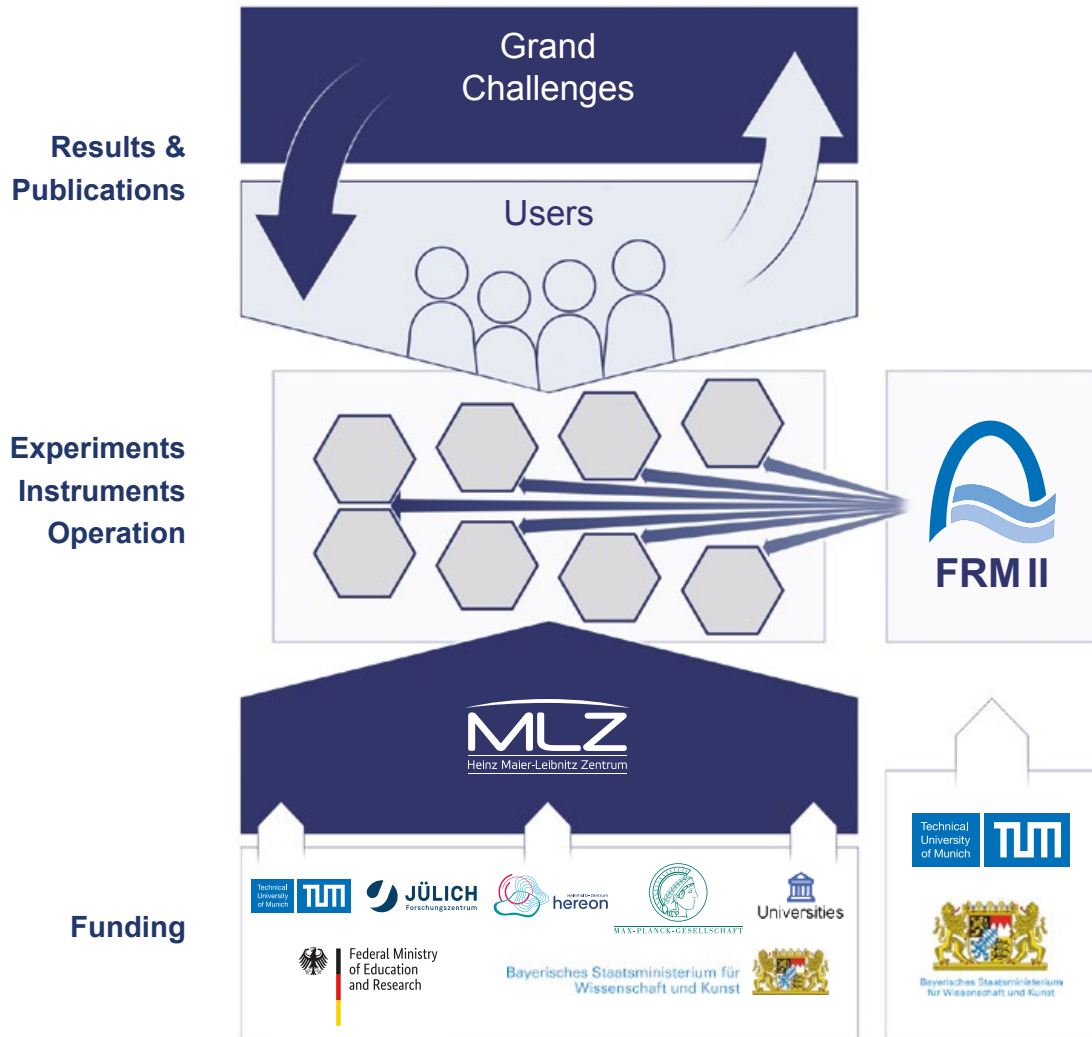


Figure 1: The neutron source FRM II and the user facility MLZ.

### Scientific Director MLZ, FRM II

Prof. Dr. Christian Pfeiderer (since 1 January, 2024)  
 Prof. Dr. Peter Müller-Buschbaum (until 31 December, 2023)

### Scientific Director MLZ, HGF

Prof. Dr. Martin Müller

### Technical Director FRM II

Dr. Axel Pichlmaier

### Administrative Director FRM II

Robert Rieck

## Scientific Cooperation at the Heinz Maier-Leibnitz Zentrum (MLZ)

The Heinz Maier-Leibnitz Zentrum with its cooperating partners, the Technical University of Munich (TUM), Forschungszentrum Jülich GmbH (FZJ) and Helmholtz-Zentrum hereon GmbH is rooted in a network of strong partners including the Max Planck Society (MPG) and numerous university groups that benefit from scientific use of the Forschungs-Neutronenquelle Heinz Maier-Leibnitz. The organizational chart of the MLZ is shown below.

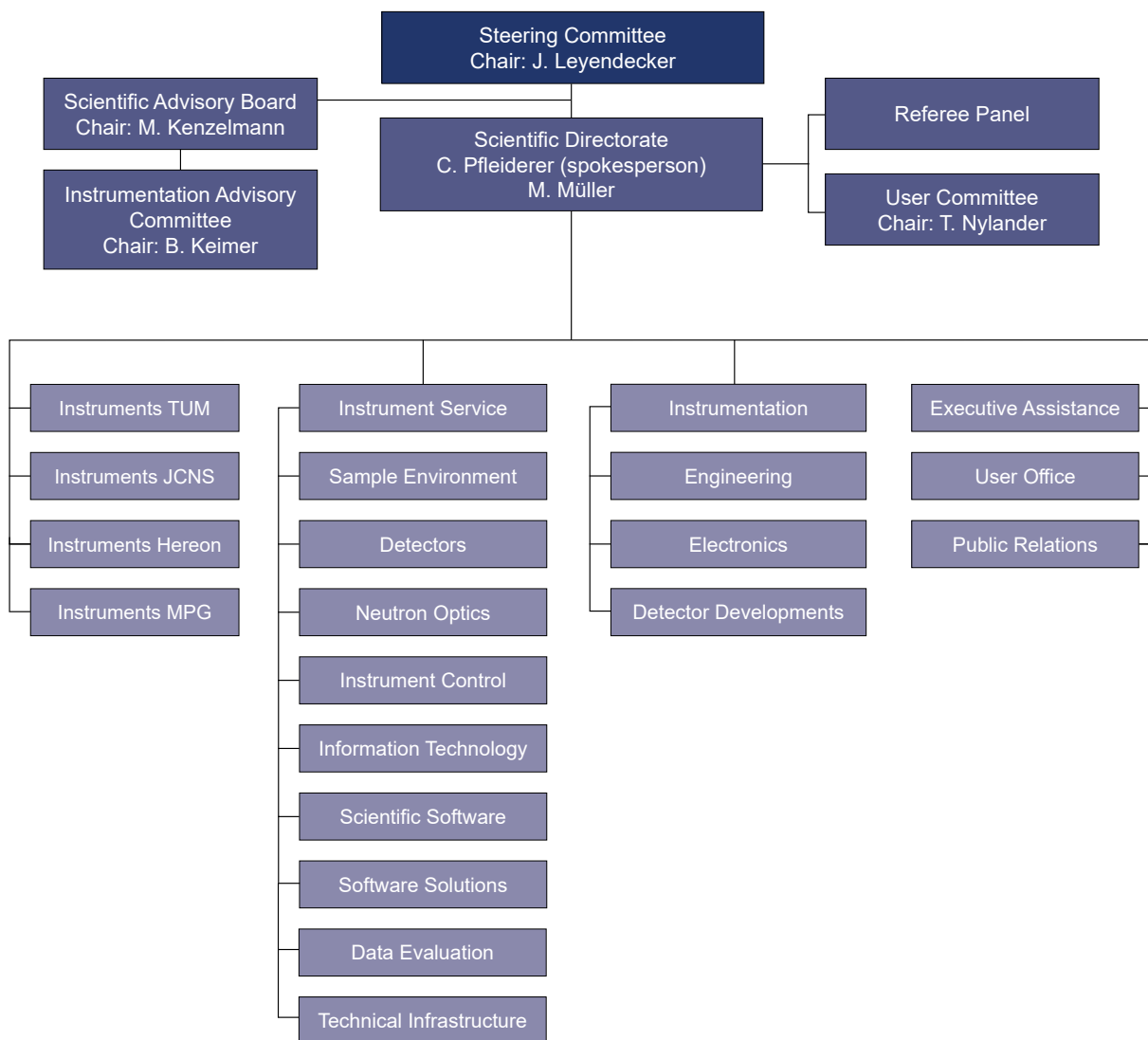
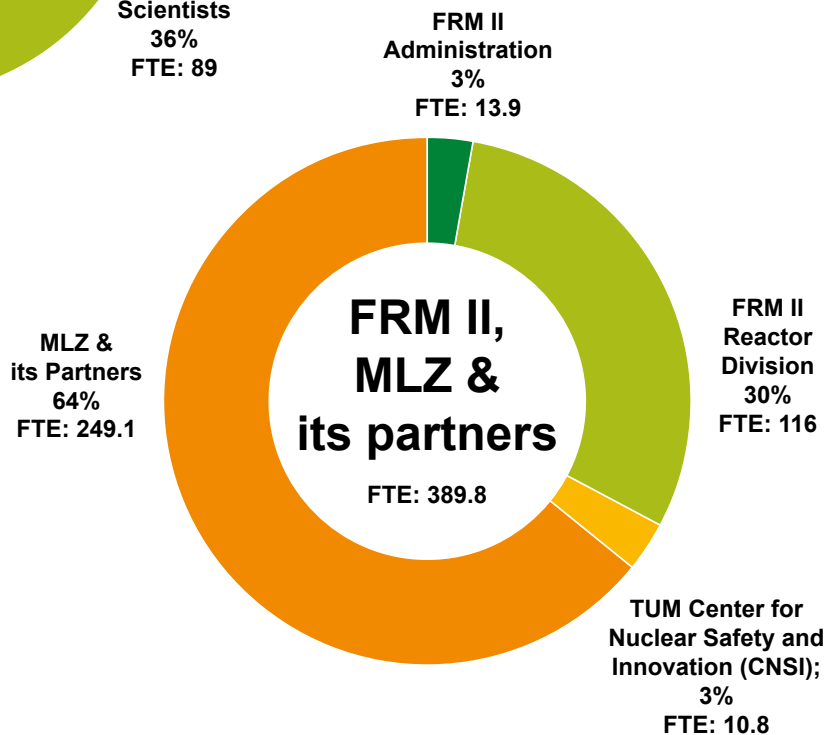
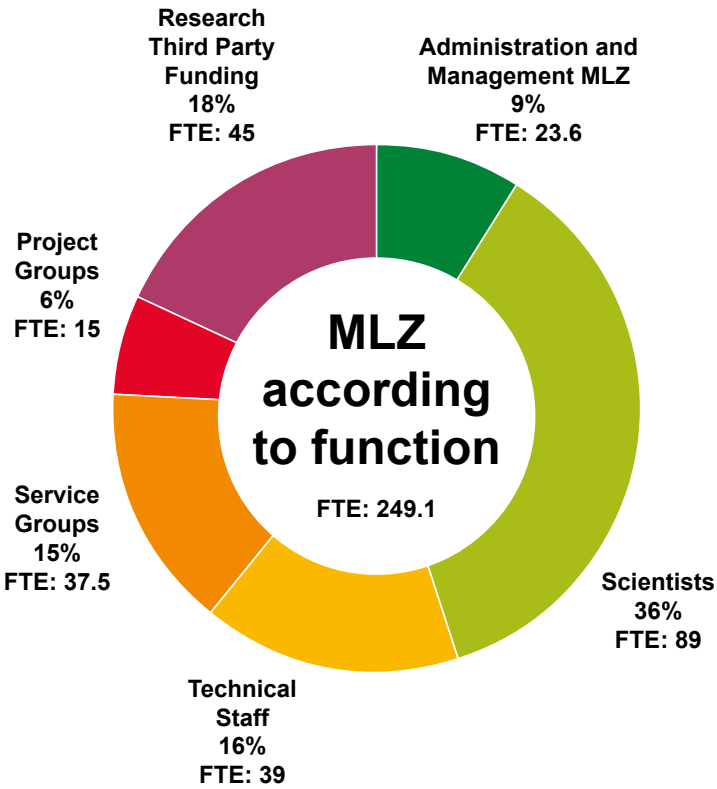
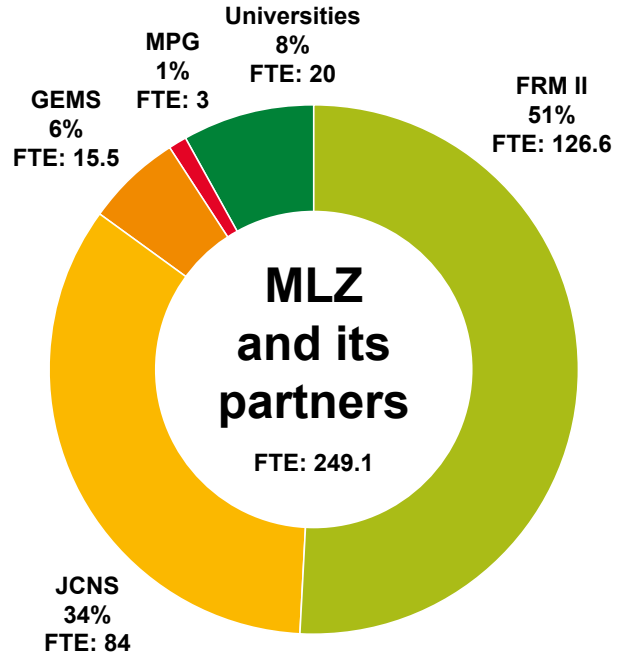


Figure 2: Organizational chart MLZ.

# Staff

The charts below show the staff of MLZ and FRM II. The staff of MLZ, as per their share among the partners with a detailed break-down of their function within the MLZ is also depicted.



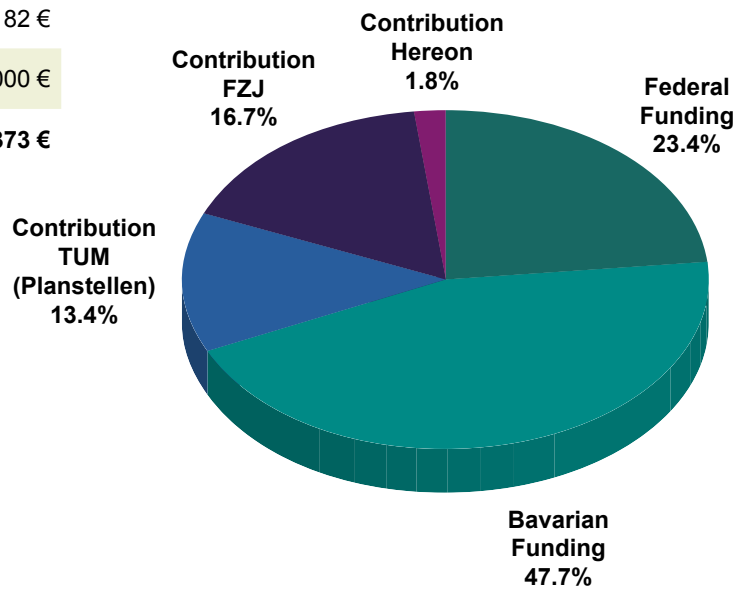
FTE = Full Time Equivalent

# Budget

The tables and charts below show the revenue and expenses for 2023.

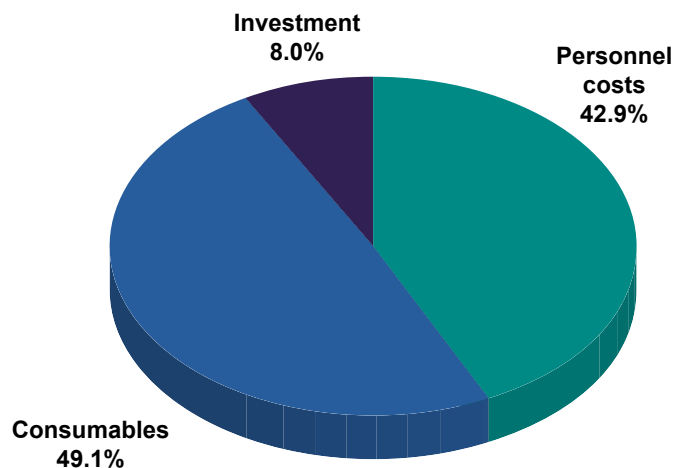
## Revenue 2023

Federal Funding	16.700.000 €
Bavarian Funding	31.971.270 €
Contribution TUM (Planstellen)	9.551.921 €
Contribution FZJ	11.915.182 €
Contribution Hereon	1.320.000 €
<b>Total</b>	<b>71.458.373 €</b>



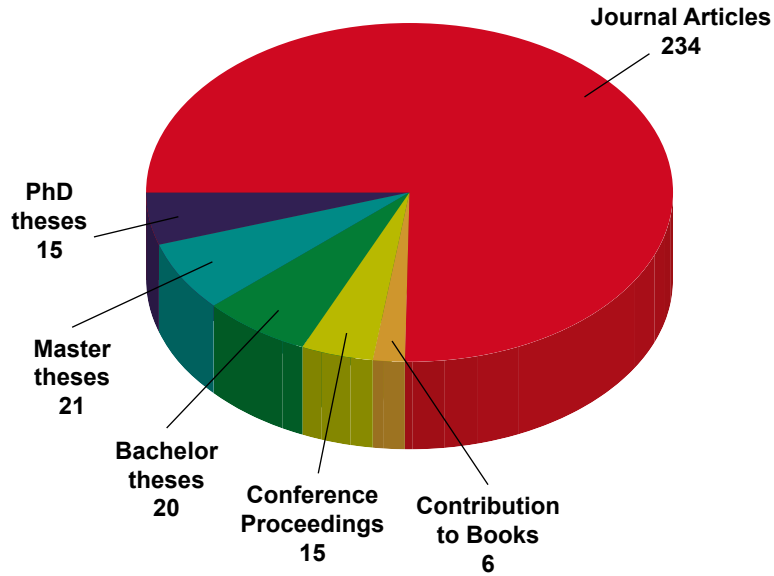
## Expenses 2023

	TUM	FZJ	Hereon	Total
Personnel costs	18.354.216 €	10.847.951 €	1.575.000 €	30.777.167 €
Consumables	31.190.950 €	3.633.011 €	340.000 €	35.163.961 €
Investment	2.740.423 €	2.624.220 €	361.000 €	5.725.643 €
<b>Total</b>	<b>52.285.589 €</b>	<b>17.105.182 €</b>	<b>2.276.000 €</b>	<b>71.666.771 €</b>



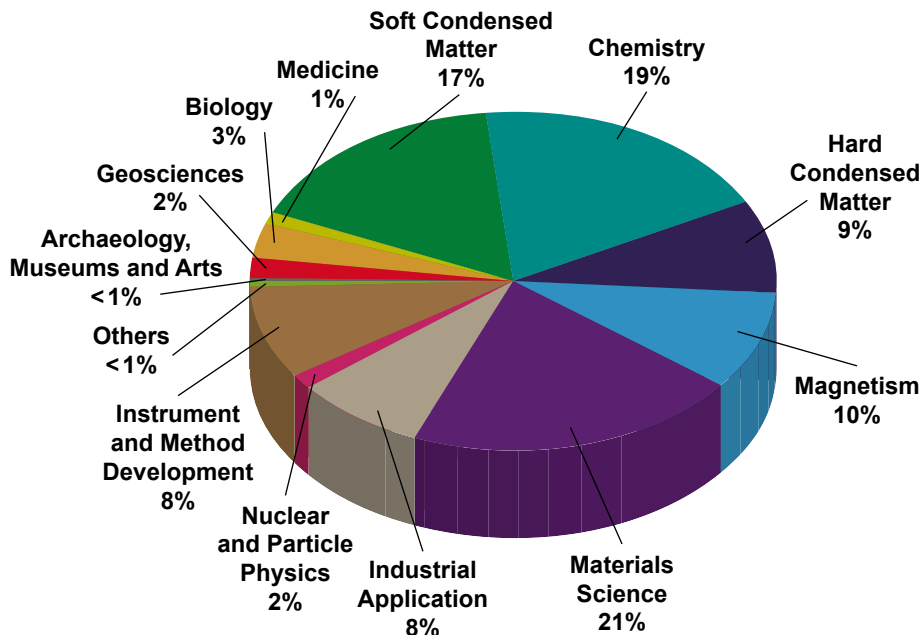
# Publications & Theses

In 2023, we received notice of a total of 255 scientific publications, including journal articles, contributions to books and conference proceedings (<https://impulse.mlz-garching.de/> and figure below). Furthermore, in total 56 theses supervised by staff of the MLZ and its partner institutions were completed in 2023.

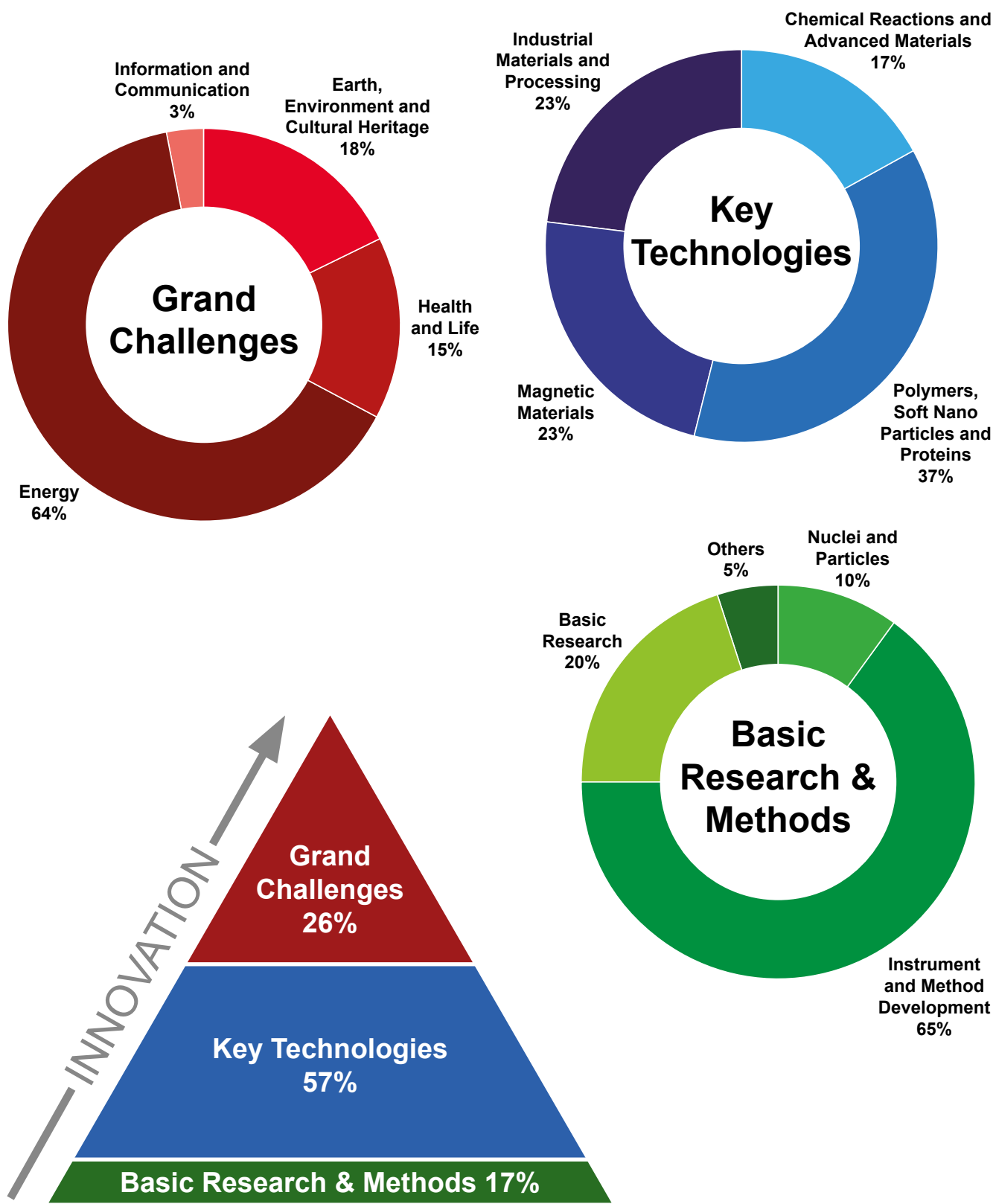


In 2023, 141 PhD theses, based on experiments at the MLZ or method and instrument developments for the MLZ, were either ongoing or completed. Of these, 113 are under the direct supervision of staff at the MLZ and its collaboration partners while the others involve external users. In total, 30 of the 141 PhD theses have been completed in 2023, including external users. Of all the doctoral students, around 95% come from German universities, around 5% from other universities in Europe.

The next figure shows the classification of the journal articles by Scientific Area (several tags per journal article are possible):

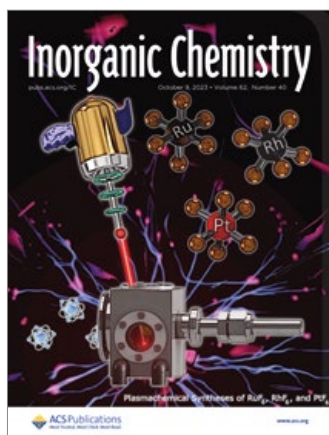


The journal articles at the MLZ can be pictured as a pyramid: Basic Research & Methods (17%) required to tackle the Key Technologies (57%) and articles that address directly the Grand Challenges of our society today (26%). The circular charts represent the individual subjects being dealt with within these three categories.

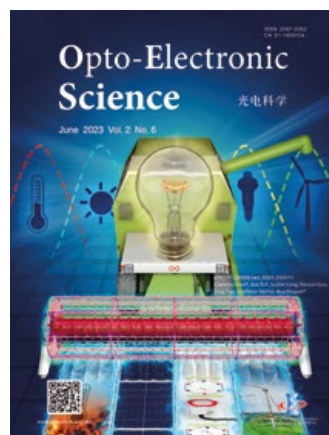


# Cover pages

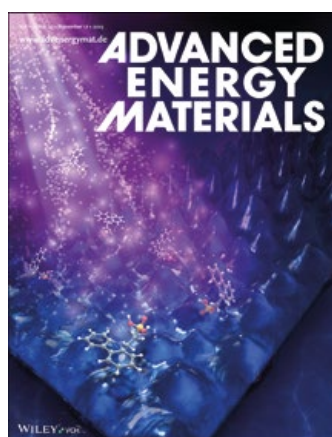
Research by MLZ scientists and at the FRM II made it to the cover pages of several journals in 2023 (see selection below).



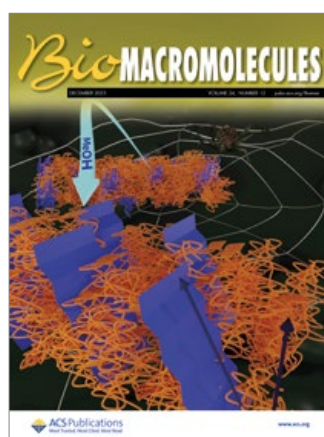
**T. Chemnitz et al.,**  
Plasmachemical Syntheses of RuF<sub>6</sub>, RhF<sub>6</sub>,  
and PtF<sub>6</sub>, *Inorg. Chem.* 62(40), 16263 (2023)  
DOI: 10.1021/acs.inorgchem.3c02452



**T. Xiao et al.,**  
Solar cell-based hybrid energy  
harvesters towards sustainability,  
*Opto-Electron. Sci.* 2(6), 230011 (2023)  
DOI: 10.29026/oes.2023.230011



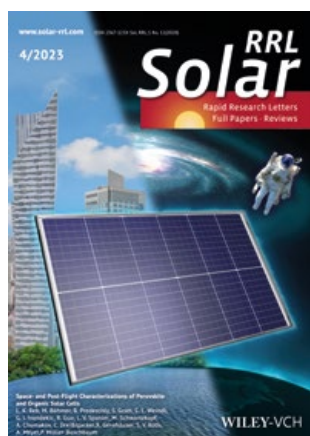
**R. Guo et al.,**  
Refining the substrate surface morphology for  
achieving efficient inverted perovskite solar cells,  
*Adv. Energy. Mater.* 13(43), 2302280 (2023)  
DOI: 10.1002/aenm.202302280



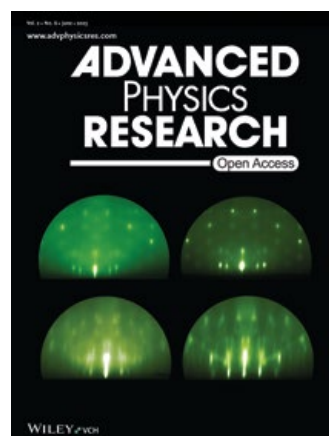
**M. Hofmaier et al.,**  
Influence of the sequence motive repeating num-  
ber on protein folding in spider silk protein films  
*Biomacromolecules* 24(12), 5707 (2023)  
DOI: 10.1021/acs.biomac.3c00688



**A. Vagias et al.,**  
The topology of polymer brushes  
determines their nanoscale hydration,  
*Macromol. Rapid Com.* 44(9), 2300035 (2023)  
DOI: 10.1002/marc.202300035



**L. K. Reb et al.,**  
Space- and post-flight characterizations  
of perovskite and organic solar cells,  
*Solar RRL* 7(9), 2300043 (2023)  
DOI: 10.1002/solr.202300043



**L. Guasco et al.,**  
Tuning Epitaxial Growth of Nb on MgO(100),  
*Adv. Phys. Res.* 2(6), 2200122 (2023)  
DOI: 10.1002/apxr.202200122

# Committees

## Steering Committee

### Chair

Jochen Leyendecker  
Federal Ministry for Education and Research

### Members

Albert Berger  
Technical University of Munich

Prof. Dr. sc. techn. Gerhard Kramer  
Technical University of Munich

Prof. Dr. Astrid Lambrecht  
Forschungszentrum Jülich GmbH

Prof. Dr. Matthias Rehahn  
Helmholtz-Zentrum hereon GmbH

Dr. Albert Schmid  
Bavarian State Ministry of Science and the Arts

### Guests

Prof. Dr. Peter Müller-Buschbaum  
FRM II, Technical University of Munich

Prof. Dr. Martin Müller  
Helmholtz-Zentrum hereon GmbH

Prof. Dr. Stephan Förster  
Forschungszentrum Jülich GmbH

Dr. Axel Pichlmaier  
FRM II, Technical University of Munich

Robert Rieck  
FRM II, Technical University of Munich

Dirk Schlotmann  
Forschungszentrum Jülich GmbH



Figure 1: Steering Committee meeting in May 2023 with R. Rieck, M. Rehahn, A. Schmid, A. Berger, G. Kramer, P. Müller-Buschbaum, J. Leyendecker, S. Förster, M. Müller, D. Schlotmann, and A. Pichlmaier (from left to right).

## Scientific Advisory Board

### Chair

Prof. Dr. Michel Kenzelmann  
Paul Scherrer Institute, Villigen

### Members

Prof. Dr. Lise Arleth  
University of Copenhagen

Prof. Dr. Giovanni Bruno  
Bundesanstalt für Materialforschung und -prüfung (BAM)

Dr. Jens Gibmeier  
Karlsruhe Institute of Technology (KIT)

Prof. Dr. Martin Fertl  
Johannes Gutenberg University, Mainz

Prof. Dr. Thomas Hellweg  
Bielefeld University

Prof. Dr. Bernhard Keimer  
Max Planck Institute for Solid State Research, Stuttgart

Prof. Dr. Rainer Niewa  
University of Stuttgart

Prof. Dr. Julian Oberdisse  
Université de Montpellier

Dr. Victoria Garcia Sakai  
ISIS Neutron and Muon Source, Didcot

Prof. Dr. Helmut Schober  
European Spallation Source, Lund

Prof. Dr. Regine v. Klitzing  
Technical University of Darmstadt



Figure 2: Scientific Advisory Board meeting in April 2023 with M. Müller, R. v. Klitzing, L. Arleth, M. Kenzelmann, V. Garcia Sakai, M. Fertl, B. Keimer, G. Bruno, J. Oberdisse, J. Gibmeier, R. Niewa, P. Müller-Buschbaum, and T. Hellweg (from left to right).



Figure 3: Instrumentation Advisory Committee meeting in March 2023 with J. Neuhaus, C. Hesse, S. Mattauch, W. Lohstroh, J.-F. Moulin, R. Woracek, M. Fernández-Díaz, B. Keimer, U. Köster, M. Müller, and P. Müller-Buschbaum (from left to right).

### Instrumentation Advisory Committee

#### Chair

Prof. Dr. Bernhard Keimer  
Max Planck Institute for Solid State Research, Stuttgart

#### Members

Dr. Maria Teresa Fernández-Díaz  
Institut Laue-Langevin, Grenoble

Prof. Dr. Ulli Köster  
Institut Laue-Langevin, Grenoble

Prof. Dr. Christof Niedermayer  
Paul Scherrer Institute, Villigen

Dr. Frédéric Ott  
Laboratoire Léon Brillouin, Saclay

Prof. Dr. Catherine Pappas  
Delft University of Technology

Prof. Dr. Henrik Rønnow  
Ecole Polytechnique Fédérale de Lausanne

Dr. Robin Woracek  
European Spallation Source, Lund

### MLZ User Committee

#### Chair

Prof. Dr. Tommy Nylander  
Lund University

#### Members

Dr. Andrea Scotti  
RWTH Aachen University

Dr. Jens Gibmeier  
Karlsruhe Institute of Technology

Dr. Ana Brás Würschig  
University of Cologne

Dr. Sandra Cabeza  
Institut Laue-Langevin, Grenoble

Prof. Dr. Holger Kohlmann (Observer on behalf of the KFN)  
Leipzig University

## Evaluation of Beam Time Proposals: Members of the Review Panels

Dr. Markus Appel  
Institut Laue-Langevin, Grenoble

Prof. Dr. Lise Arleth  
Niels Bohr Institute  
University of Copenhagen

Dr. Mikhail Avdeev  
Frank Laboratory of Neutron Physics  
Joint Institute for Nuclear Research, Dubna

Prof. Dr. Piero Baglioni  
University of Florence

Dr. Luis Fernández Barquín  
University of Cantabria, Santander

Prof. Dr. Peter Battle  
University of Oxford

Dr. Matthew Blakeley  
Institut Laue-Langevin, Grenoble

Dr. Johann Bouchet  
Commissariat à l'énergie atomique et  
aux énergies alternatives, Arpajon

Dr. Philippe Bourges  
Laboratoire Léon Brillouin, Saclay

Prof. Dr. William Brant  
Uppsala University

Prof. Dr. Richard Campell  
University of Manchester

Dr. Petr Čermák  
Charles University, Prague

Dr. Robert Cubitt  
Institut Laue-Langevin, Grenoble

Dr. Sabrina Disch  
University of Cologne

Dr. Stephan Eijt  
Delft University of Technology

Prof. Dr. Ulli Englert  
RWTH Aachen University

Prof. Dr. Björn Fåk  
Institut Laue-Langevin, Grenoble

Dr. Bela Farago  
Institut Laue-Langevin, Grenoble

Prof. Dr. Rafael Omar Ferragut  
L-NESS, Como

Dr. Anne-Caroline Genix  
Laboratoire Charles Coulomb  
Université Montpellier

Dr. Francesco Grazzi  
National Research Council of Italy,  
Florence Research Area

Dr. Christian Grünzweig  
Paul Scherrer Institute, Villigen

Dr. Klaus Habicht  
Helmholtz-Zentrum Berlin für  
Materialien und Energie

Prof. Dr. Thomas Hellweg  
Bielefeld University

Prof. Dr. Paul Henry  
ISIS Neutron and Muon Source, Didcot

Dr. Ingo Hoffmann  
Institut Laue-Langevin, Grenoble

Dr. Dirk Honecker  
ISIS Neutron and Muon Source, Didcot

Dr. Christy Kinane  
ISIS Neutron and Muon Source, Didcot

Dr. Joachim Kohlbrecher  
Paul Scherrer Institute, Villigen

Dr. Reinhard Kremer  
Max Planck Institute for  
Solid State Research, Stuttgart

Prof. Dr. Christian Krempaszky  
Technical University of Munich, Garching

Prof. Dr. Jeremy Lakey  
University of Newcastle

Dr. Reidar Lund  
Oslo University

Dr. Sandrine Lyonnard  
Commissariat à l'énergie atomique et  
aux énergies alternatives, Grenoble

Dr. Nicolas Martin  
Laboratoire Léon Brillouin, Saclay

Dr. Gwilherm Nénert  
PANalytical B.V., Almelo

Dr. Thomas Nitschke-Pagel  
TU Braunschweig

Dr. Esko Oksanen  
European Spallation Source, Lund

Prof. Dr. Andrea Orecchini  
Università degli Studi di Perugia

Dr. Alessandro Paciaroni  
Università degli Studi di Perugia

Prof. Dr. Christine Papadakis  
Technical University of Munich, Garching

Dr. Oleg Petrenko  
University of Warwick

Dr. Thilo Pirling  
Institut Laue-Langevin, Grenoble

Prof. Dr. Radosław Przeniosło  
University of Warsaw

Prof. Dr. Diana Lucia Quintero Castro  
University of Stavanger

Dr. Navid Qureshi  
Institut Laue-Langevin, Grenoble

Dr. Florin Radu  
Helmholtz-Zentrum Berlin für  
Materialien und Energie

Dr. Sarah Rogers  
ISIS Neutron and Muon Source, Didcot

Dr. Emmanuel Schneck  
Max Planck Institute of  
Colloids and Interfaces, Potsdam

Prof. Dr. Roland Schwab  
University of Tübingen

Dr. Romain Sibille  
Paul Scherrer Institute, Villigen

Dr. Thorsten Soldner  
Institut Laue-Langevin, Grenoble

Prof. Dr. Thomas Sottmann  
University of Stuttgart

Dr. Andreas Stark  
Helmholtz-Zentrum hereon GmbH

Dr. Johannes Sterba  
Atominstytut Wien, TU Wien

Dr. Christopher Stock  
University of Edinburgh

Dr. Pavel Strunz  
Nuclear Physics Institute, Řez near Prague

Dr. Anne Stunault  
Institut Laue-Langevin, Grenoble

Dr. László Szentmiklósi  
Hungarian Academy of Sciences, Budapest

Dr. Kristiaan Temst  
KU Leuven

Dr. Alexander Tsirlin  
Augsburg University

Prof. Dr. Regine von Klitzing  
Technical University of Darmstadt

Dr. Oksana Zaharko  
Paul Scherer Institut, Villigen

Prof. Dr. Hongbin Zhang  
Technical University of Darmstadt

## Partner institutions



Bavarian Research Institute of  
Experimental Geochemistry and Geophysics  
University of Bayreuth  
[www.bgi.uni-bayreuth.de](http://www.bgi.uni-bayreuth.de)



Georg-August-Universität Göttingen  
• Geowissenschaftliches Zentrum  
[www.uni-goettingen.de/de/125309.html](http://www.uni-goettingen.de/de/125309.html)



German Engineering Materials Science Centre GEMS  
Helmholtz-Zentrum hereon GmbH  
[www.hereon.de/central\\_units/gems/index.php.de](http://www.hereon.de/central_units/gems/index.php.de)



Jülich Centre for Neutron Science JCNS  
Forschungszentrum Jülich GmbH  
[www.jcns.info](http://www.jcns.info)



Karlsruhe Institute of Technology

- Institute for Applied Materials – Energy Storage Systems (IAM-ESS)  
[www.iam.kit.edu/ess/](http://www.iam.kit.edu/ess/)
- KIT Institute for Quantum Materials and Technologies (IQMT)  
[www.iqmt.kit.edu/english/index.php](http://www.iqmt.kit.edu/english/index.php)



Ludwig-Maximilians-University

- Faculty of Physics  
[www.softmatter.physik.uni-muenchen.de](http://www.softmatter.physik.uni-muenchen.de)



Max Planck Institute for Solid State Research  
Stuttgart

[www.fkf.mpg.de](http://www.fkf.mpg.de)



RWTH Aachen University

- Institute of Crystallography  
[www.ifk.rwth-aachen.de](http://www.ifk.rwth-aachen.de)
- Institute of Inorganic Chemistry  
[www.iac.rwth-aachen.de/go/id/plnz/](http://www.iac.rwth-aachen.de/go/id/plnz/)



**TECHNISCHE  
UNIVERSITÄT  
DRESDEN**

Technische Universität Dresden

- Institute of Solid State and Materials Physics  
[www.tu-dresden.de/mn/physik/ifp](http://www.tu-dresden.de/mn/physik/ifp)



Technical University of Munich

TUM School of Natural Sciences

- Chair for Functional Materials  
[www.functmat.ph.tum.de](http://www.functmat.ph.tum.de)
- Institute for Hadronic Structure and Fundamental Symmetries  
[www.e18.ph.tum.de](http://www.e18.ph.tum.de)
- Chair for the Topology of Correlated Systems  
[www.sces.ph.tum.de](http://www.sces.ph.tum.de)
- Chair of Precision Measurements at Extreme Conditions  
[www.ph.nat.tum.de/e66/home](http://www.ph.nat.tum.de/e66/home)
- Particle Physics at Low Energies  
[www.ph.nat.tum.de/ene/home](http://www.ph.nat.tum.de/ene/home)
- Chair of Biomedical Physics  
[www.ph.nat.tum.de/en/e17/home](http://www.ph.nat.tum.de/en/e17/home)

Central Scientific Institution

- RCM – Radiochemie München  
[www.rcm.tum.de](http://www.rcm.tum.de)



Klinikum rechts der Isar

Technical University of Munich

- MRI – Klinikum rechts der Isar  
[www.mri.tum.de](http://www.mri.tum.de)



Technical University of Munich

- Excellence Cluster ORIGINS  
[www.origins-cluster.de/](http://www.origins-cluster.de/)



TECHNISCHE  
UNIVERSITÄT  
WIEN  
Vienna University of Technology

Vienna University of Technology

- Neutron- and Quantum Physics  
Research area at the Atominstitut Vienna  
Abele Group  
<https://ati.tuwien.ac.at/forschungsgruppen/nqp/home/>



Universität der Bundeswehr München

- Institute of Applied Physics and Measurement  
Technology  
[www.unibw.de/lrt2](http://www.unibw.de/lrt2)

Universität zu Köln



University of Cologne

Faculty of Mathematics and Natural Sciences

- Institute for Nuclear Physics  
[www.ikp.uni-koeln.de](http://www.ikp.uni-koeln.de)
- Institute of Physics II  
[www.ph2.uni-koeln.de](http://www.ph2.uni-koeln.de)

PHYSIKALISCHES  
INSTITUT



UNIVERSITÄT  
HEIDELBERG  
ZUKUNFT  
SEIT 1386

Universität Heidelberg

- Physikalisches Institut  
[www.physi.uni-heidelberg.de/](http://www.physi.uni-heidelberg.de/)

# Imprint

## Publisher

Technische Universität München  
Forschungs-Neutronenquelle  
Heinz Maier-Leibnitz (FRM II)  
Lichtenbergstr. 1  
85747 Garching  
Germany

Phone: +49.89.289.14965  
Fax: +49.89.289.14995  
Internet: [www.mlz-garching.de](http://www.mlz-garching.de)  
[www.frm2.tum.de](http://www.frm2.tum.de)  
E-Mail: [jahresbericht@frm2.tum.de](mailto:jahresbericht@frm2.tum.de)

## Editorial Office, Design and typesetting

Anke Görg  
Connie Hesse  
Karin Kleinstück  
Christoph Kreileder  
Reiner Müller  
Björn Pedersen  
Robert Schulze (getyourdesign, Berlin)  
Andrea Voit

## Editors

Henrich Frielinghaus  
Robert Georgii  
Francesco Guatieri  
Markus Hölzel  
Michael Hofmann  
Olaf Holderer  
Johanna Jochum  
Martin Meven  
Andreas Ostermann  
Zsolt Revay  
Anatoliy Senyshyn  
Nicolas Walte  
Marcell Wolf

## Photographic credits

Front cover  
and p. 14 Sabine Steidl, LEIZA (Photo: Reliquary),  
Editing: Reiner Müller (FRM II)

p. 6 top: Juli Eberle  
bottom left: Astrid Eckert (TUM)  
bottom 2<sup>nd</sup> left: Christian Schmid (hereon)  
bottom 2<sup>nd</sup> right: Alessandra Schellnegger  
bottom right: Astrid Eckert (TUM)

p. 8/9 Bernhard Ludewig

p. 17 Dennis Möbus/Südzucker (Photo: Beet),  
From Leuband, CC BY-SA 3.0,  
<https://commons.wikimedia.org/w/index.php?curid=31310507> (Photo: Dairy),  
Editing: Reiner Müller (FRM II)

p. 20/21 Bernhard Ludewig

p. 56/57 Astrid Eckert (TUM)

p. 62 left Bernhard Ludewig

p. 64/65 Bernhard Ludewig

p. 70/71 Bernhard Ludewig

p. 74 top Bernhard Ludewig

p. 74 middle Bernhard Ludewig

p. 75 Christian Schneider-Broecker

p. 76 top Susanne Kurz

p. 76 middle Axel Griesch (IPP)

p. 76 bottom Danas Ridikas

p. 80 middle Klaus D. Wolf

p. 82 top TUM

p. 82 middle Bernhard Ludewig

p. 82 bottom TUM

p. 82 top Bernhard Ludewig

p. 83 top Bernhard Ludewig

p. 84 top Laboratoire Léon Brillouin

p. 86 Bernhard Ludewig

p. 87 top Dr. Jennifer Fischer

p. 88 top left JCNS

p. 88 bottom left Haydar Koyupinar

p. 92 bottom Christian Schneider-Broecker

p. 93 top Susanne Kurz

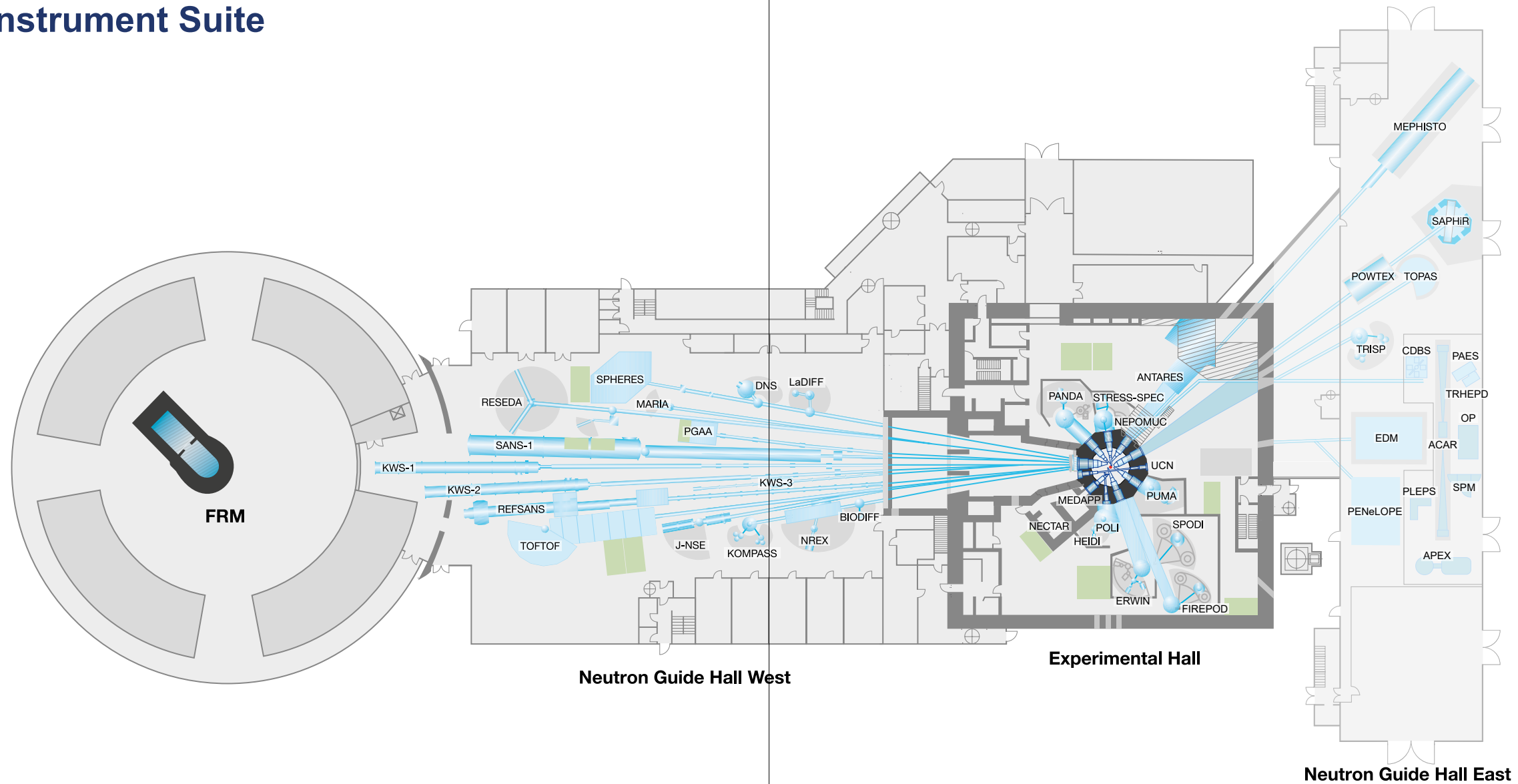
p. 95 Bernhard Ludewig

Editors, authors or FRM II/TUM:  
other images





# MLZ Instrument Suite



Instrument	Description	Neutrons	Operated by	Funding	Instrument group at MLZ
ANTARES	Radiography and tomography	cold	TUM, GEMS	TUM, Hereon	FRM II, GEMS
BIODIFF	Diffractometer for large unit cells	cold	TUM, JCNS	TUM, FZJ	FRM II, JCNS
DNS	Diffuse scattering spectrometer	cold	JCNS	FZJ	JCNS
ERWIN	Powder diffractometer	thermal	TUM	TUM	FRM II
FIREPOD	Powder diffractometer	thermal	TUM	TUM	FRM II
HEIDI	Single crystal diffractometer	hot	RWTH Aachen	FZJ	JCNS
J-NSE	Spin-echo spectrometer	cold	JCNS	FZJ	JCNS
KOMPASS	Three axes spectrometer	cold	Uni Köln, TUM	ErUM, TUM	FRM II
KWS-1	Small angle scattering	cold	JCNS	FZJ	JCNS
KWS-2	Small angle scattering	cold	JCNS	FZJ	JCNS
KWS-3	Very small angle scattering	cold	JCNS	FZJ	JCNS
LaDIFF	High resolution larmor diffraction and inelastic scattering	cold	TUM	TUM	FRM II
MARIA	Magnetic reflectometer	cold	JCNS	FZJ	JCNS
MEPHISTO	Instrument for particle physics, PERC	cold	TUM	TUM, DFG	FRM II
MEDAPP	Medical irradiation treatment	fast	TUM	TUM	FRM II
NECTAR	Radiography and tomography	fast	TUM, GEMS	TUM, Hereon	FRM II, GEMS
NEPOMUC	Positron source, CDBS, PAES, PLEPS, SPM, TRHEPD, OP, ACAR, APEX	-	TUM, UniBw München	TUM	FRM II

\*construction  
ErUM: instrument construction funded by ErUM-Pro (BMBF)

Instrument	Description	Neutrons	Operated by	Funding	Instrument group at MLZ
NREX	Reflectometer with X-ray option	cold	MPI Stuttgart	MPG	MPI Stuttgart
PANDA	Three axes spectrometer	cold	JCNS, TU Dresden	FZJ	JCNS
PGAA	Prompt gamma activation analysis, Neutron activation analysis (NAA), Neutron depth profiling (NDP)	cold	Uni Köln	TUM	FRM II
PUMA	Three axes spectrometer	thermal	KIT	TUM	FRM II
POLI	Single-crystal diffractometer polarized neutrons	hot	RWTH Aachen	FZJ	JCNS
POWTEX	Time-of-flight diffractometer	thermal	RWTH Aachen, Uni Göttingen, JCNS	ErUM, FZJ	JCNS
REFSANS	Reflectometer	cold	GEMS	Hereon	GEMS
RESEDA	Resonance spin-echo spectrometer	cold	TUM	TUM	FRM II
SANS-1	Small angle scattering	cold	TUM, GEMS	TUM, Hereon	FRM II, GEMS
SAPHIR	Six anvil press for radiography and diffraction	thermal	Uni Bayreuth	TUM	FRM II
SPHERES	Backscattering spectrometer	cold	JCNS	FZJ	JCNS
SPODI	Powder diffractometer	thermal	KIT	TUM	FRM II
STRESS-SPEC	Materials science diffractometer	thermal	TUM, GEMS	TUM, Hereon	FRM II, GEMS
TOFTOF	Time-of-flight spectrometer	cold	TUM	TUM	FRM II
TOPAS	Time-of-flight spectrometer	thermal	JCNS	FZJ	JCNS
TRISP	Three axes spin-echo spectrometer	thermal	MPI Stuttgart	MPG	MPI Stuttgart
UCN*	Ultra cold neutron source, EDM, PENeLOPE	ultra-cold	TUM	TUM, DFG	FRM II

**Front page:**

The restored reliquary. The outside is decorated with pictures of Jesus and Mary. The neutron tomography shows the inside of the reliquary. Five relic packets can be seen inside.

**Back page:**

A morning view of the Garching Atomic Egg, the first German research reactor.



**Heinz Maier-Leibnitz Zentrum (MLZ)**

[www.mlz-garching.de](http://www.mlz-garching.de)

DOI: 10.14459/2023md1724727